Whispers of Ancient Air Bubbles in Polar Ice

A novel approach to total air content studies based on the acoustical signal of air bubbles in ice cores

Master's Thesis

Written by *Mikkel Rasmus Schmidt*

June 16^{th}, 2021

Supervised by
Vasileios Gkinis and Bo Møllesøe Vinter

University of Copenhagen

UNIVERSITY OF COPENHAGEN

FACULTY:	SCIENCE
INSTITUTE:	Niels Bohr Institute
AUTHOR(S):	Mikkel Rasmus Schmidt
EMAIL:	Mikkel.schmidt@hotmail.com
TITLE AND SUBTITLE:	Whispers of Ancient Air Bubbles in Polar Ice - A novel approach to total air content studies based on the acoustical signal of air bubbles in ice cores
SUPERVISOR(S):	Vasileios Gkinis and Bo Møllesøe Vinter
HANDED IN:	June 16th, 2021
DEFENDED:	Oh god who knows......

NAME ______________________________

SIGNATURE ______________________________

DATE ______________________________

Abstract

This thesis presents a novel approach to ice core research which investigate the audio signal radiated from ice cores as sound due to air bubbles formed under pressure are being released as ice is being melted. [Minnaert, 1933] used the frequencies of the sound radiated by bubbles to estimate their radius. This method is applied on ice cores to estimate the total air content (TAC). Through initial measurements during a melt campaign in Bern in February 2020, design and production of test ice with and without bubbles and through analysis of the continuous flow analysis (CFA) system in Copenhagen and improvements of this, a first order setup has been designed. Four types of ice were melted on this setup and has been analyzed for total air content estimates. This worked as proof of concept though many parameters and the data analysis needs to be improved upon.

Disclaimer

This work is part of a three year Villum Foundation Experiment Grant (Grant 00028061) called: Whispers of Ancient Air Bubbles in Polar Ice provided to Anders Svensson. The work carried out in this thesis is the initial work on using audio to estimate the total air content in an ice core and more work will follow this.

This thesis concludes my Masters degree in Geophysics. Prior to this project, I had very little experience with the parts on studio recordings, audio and audio processing. It has been an interesting topic to self learn, and it has served as a great topic to learn through trial and error.

Audio and video files

Throughout this thesis several audio and video files will be linked, but are not embedded in the document since flash is not available post December 2019. All audio and video files can be accessed through this [link] or by copying this path: `https://sid.erda.dk/sharelink/HLT9J8pOID`

Acknowledgements

First and foremost, I would like to thank my supervisor Vasileios Gkinis - for his never ending ideas on improvements and what to pursue next, his great knowledge and for pushing me to continue even when life was tough. Even though we have had our differences I have truly valued your input. Secondly I would like to thank Thea Quistgaard, Rebecca Frøystad, Alexander Friisnæs, Maureen Eyers, Meg Harlan, Iben Koldtoft and even more for being great companions at PICE through thick and thin, and one corona lockdown after the other. A huge thanks to Thea Quistgaard and Caroline Munck Nielsen for reading through and giving valuable comments on the thesis. Thanks to my boyfriend Rasmus Jørgensen for listening to all of my problems and helping me through the tough times.

There are so many more that has been such a huge part of this journey both professionally and personally and I would like to appreciate every single one of you.

Contents

Introduction

Ice cores have been at the center of climate studies since the first ice cores were drilled and investigated back in the 50's, 60's and 70's due the stable water isotopes which serva as temperature proxxies for a climate history book [Jouzel, 2013]. Since then a multitude of new methods of ice cores studies have emerged as studies of chemistry, tephra (volcanic ash), physical properties and gas have been developed. When combined these studies give an overview of the climatic history of planet Earth during the last 800.000 years.

Once the ice core is drilled it is separated into several precisely divided pieces to gain as much knowledge as possible from each core. Every single piece of knowledge is extracted from the frozen water - except one.

As the ice core is melted for investigation of impurities and gasses the air bubbles burst with loud pops as the ancient atmosphere is finally released from its captivity and pressure of tonnes upon tonnes of overburden ice. This acoustic signal has not yet been investigated as a signal with connection to scientific variables. And the best thing - it does not require any extra ice as this signal is found during melt campaigns already happening!

This thesis conducts a first degree investigation of this signal and how to optimize the signal found. Freezers are a noisy environment - loud fans are keeping the temperature steady and during a measurement several people and instruments heat up the air, microphones come in various configurations and air bubbles go through a most complicated journey through the depth of an ice sheet. All these are complications that have been questioned, investigated and researched throughout this thesis.

During the next many pages we will go through the basic journey of an air bubble, studio recordings, and from initial measurements in Bern, Switzerland with a podcast microphone and corona implications to a full experimental setup measuring a piece of the DYE-3 ice core.

Welcome to my journey of learning about complicated and unruly air bubbles, total air content measurements, what even is sound? can it even be used for anything? and experimental tests, successes and failures.

Part I

THEORY

1 Journey of an Air Bubble

THIS CHAPTER PUTS THE FOCUS ON THE JOURNEY OF AN AIR BUBBLE from formation through densification to transformation into clathrates.

Air bubbles are the main focus of this study and the complex process from forming through densification to a state of clathrates needs to be understood and considered. In the next pages the journey of an air bubble will be explained. The variation of bubbles in size and properties will be the subject of future work but for simplicity this thesis will focus on the zone with visual bubbles. Here we know from observation that air bubbles are prominent, both from visual inspection and from pore studies [Cuffey and Paterson, 2010, Lipenkov, 2018].

Contents

The densification process is the process of turning snow into ice. This is also where air bubbles are formed and since air bubbles are the center of attention for this project this is a good place to start.

1.1 *Densification and formation of air bubbles*

1.1.1 *Densification of ice*

The process of snow turning into ice is called densification, as more snow is gradually deposited on the surface of the ice sheet, the snow grains transform into ice, getting less porous and denser with depth as the weight of the overburden snow increases [Cuffey and Paterson, 2010, Herron and Langway, 1980]. The intermediate state of compacted snow - before the close-off of air bubbles (red arrow in Figure 1.1) - is called firn. Once the air bubbles have been completely isolated from the atmosphere at the close-off depth the compacted snow is defined as ice.

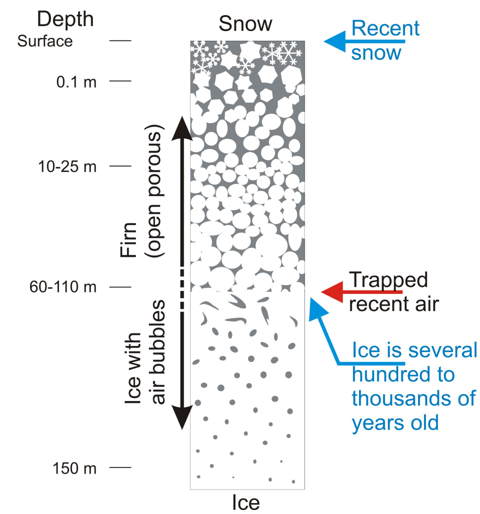

Figure 1.1: [Blunier & Schwander, 2000], Gas enclosure in ice: age difference and fractionation

The initial increase in density is due to settling, which is the displacement of individual particles in relation to the others. The fresh snow is light and irregularly placed. As more overburden pressure is introduced the ice particles fill up the empty space between them. This process takes place down to a density of 550 kgm^{-3} [Cuffey and Paterson, 2010]. Between 550 and 830 kgm^{-3} the densification processes are dominated by sublimation (parts of ice crystals turn into vapor, the vapor is displaced and then turned back to solid) and reshaping and recrystallization of the ice crystals to reduce the stress of weight and minimize empty space [Cuffey and Paterson, 2010]. At around 50-80 meters the pores containing air are isolated from the atmosphere, at which the firn layer ends and the crystals are defined as ice. This transition depth is called the bubble close-off and happens at densities close to 820 kgm^{-3} [Cuffey and Paterson, 2010]. The time duration for ice to reach this density varies greatly with the accumulation, extending to years for land based glaciers, hundreds of years for Greenland Ice Sheet ice cores and thousands of years in central Antarctica. For GRIP (central Greenland) at the depth of 50% close off (75$\pm$2 m) the age is 235$\pm$10 years [Schwander et al., 1997]. Any further increase in density happens due to disintegration of air pores and compression of air bubbles [Lipenkov, 2018].

Several models [Herron and Langway, 1980, Barnola et al., 1991, Wilkinson and Ashby, 1975] have been developed to understand the densification processes. They show that the models depend heavily on the changes in atmospheric conditions such as accumulation and temperature as well as the initial snow density. The Herron-Langway model only use these three parameters to simplify the model which fits the data. The model defines three stages which are parameterized by density, with the first going from initial snow density to critical density of 550 kgm^{-3} as explained above, due to rapid densification and snowpacking. A slower stage of densification is the second from the critical density to the air close-off density $550 - 820$ kgm^{-3}. The final stage of densification is further compaction and compression of air bubbles in the ice from 820 to 917 kgm^{-3}. The main assumption is that the densification is proportional to the stress of the load of overburden snow. For the NGRIP ice core in central Greenland the model has been run with the surface temperature (242 K), accumulation (0.19 m/yr) and initial snow density (340 kg/m^3). The model can be seen in Appendix A. In Figure 1.2 the model and the model with optimized parameters to fit the data is shown with the measured density values. The rapid densification can be seen down to 16 meters and afterwards the slower compaction stage is present. As the ice particles moves down through the ice they reach the close-off depth and the only further increase in densification happens due to air bubble compaction down to 917 kgm^{-3} [Cuffey and Paterson, 2010].

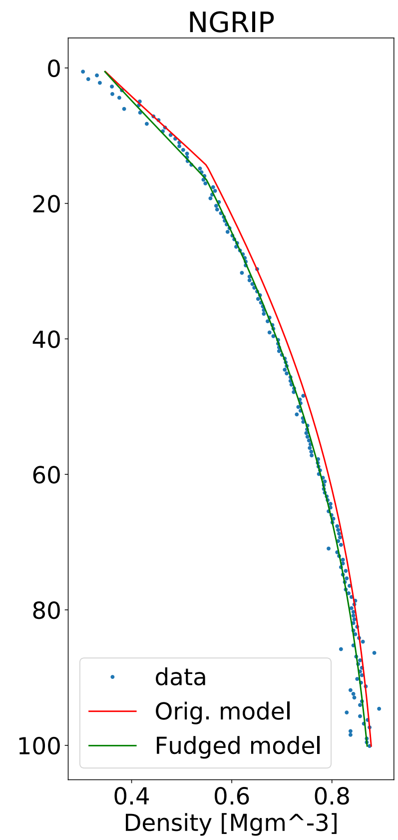

Figure 1.2: NGRIP density profile using an H-L model and an H-L model with optimized parameters.The blue dots indicate measured data points, the red line the original model and green the fudged model with scaled parameters. The parameters are Temp = 242 K, Acc = 0.19 m/yr, ρ_0 = 340 kg/m^3.

The densification process provides us with important tools to understand the past climate. Understanding the densification process is important as it has grave impact on the air bubble amount, composition, size and properties [Lipenkov et al., 1997, Lipenkov, 2018]. Factors that affect the air bubbles are accumulation, atmospheric pressure, temperature and properties of the ice [Cuffey and Paterson, 2010]. One example is the amount of accumulation from Greenland to Antarctica with Greenland having much higher accumulation rates at 0.5 m/yr and Antarctica as low as 0.02 m/yr [Cuffey and Paterson, 2010]. This changes the densification processes as the time before close off depth is hundreds of years on Greenland and thousands of years on Antarctica [Buizert, 2013]. Furthermore the transition from the last glacial maximum (LGM) to the Holocene shows a significant increase in number of air bubbles as temperature and accumulation rises [Lipenkov, 2018].

The process of densification is complex and depends on various parameters and variations from location to location. Some areas are dry like the inner ice sheets in Greenland and Antarctica, whereas several smaller ice caps experience periods of melting and refreezing in lower ice layers due to percolation. To understand the densification one has to know the parameters of the ice cap of interest [Cuffey and Paterson, 2010].

1.1.2 *Density of ice*

If a certain percentage of a column, ν, is closed off as air bubbles the density of ice is expressed as:

$$\rho = \nu\rho_a + (1-\nu)\rho_i \tag{1.1}$$

where ρ_i is the density of ice 917 kgm^{-3} and ρ_a the density of atmospheric air. This expression is only valid for the part classified as ice. An empirical density-depth relation was first derived by Schytt in 1958

$$\rho(z) = \rho_i - [\rho_i - \rho_s]\exp(-z/z_\rho) \tag{1.2}$$

where the change in density ρ at depth z depends on the density of ice ρ_i and the surface snow density ρ_s. z_ρ is the characteristic depth of the firn and is constant for each site. It is obtained by fitting to the data, though often a first estimate is based upon the firn-ice transition depth z_t using the relation $z_\rho = z_t/1.9$ [Cuffey and Paterson, 2010].

1.1.3 From porous air to air bubble

As snow deposits on the ice sheet it gets more and more compressed causing the air to form pores within the firn. These pores are long, narrow and complex forms that are undergoing internal convection of gases with the atmosphere down to the close-off depth, at which depth the pores close off completely and become isolated from atmospheric air and pressure. The further evolution of air bubble systems below the close-off depth consists of disintegration of the pore systems and elongated bubbles and by compression of air bubbles [Lipenkov, 2018]. The disintegration of pores does not change the volumetric content, but does increase the number of bubbles present in the ice as it disintegrates into more individual bubbles. Because the air can be exchanged down until close-off there will be a difference in the age between the gas in the air bubbles and the surrounding ice crystals at the same depth [Cuffey and Paterson, 2010, Schwander et al., 1997].

1.2 Bubble classification

There are various types of bubbles present in polar ice. As the bubbles move deeper in the ice they undergo transitions from bubbles to clathrates.

1.2.1 Normal air bubbles

Normal air bubbles are the result of the disintegration of pores in the ice matrix. Some pores close-off continuously down through the densification process until the close-off depth at which point all of the pores will be isolated [Lipenkov, 2018]. Any further compression causes these pores to disintegrate into individual unique smaller

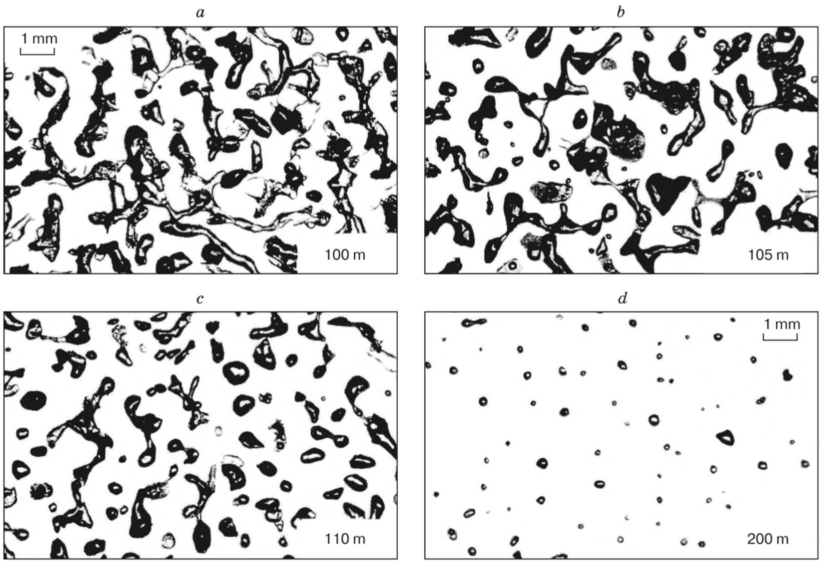

Figure 1.3: Pores and air bubbles in Vostok ice core from [Lipenkov, 2018]. a: 100 m depth: close-off of firn pores and their isolation from atmospheric air, according to gas contents in ice; b: 105 m depth: close-off of firn pores, according to open porosity measurements; c: 110 m depth: disintegration of elongated air bubbles; d: 200 m depth: isometric air bubbles. Microbubbles occur as nearly spherical small bubbles (a–c) or as black points (d).

pores or air bubbles that gets rounded off due to pressure [Lipenkov, 2018]. The pore disintegration is seen in figure 1.3 right at close-off and fast disintegration in the next meters until all remaining air is shaped as spherical bubbles due to pressure. The compression of the air bubbles due to the overburden snow is clearly seen from 1.3.a-c compared to 1.3.d with all white surfaces being ice particles.

1.2.2 *Microbubbles*

Besides normal bubbles, polar ice also contains very small air bubbles which are defined as microbubbles. These are bubbles that are captured by ice grains before the pore close-off from the atmosphere. Early in the process they are seen as small bubbles but after close-off they are very small bubbles compared to pore inclusion bubbles seen in Figure 1.3 [Lipenkov, 2018]. The microbubbles are seen in Figure 1.3.a-c as nearly spherical small bubbles and in 1.3.d as black points [Lipenkov, 2018].

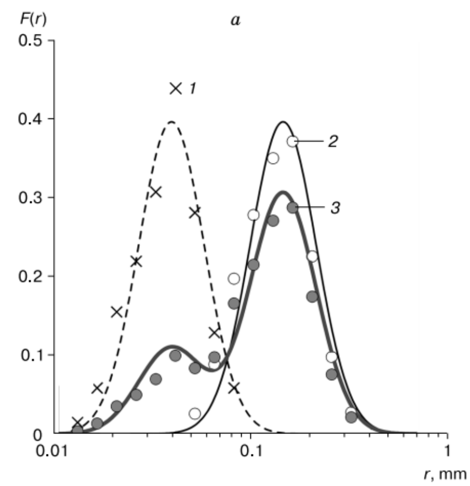

Figure 1.4: Size distribution of air bubbles in polar ice from [Lipenkov, 2018]. Normalized distributions of 1) microbubbles, 2) normal bubbles and 3) all air bubbles by their radius in the Vostok ice core in Antarctica from the depth of 183 meters including 2500 inclusions. Symbols are data and curves are size distributions.

The two types of air bubbles are confirmed through experimental observation and direct measurements of gas pressure in [Lipenkov, 2018] and [Lipenkov, 2000]

By observation the normalized size distributions from measuring 2500 bubble inclusions can be seen in Figure 1.4, where microbubbles and normal bubbles as well as all air bubbles can be seen. By gas pressure measurements it is shown that the gas pressure at the firn/ice transition of normal bubbles is on average 0.6 MPa lower than the overburden ice pressure, whereas the average gas pressure in microbubbles is 0.25 MPa lower [Lipenkov, 2000]. This further proves that two types of bubbles are present.

From these studies of antarctic ice cores it is shown that microbubbles make up commonly (20±5) % of the total number population of air bubbles, but less than 0.3% of the total gas content [Lipenkov, 2018].

1.2.3 *Clathrates*

As the overburden pressure due to the weight of snow keeps increasing the bubbles keep shrinking in size. As they decrease in size the gas pressure inside the bubbles rises. At a sufficient pressure and depth the gas pressure is in equilibrium with the surrounding ice at the given temperature. With these conditions the bubbles begin to disappear as clathrate hydrates. At this stage the ice crystal lattices form cages in which the air bubble molecules can "hide" within the lattice [Miller, 1969]. The air bubbles transform into clathrates over a broad depth range of several hundred meters, e.g. 900-1600 meters in central Greenland, but as the pressure increases they are more likely to transform [Cuffey and Paterson, 2010].

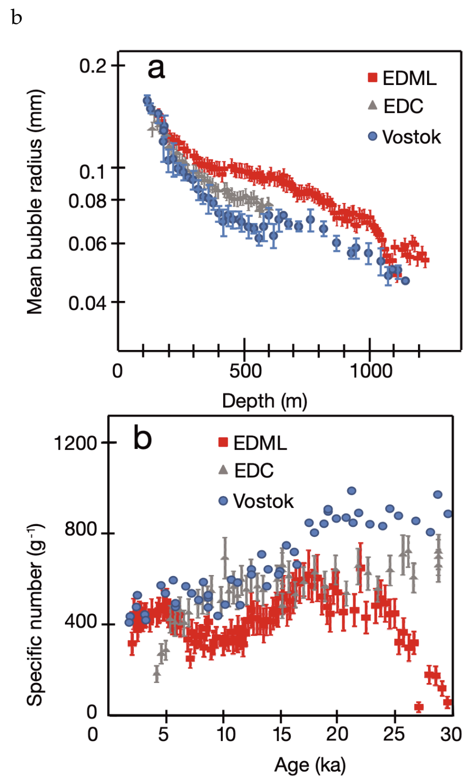

Figure 1.5: a) Mean equivalent bubbles radius showing a decrease in bubble radius as depth increases and b) specific bubble-number profiles of EDC and EDML. EDC and Vostok shows a slow increase back in time, whereas EDML (closer to the coast) shows higher variation with time. The figure is from [Ueltzhöffer et al., 2010].

1.3 *Bubble-size and bubble-number distributions*

For future measurements some reference is needed in order to estimate whether the results are consistent with previous results presented in a variety of papers. These results will be presented in the next sections.

1.3.1 *Bubble-size distributions*

Studies from [Lipenkov, 2000, Ueltzhöffer et al., 2010, Lipenkov and Salamatin, 2015, Bendel et al., 2013] have investigated bubble-size distributions of Antarctic ice core from Vostok, EDC and EDML. It varies for each study whether the air bubbles have been classified as the collected air bubble distribution or whether the microbubbles and normal bubbles have been studied separately. Despite this, all distributions show the left distribution tail towards the microbubbles as can be seen in Figure 1.4.

Figure 1.5.a shows the comparison of mean bubble radius across the three cores by the depth. The decrease in size matches the intuition by the compression of air bubbles by depth due to weight. The bubble radius goes from around 150μm in radius to around 60 μm at the same depth as the ice transforms to clathrate hydrates where both clathrates and bubbles exist [Ueltzhöffer et al., 2010]. According to [Lipenkov and Salamatin, 2015] the normal bubble radius in the

Vostok core decreases from 300µm at 100m depth to below 100µm at 500m whereas the microbubbles radius is close to 50µm already at 100m decreasing to 30µm at 500m.

The physical bubble size in the ice core is not equivalent to the air bubble size released during melting as the air bubble volume is the same as the depth at which the core was drilled and the ice is compressed by the weight. Therefore the air bubble size estimated is the one at close-off, prior to any physical compression. This is also the bubble size at atmospheric pressure. In [Lee et al., 2013] air bubbles released from glacier ice from Gulkana Glacier in Alaska (depth not mentioned) were examined. The bubble sizes were estimated both optically and using sound as will be explained in section 3.5. They estimated the bubble sizes between 230µm and 500µm, which is vastly greater than the values from the Antarctic ice cores.

1.3.2 *Bubble-number densities*

Many of the studies mentioned in the previous section has worked with bubble-number densities e.g. [Ueltzhöffer et al., 2010, Lipenkov and Salamatin, 2015, Bendel et al., 2013]. The bubble-number is usually given in values of number of bubbles N per gram. The comparison of the Vostok, EDC and EDML ice cores in bubble-sizes by age is seen in Figure 1.5.b. The bubble-number values vary with time and the two central ice cores Vostok and EDC show a decreasing tendency from 700-800 bubbles g^{-1} to 400 bubbles g^{-1} whereas EDML show more variations possibly with climatic signals [Ueltzhöffer et al., 2010, Bendel et al., 2013].

Besides this [Spencer et al., 2006] has developed a paleoclimatic indicator from the bubble-number densities resulting in Figure 1.6 showing high variability in bubble-number densities by variations in accumulation and temperature [Spencer et al., 2006].

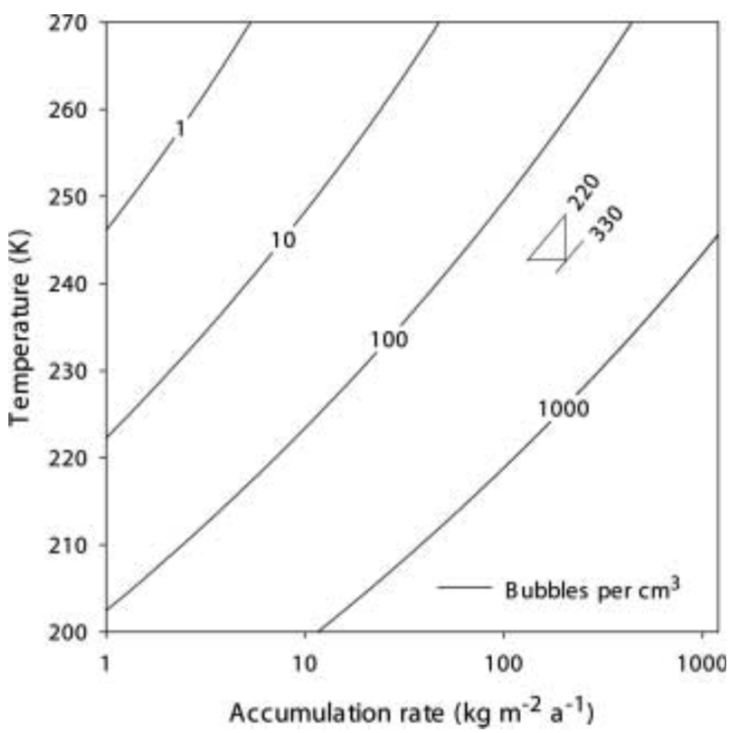

Figure 1.6: Bubble number-density reached under steady-state conditions from [Spencer et al., 2006]. The triangle between the isolines for 330 and 220 bubbles cm^{-3} represents possible climatic change over the past 5 kyr allowed by our model and measured bubble number-density. The lower right corner of the triangle represents modern conditions.

2 Total Air Content of Ice Cores

In this chapter the focus is on total air content (TAC), its relation to the air pressure and densification and give an overview of other measurement techniques and results from various ice cores. Total air content is understood as amount of air per unit mass of ice.

Contents

2.1 Relation between TAC and atmospheric pressure

Since the densification process is mostly affected by atmospheric conditions, particularly barometric pressure and temperature, the total air content is also directly related to this. According to [Martinerie et al., 1992] [Raynaud and Lebel, 1979] the relation between TAC (V), temperature and atmospheric pressure is given by:

$$V = V_c \frac{P_c}{T_c} \frac{T_0}{P_0} \tag{2.1}$$

with V_c, P_c and T_c being the volume of air per gram, pressure and temperature at pore close-off and T_0 and P_0 being standard values of pressure (1013 mbar) and temperature (273°K).

Due to this relation between the volume of air in polar ice and the atmospheric pressure the TAC has been suggested as a proxy of changes in the surface elevation for the ice sheets mainly during glacial-interglacial cycles. If the temperature variations in the past is known, then the pressure can be found using this method. This estimate of the pressure can also be used to do some upstream corrections of ice that has drifted under pressure towards the margins of the ice sheet. But since the relation needs to know the pore-volume at close-off this can lead to major uncertainties to be accounted for.

According to [Martinerie et al., 1992] there are two major uncertainties using V as a proxy for paleoelevations:

- The pressure P_i can be influenced not only by changes in pressure due to surface elevations but also changes in atmospheric patterns affecting the atmospheric pressure
- The volume of the pores during close-off is not well known.

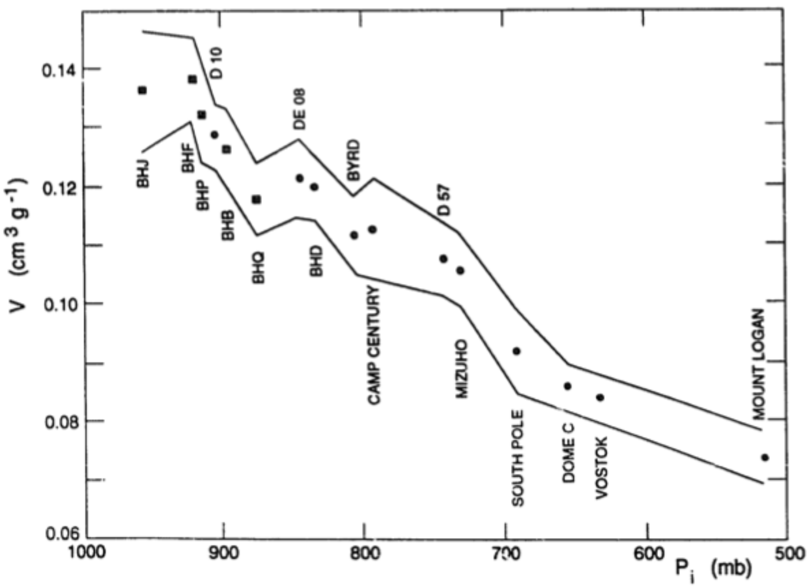

Figure 2.1: [Martinerie et al., 1992]. Air content versus pressure at the air isolation level from 16 different location. The dots show the the mean values for each site and the line the maximum uncertainty. The squares correspond to the five sites which undergo summer snow melting.

As can be seen in Figure 2.1 there is a relation between the TAC and the pressure at the air isolation level for the 16 sites in [Martinerie et al., 1992]. This shows a decrease in TAC with pressure decrease and hence increasing site elevation. The correlation between various parameters as temperature, elevation and pressure is discussed in [Raynaud and Lebel, 1979] and [Martinerie et al., 1994] and according to [Raynaud and Lebel, 1979], an elevation increase of 1000 meters corresponds to an air volume decrease of approximately 0.017 cm^3/g of ice, and a temperature reduction of 5°C corresponds to a decrease of about 0.001 cm^3 per g of ice. These relations can be seen plotted in Figure 2.2 which displays Fig. 1 in [Raynaud and Lebel, 1979], the values for 6 different ice cores at various elevations and variations in temperature at close-off which changes with elevation. Expressed in percentages of change in long term variation parameters [Lipenkov et al., 1995]:

1. Elevation: A change of about 50 m in elevation may generate a change of 1% in air content

2. Atmospheric pressure: Long-term changes in atmospheric pressure may generate a change of 1% per 7 mbar.

3. Temperature: Changes in temperature of 2°C may introduce a 1% change in air content.

There is a seasonal variation in the total air content of up to 9% due to atmospheric conditions and precipitation [Raynaud and Lebel, 1979]. This effect is in most studies neglected due to using samples deeper in the cores when annual layer thickness is 2-5 cm. Using samples of greater sizes (3-4 cm) should be enough to neglect annual bias below a certain depth which varies from core to core. Above this depth, where the sample sizes are equal to or smaller than the annual layer thickness, there is a significant short term variation which calls for sequential samples ranging at least a full year [Herron and Langway, 1987]. If annual melt is present, this introduces yet another variation. This melt percolates through the ice, spreads laterally and freezes, creating ice layers with a virtually void of bubbles and surely not densified air bubbles relating to air pressure.

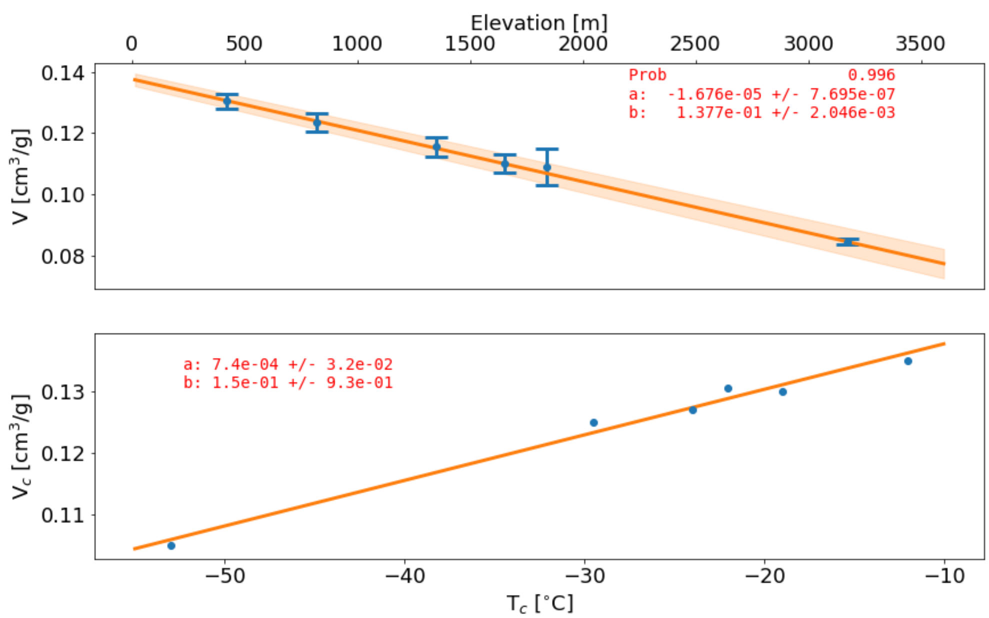

Figure 2.2: Variations in TAC values with changes in elevation and temperature from [Raynaud and Lebel, 1979]

Many other parameters besides the atmospheric pressure due to elevation changes might come into play and especially during rapid alterations such as temperature variation and dependence, changes in the pressure-elevation gradient and wind stress [Raynaud et al., 1997]. Antarctic records also show an insolation signature in the TAC records [Eicher et al., 2016].

2.2 *Previously used measurement methods*

Various techniques have formerly been used to measure TAC in ice cores. Each technique has its advantages and disadvantages. Some produce more or less precise measurements and uncertainties, introduce systematic errors or use more ice. Some take seasonal variations and short-term pertubations as melt features into account.

For all methods, all discretely sampled TAC measurement samples were chosen for optimal conditions of the gas trapped. Meaning samples from unfractured sections and as little percolating meltwater as possible. The samples are also collected well below the close-off depth as pore seals may be delicate and consequently can result in changes between core-recovery and measurement.

Gas extraction (methane) method: Ice samples of 20-40 g are taken from a central part of the ice core and are placed in a gas vessel sealed using vacuum grease. The air surrounding the ice sample is evacuated to a vacuum and the ice is then melted and slowly re-frozen from the bottom. In this way most air is pushed out of the water sample. The same method is used for artificial bubble-free ice, see sec: 5.2. The efficiency is estimated to 99% from experimental tests [Raynaud et al., 1988]. After refreezing, the gas is expanded in an extraction line and measured. These measurements were analyzed for relative precision and showed an average change of 0.7% and never exceeded 2% [Raynaud et al., 1988]. This method does show systematic differences in results using different procedures for gas extraction under vacuum. This should be taken into account when comparing results but does not affect a single procedure. This method is a by-product of the method used for methane measurements of air in ice cores [Raynaud et al., 1988].

Gas extraction melting under a liquid in a burette: This method melts ice beneath another liquid and uses gas extraction in a burette for air-volume measurements. The errors for this methods are significant up to 5%, but the precision of the measurements has been improved using new liquids [Lipenkov et al., 1995, Kameda et al., 1990]. Much of the method follows the previous method of gas extraction.

Barometric air extraction by ice crushing: Air-content measurements have been measured along a dry-extraction procedure. The ice is crushed into less than 0.1 mm grain size and the released air is introduced in another pre-evacuated vessel. The temperature and pressure changes of the second vessel gives the total air content. The total amount of air extracted when crushing the ice sample under vacuum has an estimated uncertainty of 1%, though the error might be greater due to inefficient crushing and air still being stuck [Lipenkov et al., 1995]. Various methods have been applied for more efficient crushing [Kameda et al., 1990].

Vacuum-volumetric method and barometric method optimization: The sample is contained in a glass vessel and by melting-refreezing, the air is collected after trapping the water vapor in the burette of a Toepler pump [Lipenkov et al., 1995]. This has a high accuracy but several disadvantages as long measurement times and use of health hazard products, as the Toepler pump uses mercury, and fragility of the glass vessel. [Lipenkov et al., 1995] has optimized this method and analyzes samples with a Barocel using the pressure rather than a volume measurement. It also uses stainless steel vessel and tubes contrary to the glass. This makes it suitable for field use.

In general measurement techniques have to account for the cut bubble effect, which is the estimation of air volume lost on the edge of ice sections, as the bubbles air has been released, when the core section is cut [Martinerie et al., 1990]. The higher the ratio between surface area and volume the higher the effect. [Kameda et al., 1990]

2.3 *Total air content in ice cores*

The air content has been measured in all previously drilled ice cores using the techniques mentioned above. The variations in air content are small across various ice cores as displayed in table 2.1 and Figure 2.3. The table values are just average values and each core has variations in them. Figure 2.3 show the TAC data vs. depth for each core mentioned. In the following paragraphs each core will be presented in more depth.

Ice core	Average TAC [cm^3/g]
NGRIP	0.09329 ± 0.00533
DYE-3	0.10207 ± 0.01141
GRIP	0.08870 ± 0.00435
GISP-2	0.08700 ± 0.01952
NEEM	0.09192 ± 0.00903
Camp Century	0.09730 ± 0.01893
Combined	0.09338 ± 0.03159

Table 2.1: The average of the volume of air content in various ice cores.

DYE-3 [Herron and Langway, 1987] According to [Herron and Langway, 1987] there are significant short term variations in the total air content measurements in the first 900 m due to seasonal variations.

Below this depth the annual layer thickness gets small enough for sample sizes to account for annual variation. This short term variation is up to 10 to 15% within consecutive samples. Therefore, several consecutive samples were studied to accommodate both seasonal variations and short-term pertubations. The DYE-3 scatter in figure 2.3 reflects seasonal variations and shows the need for consecutive samples to reflect a year. This is why the data points look stacked as they are consecutive samples with high variation.

Camp Century [Herron and Langway, 1987] The data provided in [Herron and Langway, 1987] shows an approximately constant average air volume in the upper 800 meters of the Camp Century ice core of 0.110 ± 0.006 cm^3/g. From 950 to 1100 m there is a slow decrease to 0.101 ± 0.005 cm^3/g followed by a sharp decrease below 1350 m. This is basal ice and the values can be contributed to refreezing and basal processes. This tendency is observed in other cores as well.

GRIP [Raynaud et al., 1997] These data cover two wide periods in the GRIP ice core. The first up to 40,000 years back and the second includes the Eemian ice from the last interglacial. The main findings show a decrease of around 13% between the last glacial maximum (LGM) and the earliest parts of the Holocene and it shows a steady increase of about 8% during the Holocene. The decrease in TAC from the LGM to Holocene transition contradicts the hypothesis that an increase in temperature will lead to an increase in TAC. From ice sheet modelling, the elevation increase of up to 250 m during the transition to Holocene is not enough to explain even half the decrease. To account for the full drop, densification processes as temperature, pressure and wind have to be taken into account. Here the changing wind stress and changes in ratio between summer-winter precipitation would have a significant impact. Ice sheet modelling shows a change in elevation of several hundred meters and constrains the probable change in elevation. This does not account for enough change and suggests that various climate parameters may have changed during the Holocene.

The air content found in the Eemian period is of the same order as the previous 40 kyr with generally lower air content for warmer periods.

NGRIP [Eicher et al., 2016] The NGRIP drilling site is comparable to the GRIP ice core site. The elevation at GRIP is 300m higher but the temperature is essentially the same as the higher elevation is compensated by the higher latitude. The two datasets are in good agreement, though the TAC is on average lower by 1.7-2.4 ml kg^{-1}

[Eicher et al., 2016]. These data show a dependency on local summer insolation and thus the orbital parameters on a low frequency scale. On high-frequency changes the TAC match with the D-O events during the last glacial and show a variation with the temperature experienced during these events. These alterations in TAC would not be due to elevation changes as the change is on too short a time scale for the ice sheet to build up.

NEEM [Jensen et al., 2013] TAC measured in NEEM is only done for the bottom part of the ice core. This is done for reconstruction of the last interglacial, the Eemian, in the NEEM community paper [Jensen et al., 2013]. Since the Eemian is estimated to be up to 8°C warmer than present it was dominated by many melt layers reducing the air content and resulting in highly variable measurements with a decreasing tendency following the summer insolation decrease. At the onset of the Eemian the TAC was stable at 85.0 ml kg^{-1} compared to the present level of 97,5 ml kg^{-1}. Correcting for summer insolation the elevation at the depositional site is estimated to 540±300 m higher than the present NEEM elevation. Very little TAC data has been published of NEEM above 2200 m depth.

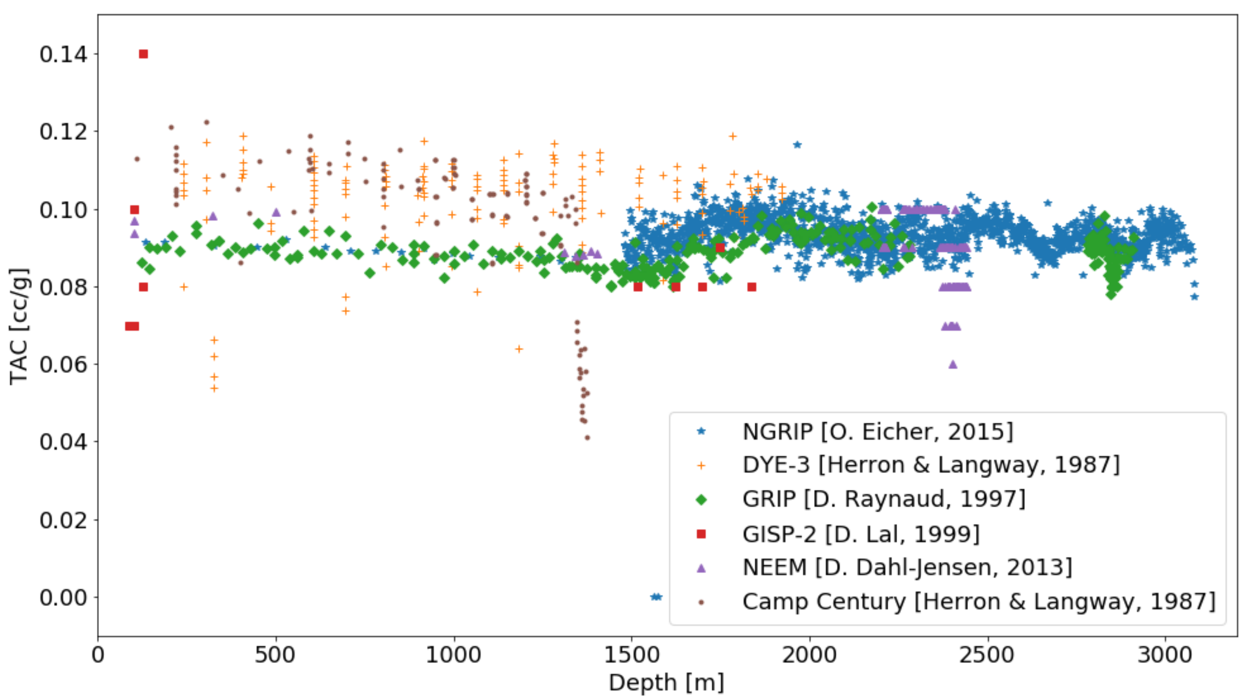

Figure 2.3: Total air content (TAC) of Greenland ice cores.

3 *Acoustics and Studio Recordings*

This chapter focuses on audio, studio recordings and noise from a basic point of view.

Contents

Sound is the wave motion of gases, liquids and solids, and the effects of these motions. The wave motion is a consequence of small disturbances in the air which then propagate through the air from a source, for example when you clap your hands [Lautrup, 2004, Jacobsen et al., 2011].

3.1 *Acoustics basics*

A key characteristic of fluids - gasses and liquids - is a lack of constraint to deformation, which we see in solids, and the inability to transmit shearing forces as e.g. S-waves in an earthquake [Jacobsen et al., 2011, Lautrup, 2004]. Since fluids react to a change in volume with a change in pressure these waves are compressional oscillatory disturbances (longitudinal) that involve molecules moving back and forth in the direction of propagation, but with no net flow. This results in extremely small changes in pressure, density and temperature due to adiabatic processes, meaning there is no flow of heat as the vibrations are so rapid that an equilibrium is never reached [Jacobsen et al., 2011, Lautrup, 2004].

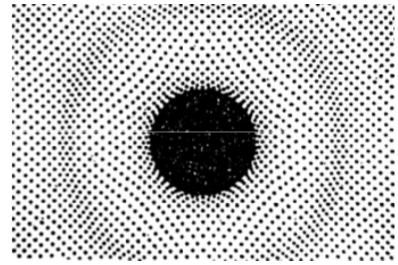

Figure 3.1: Particle motion of a propagating spherical longitudinal sound field from a pulsating source.

Sound waves, as all other waves, exhibit phenomena characteristic for waves. Waves interfere, and they are reflected on rigid surfaces and absorbed by soft ones; they are scattered by small obstacles and diffracted around corners, and refracted, meaning a change in direction at boundaries between mediums [Lautrup, 2004].

A mathematical description can be obtained. By combining equations and making some basic assumptions such as conservation of mass and that sound is close to being an adiabatic process. Then it is based on the local longitudinal force caused by a difference in the local pressure balanced by the inertia of the medium. Pertubations are of several orders of magnitude smaller than the equilibrium values and the linearised wave equation is therefore simplified:

$$\frac{\partial^2 p}{\partial x^2} + \frac{\partial^2 p}{\partial y^2} + \frac{\partial^2 p}{\partial z^2} = \frac{1}{c^2}\frac{\partial^2 p}{\partial t^2}, \tag{3.1}$$

with c for the speed of sound, p is the pressure.

Since the diversity of possible sound fields is enormous, Eq. 3.1 has to be supplied with boundary conditions describing sources that generate the sound field, surfaces that reflect or absorb sound, objects that scatter etc. The boundary conditions are often described by the particle velocity given by Euler's equation of motion relating the sound pressure to the particle velocity [Lautrup, 2004].

$$\rho\frac{\partial \mathbf{u}}{\partial t} + \nabla p = 0. \tag{3.2}$$

By assuming hydrostatic equilibrium, meaning constant density ρ_0, speed of sound for the medium c_0 and constant pressure p_0, a standard wave equation is defined as [Lautrup, 2004]:

$$\frac{\partial^2 \Delta\rho}{\partial t^2} = c_0 \nabla^2 \Delta\rho, \tag{3.3}$$

since the constant c in Eq. 3.1 has units of a velocity and is the speed of sound of harmonic waves [Lautrup, 2004]. It is given by

$$c = \sqrt{K_s/\rho}. \tag{3.4}$$

The quantity K_s is the adiabatic bulk modulus and ρ the density of the medium. The adiabatic bulk modulus can also be expressed in terms of the gas constant R (287 J Kg^{-1} K^{-1} for air), γ the ratio of specific heats, the absolute temperature T and the density of the medium [Lautrup, 2004].

$$c = \sqrt{\gamma RT}. \tag{3.5}$$

For water, with $K_s \approx 2.3$ GPa and $\rho \approx 10^3$ m^{-3}, the speed of sound comes to be about $c_{water} \approx 1500$ m s^{-1}. For air, at 20°C, it is around $c_{air} = 344$ m s^{-1}, see more in table 3.1 [Jacobsen et al., 2011, Lautrup, 2004].

Fluid	T [°C]	c [m s^{-1}]
Air	-25	315.77
Air	-20	318.94
Air	-15	322.07
Air	-10	325.18
Air	-5	328.25
Air	0	331.30
Air	10	337.31
Air	20	343.21
Fresh water	20	1481
Sea water	25	≈1550 [1]

Table 3.1: Empirical sound speeds in dry air at various temperatures and water. The temperature is also listed.

[1] Varies with salinity, depth and temperature

3.1.1 *Sound energy, power and intensity*

The energy emitted from a source of sound can be described by various definitions which describe the different properties or relations between these.

Sound pressure (level) The sound pressure is the local pressure deviation from ambient atmospheric pressure caused by a sound source [ISO 3744:2010, en]. It is defined as $p_{total} = p_{stat} + p_{dynamic}$ where p_{stat} is the ambient atmospheric pressure and $p_{dynamic}$ the pressure deviation. $p_{dynamic}$ are what is measured by microphones or hydrophones (see Sec. 3.3).

The sound pressure is most often expressed as the sound pressure level (SPL), which compares the sound pressure to a reference pressure p_0, often set to $p_0 = 20\mu$Pa (the limit of human hearing) and calculated as

$$L_p = 20 \log_{10} \frac{p}{p_0} \mathrm{dB}. \tag{3.6}$$

The sound pressure level describes the sound pressure relative to the lower limit of human hearing and is the one referenced when people talk about audio levels from e.g. airplane jet engines at 110-140 dB_{SPL} [ISO 3744:2010, en, Jacobsen et al., 2011].

Sound energy Sound is a mechanical wave which exists in mediums by oscillatory elastic compression and displacement of said medium [Jacobsen et al., 2011]. This medium stores the energy radiated by e.g. a speaker membrane and the sound energy is then the potential and kinetic energy stored in the medium.

$$E = E_{pot} + E_{kin} = \int_V \frac{p^2}{2\rho_0 c^2} \mathrm{d}V + \int_V \frac{\rho v^2}{2} \mathrm{d}V, \tag{3.7}$$

which expresses the sound energy in a volume of interest with the potential energy describing the local energy stored in the medium due to compression and the kinetic energy describing the energy represented by the mass of particles moving at velocity v [ISO 3744:2010, en, Jacobsen et al., 2011].

Sound intensity The sound intensity is given by the sound pressure and the particle velocity, though mostly used as the time-averaged sound intensity [Jacobsen et al., 2011]:

$$\bar{I} = \frac{1}{T} \int_0^T p(t)v(t)\mathrm{d}t. \tag{3.8}$$

Sound power The sound power relates to the rate per time at which airborne sound energy is radiated by a source [ISO 3744:2010, en]. It relates to the intensity as the intensity through a surface area, A

$$P = AI = Apv \tag{3.9}$$

The sound power is not dependent on the conditions of the surroundings or on distance as the sound pressure is.

3.1.2 Inverse distance law

Everyone has experienced this in their daily life - the intensity of the audio decreases by distance. This is due to the inverse distance law which is

$$I = \frac{P}{4\pi r^2} \tag{3.10}$$

where the intensity I is equal to the power P divided by the area of a sphere with the radius r being the front of the sound wave [Jacobsen et al., 2011]. This shows that the intensity is inversely proportional to the square of the distance from the source.

3.2 Signal analysis of acoustic measurements

A signal is defined as a physical quantity that varies with time, space or any other independent variable and can mathematically be described as a function of one or more variables eg. $s_1(t) = 8t$, $s_2(t) = 3t^2$ as examples varying with time t as an acoustic signal does as seen in Figure 3.2.3 [Proakis and Manolakis, 2007].

But an acoustic signal gives a much more complex expression and might not be described fully by a simple function. These signals can be better expressed with a high degree of accuracy by a sum of several sinusoids of different amplitudes, frequencies and phases as

$$\sum_{i=1}^{N} A_i(t) \sin[2\pi F_i(t)t + \theta_i(t)]. \tag{3.11}$$

A better interpretation of the signal will be to analyze small time segments and the information contained in the amplitudes A_i, frequencies F_i and phases θ_i for that small time segment [Proakis and Manolakis, 2007].

The signal measured is the pressure on the diaphragm as will be explained in the next section. Sound signal analysis explores different factors such as frequency, noise and sound pressure level. The root mean square (RMS) sound pressure (Eq. 3.12) is of great importance but gives a single value for the signal, which often is insufficient in analysis of the nature of the signal. Therefore the RMS is often analyzed in smaller bands of time [Proakis and Manolakis, 2007, Jacobsen et al., 2011].

$$p_{rms} = \sqrt{\overline{p^2(t)}} = \left(\lim_{T \to \infty} \frac{1}{T} \int_0^T p^2(t) \mathrm{d}t \right)^{1/2}. \tag{3.12}$$

Converting from sound pressure over time to frequency domain involves decomposing the signal into spectral components. This is easily achieved with digital analyzers as packages in most programming languages e.g. python or Matlab using discrete Fourier transforms 'DFT' or Fast Fourier Transforms 'FFT'.

Analyzing the signal in bands has an important property - the independent bands are uncorrelated signals. This means the sum of the individual mean square values of the bands sum to the mean square of the unfiltered signal

$$p_{rms}^2 = \sum_i p_{rms,i}^2, \tag{3.13}$$

where $p_{rms,i}$ is the rms value of the i'th element in the filter. Eq. 3.13 is known as Parseval's formula.

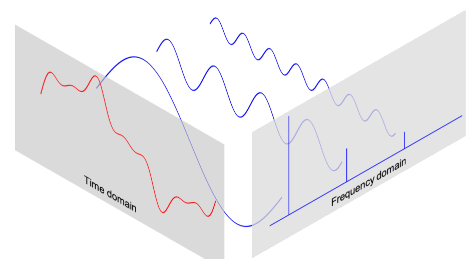

Figure 3.2: The principle of the DFT composing a complex signal into simple sine and cosine waves from [Kong et al., 2021]

3.2.1 *Discrete Fourier Transform*

The Fourier transform takes a signal and decomposes it into spatial or temporal frequencies by sine or cosine waves that are more easily studied than natural complex signals. The Fourier transform can be applied to both continuous and discrete signals, but as the audio signals studied in this thesis are discrete, only the Discrete Fourier Transform (DFT) will be discussed.

The raw time domain signal as the red in Figure 3.2 can be turned into a figure in the frequency domain as an amplitude spectrum for each of the decomposed (blue) frequencies.

By performing the DFT the information from an evenly spaced discrete signal is decomposed into information about the frequencies of all the waves that are needed to sum to the time domain signal

[Kong et al., 2021] and is defined as

$$X_k = \sum_{n=0}^{N-1} x_n e^{-i2\pi kn/N} = \sum_{n=0}^{N-1} x_n [\cos(2\pi kn/N) - i \sin(2\pi kn/N)], \tag{3.14}$$

where n is the current sample, N is the number of samples, k is the current frequency from $[0, N-1]$, x_n is the value at sample n and X_k is the magnitude at given frequency in the frequency domain with information on frequency k amplitude and phase.

The DFT contains information on both odd numbered N elements which result in negative frequencies and even numbered N elements which result in positive frequencies. If the input signal is real-valued the positive frequencies are the conjugates of the negative frequencies, resulting in a symmetric spectrum. Therefore in this thesis only the positive frequencies of the DFT are plotted as alle the signals are real-valued [Kong et al., 2021].

If the signal needs to be transformed back to the time-domain, e.g. after post-processing, this can be done using the inverse discrete Fourier transform [Kong et al., 2021, Proakis and Manolakis, 2007].

The DFT is quite slow considering it calculates all elements though they are symmetric. This is improved upon by using the fast Fourier transform (FFT) [Kong et al., 2021]. It successfully reduces the computational complexity by exploiting the symmetries in the DFT. It utilizes that some elements are going to be the same and therefore only needs to be calculated once.

3.2.2 *Random noise*

Sound signals are often disturbed by noise in various ways. These come from machinery, people and general noise in the environment around the setup.

The signal of white noise, named as an analogy to white light, has a flat frequency spectrum when plotted in a linear function of frequency as Hz. This means the power in any given band of a certain bandwidth of the signal is of equal size. For example any band of 20 Hz would contain the same amount of sound power whether its between 20-40 Hz or 960-980 Hz. Other types of noise can be described by their power response by frequency and have similar analogies to colors.

Equivalent to Eq. 3.13 the mean square sound pressures of different individual sources, intentional or noise sources, are additive due to being uncorrelated signals. This is of immense importance and use since, considering a case, where a signal is present and background noise cannot be turned off, it is possible to correct the measurement for the influence of background noise by simply subtracting the mean square value of the background from the total signal. For this to work the signal to noise ratio must not be too strong and it is necessary for it to be stationary in frequency.

3.2.3 *Nyquist sampling theorem*

By sampling at a high enough rate the discrete signal can be approximated to a continuous signal. With a small sampling frequency some of the information contained in the signal might be lost. This boundary is not defined specifically, but is characteristic to the system [Proakis and Manolakis, 2007]. In the other end the upper limit of frequencies to be studied is limited by the sampling rate. This is represented by the Nyquist sampling theorem [Proakis and Manolakis, 2007, Kong et al., 2021]. This says that only frequencies below the Nyquist frequency can be considered during analysis

$$F_s > 2F_{max}. \tag{3.15}$$

If the analysis goes beyond F_{max} the sampling of a continuous-time signal cannot be uniquely distinguished when such a signal is sampled at sampling frequency $F_s = 1/T$. This means that aliasing is experienced, in which two different frequencies might give the exact same values when sampled and it will therefore not be possible to uniquely distinguish each individual sinusoid.

For this analysis this is not of concern as the microphones are built-in with a sampling frequency of minimum 48000 Hz and the preamp sampling rate of 192000 Hz which is well beyond the human hearing from 20 to 20.000 Hz in the frequency spectrum. There might be signals worth investigating beyond human hearing and therefore these are also of interest and could be investigated later.

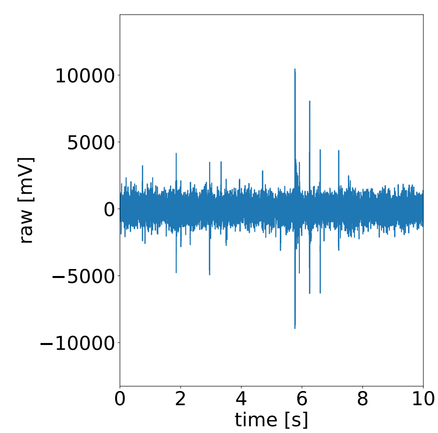

Figure 3.3: Raw signal converted from analog audio signal to a soundwave in electric/digital signal.

3.3 *The studio flow*

The central part of recording is the microphone, but the signal has to also be amplified and changed to a digital signal for processing. First microphone types, specifications and requirements are explained in depth. Next the supporting gear and its specifications are presented - what it does and why its needed.

Overall the studio flow takes a continuous complex analog signal and converts it to a discrete real-valued signal by sampling, sending it to a computer for processing and then back to an analog signal.

3.3.1 *Amplification and processing*

After the microphone the typical studio flow consists of several instruments and gear which will be presented now. The flow can also be seen in Figure 3.4.

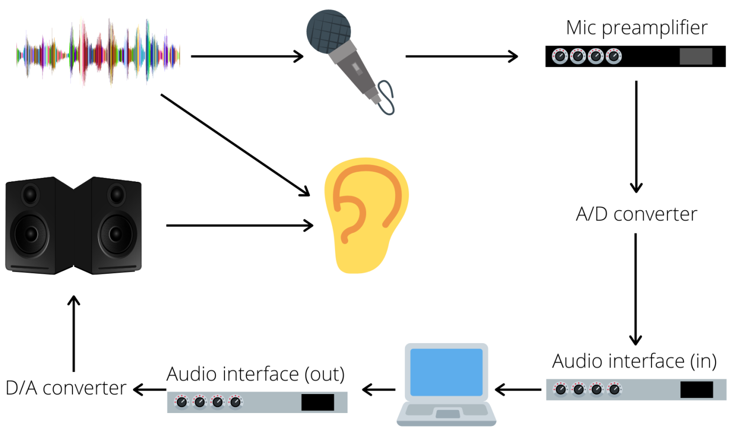

Figure 3.4: The studio flow as the source is recorded by the microphone and then amplified through the preamplifier. The signal is then converted to a digital signal through an A/D converter and send to the computer through the audio interface. If the signal is played again it is first send back to a D/A converter to an analog signal through the audio interface and played in the speakers.

The microphone signal is weak due to small changes in voltage since the diaphragms movement is small. The preamplifier is built to amplify this signal to a higher level at line level. Many preamplifiers are made to have more filters or effects built in as e.g. compression and EQ effects though some of this can also be done more controlled in post-processing.

The signal is then converted from an analog signal to a digital signal (A/D) and through the audio interface it is sent to the computer. Often the signal is recorded through a digital audio workstation (DAW) such as Audacity or Cubase. In the DAW it can be processed through a variety of filters or be even more amplified.

At this stage the audio is saved and processed through methods described later in the thesis.

If the audio signal should be played through a speaker it can be sent back through the audio interface and be converted back to an analog signal (D/A) which can then be heard through speakers or headphones.

USB microphones include most of this setup as plug 'n' play. The preamp is included in the microphone as well as the A/D converter. This causes lower audio quality due to their smaller size and less flexibility. Therefore more professional setups always have a separate preamplifier.

3.3.2 Microphones basics

Microphones and recording are complicated with many specifications and combinations to keep in mind. First the basics of microphones and recording are explained.

A microphone is by the definition from Merriam-Webster: "An instrument whereby sound waves are caused to generate or modulate an electric current usually for the purpose of transmitting or recording sound (such as speech or music)"[2].

[2] https://www.merriam-webster.com/dictionary/microphone

Microphone main types The two basic types of microphones are dynamic and condenser microphones as can be seen in Figure 3.5. Other variations of microphones use these techniques and are specified for different surroundings' sound pressure levels and other specs depending on the specific recording situation.

Dynamic mics: These usually handle louder environments since they are more sturdy and less sensitive. The sound here is aimed down the front of the microphone and are like most microphones you see on a concert stage [H., 2021b].

The technical recording is done using a diaphragm which vibrates due to sound pressures and move a magnet through a wire coil's magnetic field. This induces the electrical flow as described by Faraday's Law of Induction. The system is called a transducer and is used in many varieties of microphones [H., 2021a,b].

Condenser mics: These are often seen in recording studios as they are more sensitive to smaller changes in the sound pressure. Here the sound is aimed to the side of the microphone. Since they are more sensitive and pick up small nuances they are more often used in studios where the acoustic environment has been treated and can be controlled [H., 2021b].

The diaphragm itself is less sturdy and might break if the recording is too loud or if it is dropped. It works by vibrating closer or further away from a charged metal plate. Because this plate is charged we need phantom power or another power source, which is described later [H., 2021a,b].

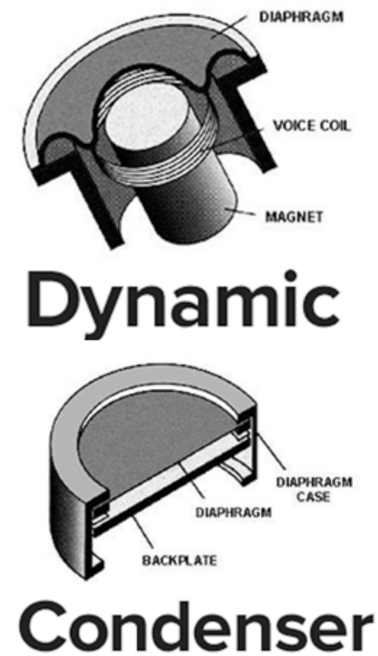

Figure 3.5: Dynamic and condenser microphone. Dynamic microphones work by using the sound pressure on a diaphragm to move a magnet inside a wire-coil. Condenser microphones work by sound pressure moving a diaphragm in relation to a charged backplate.From [Ledgernote.com] link here.

Pickup patterns Usually microphones are very easy to use since you just point the microphone at the sound source and it records. The pickup pattern describes the sound level taken in depending on the direction of the source. Polar pattern, directivity, polarity and pickup patterns all mean the same. This could e.g. be for noise reduction, as when you do not want the cheer from the crowd going into the microphone but only the singers voice [H., 2021c]. This is because microphones can be built in a way that they take in more of the signal coming from some direction and diminishes the signal from other directions.

The most common pattern is the cardioid. This pattern picks up a wide field of sound pressures coming from the front of the microphone while diminishing most noise coming from behind [H., 2021c].

Some of the other pickup patterns are described in the following paragraphs but can also be seen in Figure 3.6.

Unidirectional means that the recorded sound comes from the front. This is the case for cardioid and supercardioid and in some sense the hypercardioid. As the microphone gets more directional more of the off-angle sounds are captured as well. Unidirectional microphones, especially in acoustic controlled environments, do a good job of disregarding the noise from the back while still capturing movements of the source to the front [H., 2021c].
Bidirectional records the sound from two angles opposite each other, usually front and back. This is seen in Figure 3.6.d-e as the figure of eight recording pattern and in the hypercardioid [H., 2021c].
Omnidirectional (Figure 3.6.a) records evenly in 360 degrees to get the full soundscape [H., 2021c].
Finally lobar or shotgun is highly directional and captures directly in front of and a bit to the back and sides as can be seen in Figure 3.6.e [H., 2021c].

All of these can be examined further in Figure 3.6 which shows the polar patterns as 0 dB at zero degrees with the highest sensitivity directly in front of the mic. As the pattern moves closer to the center the sensitivity decreases. The top is in front of the microphone and bottom is backside and this should be seen as a 360 degrees view around the pickup pattern [H., 2021c].

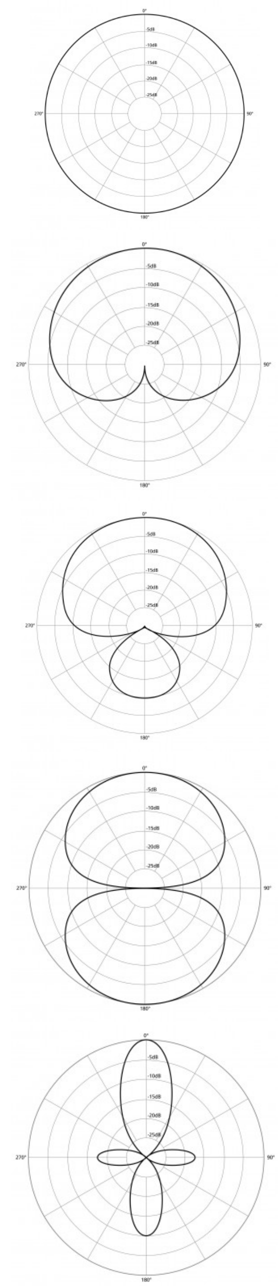

Figure 3.6: Pickup patterns of microphones. From the top: omnidirectional, cardioid, supercardioid, bidirectional and lobar/shotgun. The sensitivity is highest in front of the microphone at zero degrees with zero dB. Every circle towards the center is a decrease in sensitivity by 5 dB.

Special microphone types Contact microphones are microphones that measure the vibrations through a material rather than the pressure from the molecules moving through air.

Hydrophones are made specifically for measuring in water and measures the vibrations radiating through water from a sound source. This is e.g. utilized in [Lee et al., 2013].

Proximity effect Usually for a recording the microphone would be placed closely to the sound source to get a high sound pressure compared to the noise. But as the source gets close to the microphone there will be a boost in the bass with an increase in volume and decrease in frequency. This is called the proximity effect [H., 2021a].

To start with this will not be considered, but is an effect which might be experienced. Different pickup patterns and different microphones have more or less pronounced proximity effects. It is also most prominent in dynamic mics as the source needs to be very close to condenser mics to get the effect due to the high sensitivity [H., 2021a].

Gain staging and volume When microphones record, they measure an extremely low electrical amplitude (directly related to volume) also known as mic level. Therefore the mic level has to be boosted to line level. This could be done by just boosting the volume, but then the noise floor is also risen and the signal-to-noise ratio (SNR) decreases. To avoid this problem a preamplifier is used. These turn up the signal without turning up the noise level and is the only way to get a high-quality recording [H., 2021a].

The preamplifier is at least as important as the mic itself. The very basic understandingof gain is that the volume of the mic is adjusted by outputting the signal to the preamp and then adjusting the gain knob [H., 2021a].

Gain might seem closely related to volume as they both increase the loudness of the signal when turned up and they do both modulate the amplitude. So what is the difference between gain and volume? Volume is the measure of sound coming out of a system like speakers, headphones etc. You turn up the volume and the speakers get louder. By changing the volume neither the tone nor quality of the signal is changed (if the speakers do not distort at high volumes). Volume is the output and therefore does not change the audio signal.

Gain is the ratio between the volume at input and output of an electrical current but is often understood as the volume at input. There is a peak amplitude of the voltage through the electrical system before distortion is experienced, which is the voltage controlled by gain [H., 2021a].

As the signal goes through an Analog-to-Digital (A/D) converter there is an optimum loudness that gives the A/D converter as much information as possible to convert the signal with the highest quality to a digital signal. This way it fills the bits of data with as much information as possible. If the signal gets too loud there will be distortion in the form of audio clipping, which is frequencies being cut out, since there is a maximum voltage [H., 2021a].

Gain makes sure the highest quality audio is achieved instead of a mediocre signal with lost information. It is also important to adjust the gain for every step in the studio flow to get the best resolution [H., 2021a].

Phantom power Looking back at the two types of microphones and how they technically work the dynamic mic will not need an external power source as you are moving a magnet through a coil inducing its own electrical current [H., 2021a].

The condenser mics use the charged metal plate and therefore need an external power source such as a battery, built-in power supply or as most use the phantom power from a preamp [H., 2021b].

Phantom power is +48 volts supplied by the preamp up through the XLR cable used to connect the preamp and mic.

Frequency response This is a chart showing the response from the mic across the range of frequencies measured. An example can be seen for the Shure VP82 microphone in Figure 3.7. Most microphones have a mostly flat or transparent signal response meaning the electrical current is not amplified or diminished at some frequencies [H., 2021a].

Some microphones have built-in options to change the frequency response with e.g. high/low pass filters, bass roll off or high frequency amplification. This change, especially if it is designed from the manufacturer, is called coloration and "colors" the frequency response from a transparent signal. Some mics also give the option to reduce the output amplitude by 10 or 20 dB if recording in noisy environments [H., 2021a].

The bass roll off and the high pass/low cut filters gradually reduce the volume of the bass that makes it into the signal with the low/bass frequencies. This is done in order to remove ambient noise such as vibrations in the floor or air condition (or freezer) humming. This can also be done in the post-processing part [H., 2021a].

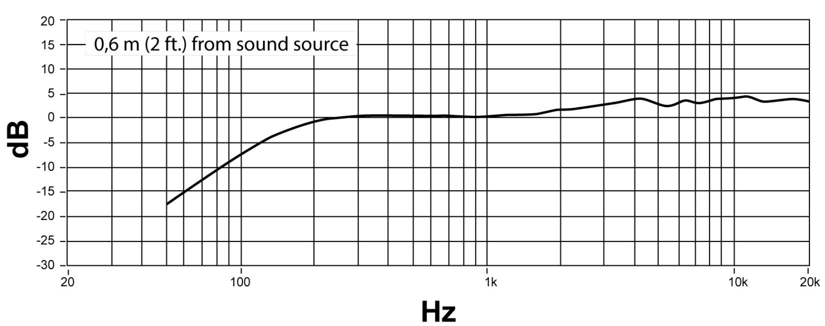

Figure 3.7: The frequency-amplitude response of the Shure VP82 microphone which is mostly flat along the frequencies but does drop out at the low frequencies.

Microphone cables Some microphones are USB microphones and cram the whole studio flow into just the mic, and sometimes reducing the audio quality significantly due to mediocre instruments.

For non-USB microphones the most common cable is the XLR cable which carries mic-level signals and does not accumulate electrical noise over longer distances [H., 2021a].

3.4 *Sound absorption and insulation*

Every room has a characteristic soundscape due to reflections off the walls, noise production and furniture placed in various ways. Recording studios are deadened into virtually sound isolated rooms. This is done to both diminish noise from external sources and reflections of internal sources. As sound hits the walls it reflects off the surfaces and creates spectral reflections which are near-perfect replicas of the original signal. Since the sound produced by a source moves in several directions some parts of the signal will reach the microphone at a later stage and possibly out of phase causing interference diminishing some frequencies while amplifying others which is known as comb filtering [Mathias, 2019].

The spectral reflection depends highly on the density of the surface it hits. Is the surface hard, then most of the signal is reflected directly whereas a soft, heavy material absorbs a high fraction of the energy from the soundwave [Mathias, 2019, Jacobsen et al., 2011].

If the room is very square with sparse furniture that can break off and reflect the sound, a room mode is introduced, both from wall to wall, but also ceiling to floor. This room mode is the resonant frequency of the room and is amplified compared to the rest of the frequencies [Mathias, 2019].

The acoustics in a room can be improved in several ways and some has already been mentioned, e.g. materials that absorb the energy from the signal. The materials used for absorption are porous and light and the thicker they are the more energy they absorb. The absorption properties are caused by viscous friction between the moving air molecules in the air and the internal surface area of the sound absorption material, where kinetic energy turns to heat. This only results in mid to high frequencies being diminished [Jacobsen et al., 2011]. For low frequencies to be absorbed the material needs a higher density and width. For the kinetic energy to have an effect the width of the material need to be at least $\lambda/4$ thick, where λ is the wavelength [Jacobsen et al., 2011]. These materials are especially important for use in corners as 90° corners reflect the sound directly back towards the source and causes a delay and comb filtering. This can both be dealt with using absorption panels but also drapes, blankets or rounded off corners [Mathias, 2019, Jacobsen et al., 2011].

Another way to improve acoustics is diffusion of the sound signals. This does not absorb the energy and diminish the signal, but rather spreads out the energy to the entire room. A good example is a bookshelf with various depths, books and decorative pieces diffusing the signal. Round surface are the best as they spread out the signal more evenly [Mathias, 2019].

Membrane absorbers work by having a cavity between the wall and a surface which causes the air to resonate between the wall and the plate and use its energy at certain critical frequencies which will be diminished [Jacobsen et al., 2011].

Just using these materials does not guarantee that the room is deadened but will cause a significant decrease of the energy of some frequencies depending on the setup.

3.5 *Minneart frequency*

This section connects the previously presented sound and air bubble perspectives by describing how the bubble radius can be estimated through sound frequency analysis.

Air bubbles are of interest in many fields from everyday phenomena to research subjects of e.g. ocean bubbles and industrial applications, often as occurring bubbles not wanted and issues that has to be dealt with.

In 1933 M. Minnaert [Minnaert, 1933] set out to investigate the sound of running water. He did this through a simple experiment by releasing air bubbles individually through a tube and investigating this phenomenon. This is the basis of using sound to investigate bubble features.

3.5.1 Pulsating bubbles

Just as a spring an air bubble in a liquid is an oscillator. Posterior to the bubble's release from a tube or being released from pressure in ice, the bubble pulsates after the first initial displacement. The bubble wall pulsates and sets the surrounding water in motion through vibration [Minnaert, 1933]. The oscillation approximates to a simple harmonic motion at low amplitudes which coincides with the natural frequencies of the bubble system. These natural frequencies were first calculated by [Minnaert, 1933]. So let us go through the process [Minnaert, 1933, Leighton, 1994]:

The pulsation after the initial displacement results in a variation in the bubble radius with an oscillating displacement about the mean radius R_0 which can be described as $R_\epsilon = -R_{\epsilon 0}e^{i\omega_0 t}$. The bubble radius is therefore described as a function of time as

$$R = R_0 + R_\epsilon(t) = R_0 - R_{\epsilon 0} \mathrm{e}^{i\omega_0 t} \tag{3.16}$$

with ω_0 as the resonance frequency. The pulsation has negative sign due to increase in radius resulting in a decrease of internal pressure which will come in to play later.

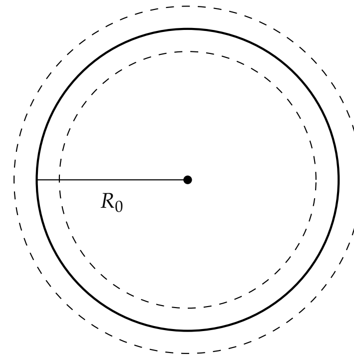

Figure 3.8: Bubble pulsating about R_0 with V_{min} when the bubble is smallest and V_{max} when the bubble is largest.

To describe the full picture of the freely oscillating bubble the external liquid movement which comes from kinetic energy is set equivalent to the internal potential energy due to change in pressure from oscillation around R_0, since the energy is constant but varying between the two as the bubble oscillates.

Kinetic energy of liquids is found by integrating over spheres of liquid from the bubble wall to infinity. Considering liquid shells at radius r with a thickness dr and mass $4\pi r^2 \rho \mathrm{d}r$ the kinetic energy is then

$$E_K = \int_R^\infty (4\pi r^2 \rho \mathrm{d}r)\dot{r}^2 \tag{3.17}$$

In time dt any mass flowing through a spherical surface around the bubble is $4\pi r^2 \dot{r} \rho \mathrm{d}t$ from the surface area of a sphere. Since most fluids are incompressible this is a fair assumption, especially considering this project works with water and ice. By conservation of mass this general flow can be equated to the flow at the bubble surface to give $\dot{r}/\dot{R} = R^2/r^2$. By substituting this into eq. 3.17 gives

$$E_k = 2\pi R^3 \rho \dot{R}^2 \tag{3.18}$$

Which gives maximum values when the bubble radius is at equilibrium position $R = R_0$ and describes the inertia of the liquid component of the gas-liquid oscillating system.

Now that the liquid kinetic energy component is found the gas potential energy is considered. As the bubble is compressed and stretched from the equilibrium radius to $R = R_0 \pm R_{\epsilon 0}$, the work done at minimum volume, V_{min}, with eqiulibrium radius presssure p_0 and minimum radius internal pressure p_g is

$$E_{\mathrm{p,max}} = -\int_{V_0}^{V_{min}} (p_g - p_0)\mathrm{d}V = -\int_{R_0}^{R_0 - R_{\epsilon 0}} (p_g - p_0) 4\pi r^2 \mathrm{d}r \tag{3.19}$$

When the bubble has decreased in radius by $R_\epsilon = R - R_0$, the volumetric change follows $\left(\frac{R - R_\epsilon}{R}\right)^3$. Assuming the gas behaves polytropically and adiabatic so that $c_p/c_v = K$, and $p_g V^\kappa =$ constant, where κ is the polytropic exponent for the thermodynamic bubble expansion. The changed pressure is then given by

$$\frac{p_g}{p_0} = \frac{v_0^\kappa}{v^\kappa} = \left(\frac{R}{R - R_\epsilon}\right)^{3\kappa} \tag{3.20}$$

The pressure inside the bubble over the pressure outside may, by binomial expansion due to small fraction, be written as

$$p_g - p_0 = \frac{3\kappa R_\epsilon p_0}{R_0} \tag{3.21}$$

This is substituted into eq. 3.19 which gives the potential energy at minimum volume and maximum internal pressure

$$E_{\mathrm{p,max}} = -\int_0^{R_{\epsilon 0}} \frac{3\kappa R_\epsilon p_0}{R_0} 4\pi R_0^2 \mathrm{d}R_\epsilon = 6\pi\kappa p_0 R_0 R_{\epsilon 0}^2 \tag{3.22}$$

Now that the maximum of the external liquid kinetic energy (eq. 3.17) and the internal potential energy (eq. 3.19) has been found they can be equated and results in the Minnaert frequency, the one specific for a certain bubble size.

$$\omega_M = \frac{1}{2\pi R_0}\sqrt{\frac{3\kappa p_0}{\rho}} \tag{3.23}$$

Which defines and relates the Minnaert resonance frequency to the bubble radius R_0, the appropriate polytropic exponent for the thermodynamic process of bubble expansion κ, the ambient pressure of the fluid p and the density of the ambient fluid ρ [Pettit et al., 2015, Minnaert, 1933].

In [Lee et al., 2013, Pettit et al., 2015], which melts glacial ice in water, the values used are $\rho = 998$ kg m^{-3} as the density of water, $p_0 = 101$ kPa is the ambient pressure and the ratio of specific heats/polytropic constant of $\kappa = 1.33$ to 1.4.

In table 3.2 the variation in frequency by change in the bubble radius can be seen using the values described above.

Frequency ω_0 [Hz]	Bubble radius R_0 [μm]
100	32829
500	6565
1000	3282
3000	1094
5000	656
8000	410
10000	328
15000	218
20000	164
30000	109

Table 3.2: Minneart frequency change with bubble radius with $\rho = 998$ kgm^{-3}, $p_0 = 101$ kPa and $\kappa = 1.4$

Minneart concludes early in his experiment that the sound radiated by the bubble happens at the moment the bubble closes at the end of the tube and not as the bubble bursts at the water-air surface as many would think. The same conclusion will be reached later in this thesis.

Part II

EXPERIMENTAL WORK

4 Preliminary Recordings in Bern

The preliminary recordings and results of the data taken during a visit to the EastGRIP Chemistry CFA campaign is the focus in this chapter.

Contents

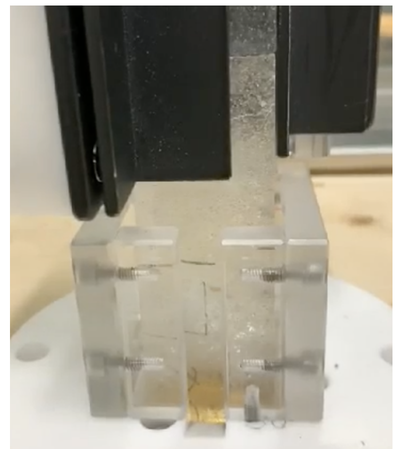

Video 4.1: Ice core melting during the CFA chemistry campaign of EastGRIP. [link]

During February and March 2020 up until lockdown due to COVID-19, the chemistry CFA campaign of a section of the East-GRIP ice core was done. This offered an opportunity for this project to execute some initial test measurements, to get a first glimpse of problems and possible solutions.

Microphone The microphone used for the Bern recordings is the RØDE Videomic NTG. With the very little level of research that was possible to carry out previously to the purchase of the microphone and measurements of the sound, this was the number one choice. The mic was chosen due to its shotgun microphone supercardioid polarity meaning it captures mostly sound from the front and ignores some of the sound fromsources from the rear. The microphone is a USB microphone and has a built-in preamp which means it plugs directly into the computer and cannot connect to an external preamp which would usually be better at amplifying the signal with finer resolution. The built-in preamp had direct digital switching with controls of high-pass filter, padding and high frequency boost, which had also been tested previously in Denmark to learn the basics. This setup did fit perfectly for a small visit to Switzerland to do some initial measurements.

Company	Røde
Model	Videomic NTG
Type	Supercardioid
Sensitivity	-26 dB re 1V/Pa
Polar pattern	Cardioid
Freq. range	20Hz - 20kHz

Table 4.1: Microphone specifications. [1]

[1] http://www.rode.com /microphones/videomicntg

4.1 Measurements

The whole EastGRIP ice core CFA Chemistry section will be melted in Bern, Switzerland. Their CFA system is of the highest standard and very well functioning and was therefore chosen for measurements of the EastGRIP ice core. The overall principle is the same as the Danish which will be explained in more detail later in section 6.3.2.

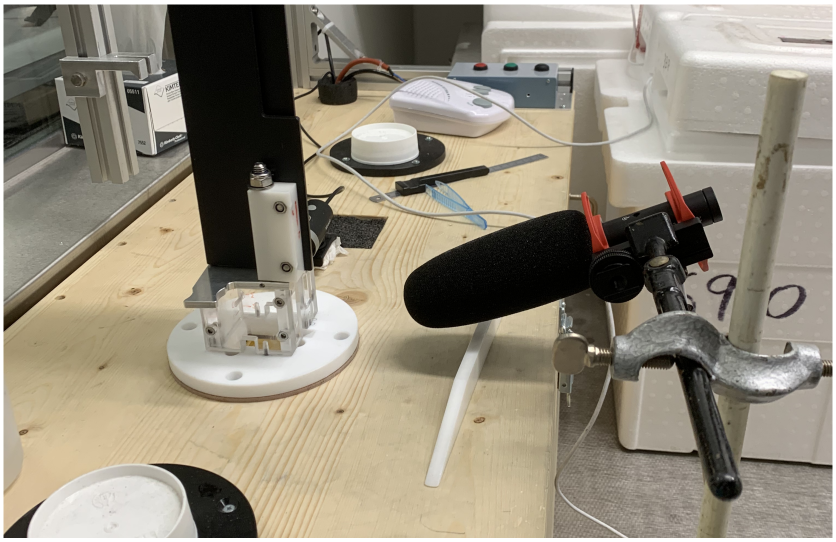

Figure 4.1: The setup of the microphone during teh Bern measurements. The mic is directed towards the ice core and is held tight on a mount.

4.1.1 Setup

The setup for sound measurements in Bern can be seen in figure 4.1. The melthead is encapsulated by a lot of plastic with a gap to the front and to the back and the sound was thus recorded from the back from the observer in which direction the sound also propagated. In video 4.1 it is clearly seen how the ice melts and the sound from the popping of the air bubbles in the ice cores is clear and very distinctive.

The microphone is held tight on a mount with clamps and directed straight towards the melt head. The microphone was moved as close as possible and even closer than that seen in figure 4.1 to capture as strong a signal as possible disregarding noise. Since this is a USB-microphone with a built-in preamp it is connected directly into the computer which also had to be in the freezer. The laptop cooled down quickly to a point where it was completely frozen during the 20 min melting and recording sessions resulting in shut downs and thus recordings being stopped midway. It was thus put in an ice

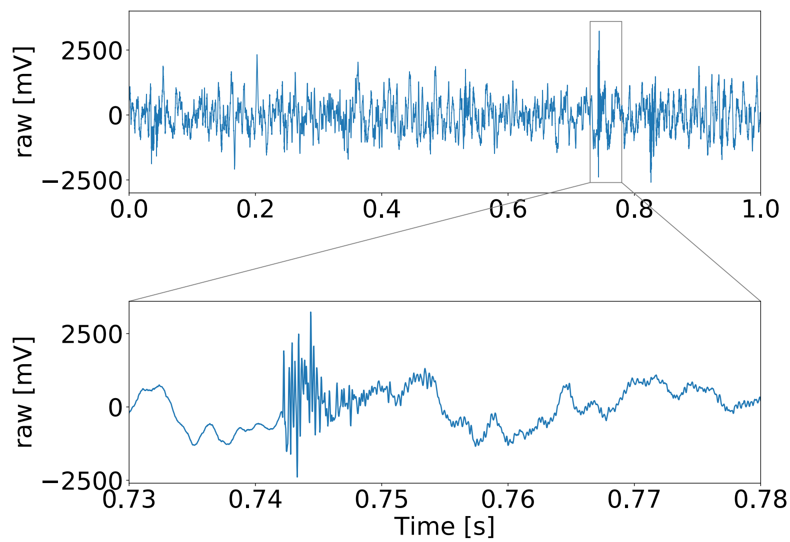

Figure 4.2: The raw signal in mV from the microphone as a function of time and a zoom in on a single bubble signal.

core box in hopes of generating a bit of heat for itself but it turned out to be unsuccessful. For every second melt the laptop had to heat up again. This provided a lot of information for optimization of the general setup in Copenhagen to be done.

4.1.2 Data

Figure 4.2 displays the raw signal in the time domain with peak indicating bubble signals. The measurements were made at a sampling rate of 44100 Hz and bit depth of 24 bit. The background noise is very stable as can be seen in figure 4.3.c and no peaks are seen along the time axis. Therefore the peaks seen in the signal must be due to bubble popping or cracks, but must be a signal that is introduced besides the background noise. An example of a raw bubble signal can be seen in 4.2 inset and somewhat resembles a theoretical bubble signal with noise. The raw signal can be heard in audio 4.1 and the background noise in audio 4.2

In figure 4.3 it is clearly seen that the level of noise in the Bern freezer is very prominent and disturbs all measurements done while the freezer is on. Only the most prominent signals are visible with the freezer on. The freezer noise is in the low frequency range as can be seen in figure 4.3.c and decreases in power as the frequency increases.

Audio 4.1: Bern audio sample

Audio 4.2: Bern background noise

Audio 4.3: Bern filtered audio

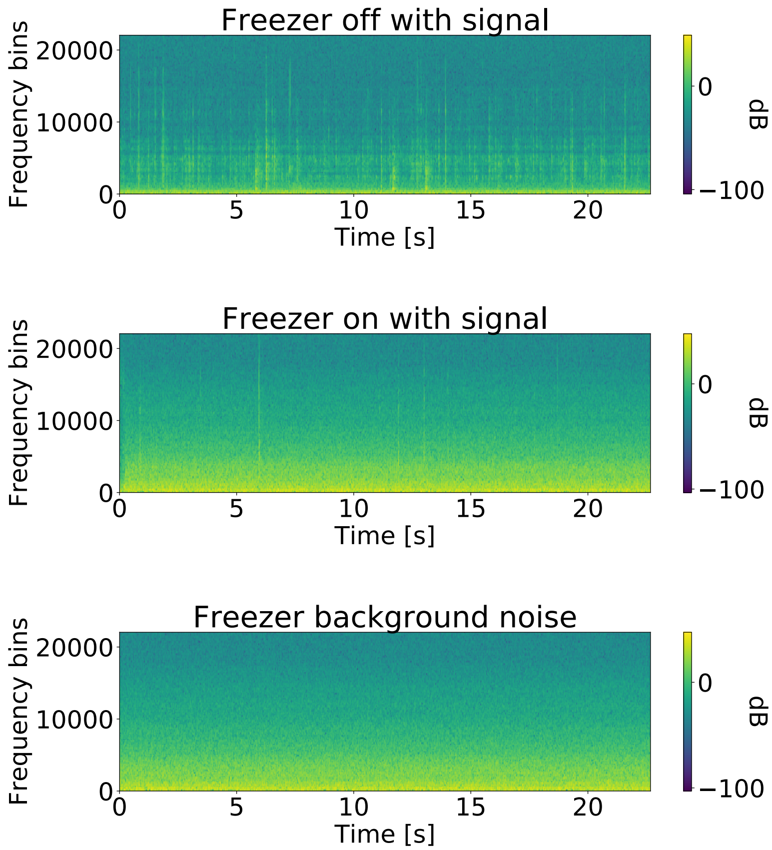

Figure 4.3: Spectrograms of the recorded signal from Bern of the signal with the freezer off and on and the background signal. The spectrograms show the frequency response by time in separate bins. This way a change in spectral density can be detected.

4.2 *Results*

After using a sinc function as high pass filter with cutoff frequency of 2 kHz the frequency bands with the most prominent energy is present in the energy levels portrayed by the signals in the 4-8 kHz bands. To compare the filtered signal with the original signals they can be heard as Audio 4.1 and 4.3. It can clearly be seen that most of the noise around the signal has been minimized and now it displays several smaller features previously hidden in the noise due to small amplitude but higher frequencies than that filtered away. From the spectrograms it can be seen that the peaks are clear in the higher frequency analyzed through time as in the spectrogram. This gives rise to further studies and a more thorough analysis based on the Minnaert frequency described in section 3.5. More work was later done to minimize noise and get a clearer signal.

The CFA campaign freezers in Bern and Copenhagen are different in the way that the Copenhagen freezer is a small vertical freezer and

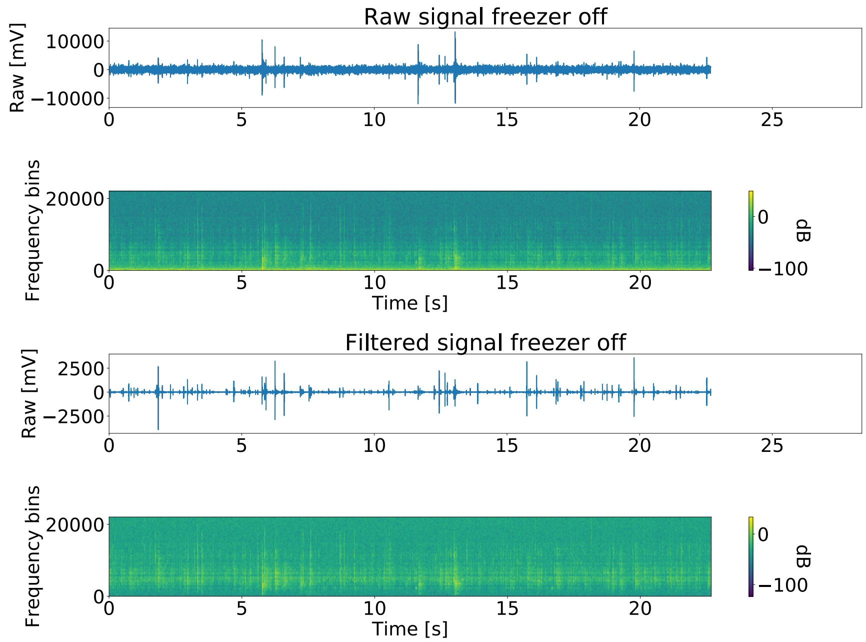

Figure 4.4: Comparison of the raw and filtered time signals and the spectrograms. Most of the low frequency noise has been filtered out and more high frequency signals are seen in the filtered signal time domain.

the Bern freezer is a ~15m^2 freezer room. Therefore the noise reduction methods will most likely divert in format and efficiency. The freezer fan in Bern is much larger and makes more noise whereas the Copenhagen freezer is smaller and quieter, but it is not possible to shut it off for a longer time span. Even though there are differences the Bern recordings showed that individual bubble signal are clear in the spectrograms and the initial points of focus for noise reduction.

Using the gained knowledge from the measurements in Bern led to several improvements of both the Danish CFA system and the idea to produce artificial test ice - both ice with bubbles of varying size and ice that is bubble-free. This ice would be ideal to test the setup and record with microphones to analyze noise signals and suggest more improvements.

5 Creating Bubbly and Bubble-Free Ice

This chapter focuses on test ice for the measurements by trying to create controlled ice with bubbles as well as bubble-free ice cores with the potential of ice transitions between bubble-free and bubbly ice.

Contents

Drilling an ice core on the Greenland ice sheet or on any other glacier is an expensive endeavour. Therefore to be able to test our instrument on something cheaper an experiment was set up to create an artificial ice core with variable amounts and sizes of air bubbles. Besides this the setup for bubble-free ice was optimized and adjusted for a bubble-free/bubble transition. These ice cores could then be used to test for audio signals from air bubbles popping using various microphones before testing the instrument on actual Greenland ice. The bubble-free ice can be used to get a sense of background signals to be removed in post-processing.

5.1 *Ice core with bubbles*

In order to conduct our first measurements a setup consisting of three parts was designed to create the resemblance of a true ice core

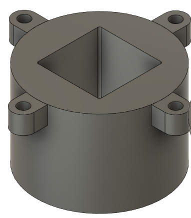

(a) Setup 5.0 bottom part.

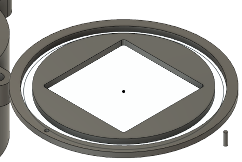

(b) Setup 5.0 connector piece.

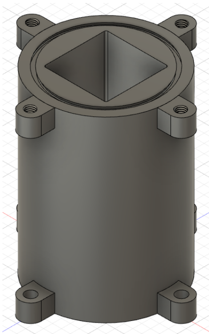

(c) Setup 5.0 middle part.

Figure 5.1: The bottom piece has a whole in the bottom for the air to get through and a connector piece is used to hold the o-ring in place and prevent leaks. The bottom and middle parts are connected by bolts and is used for further extension.

with varying degrees of bubble amount and sizes. These parts can be seen in Figure B.1 and will be explained more in depth in the following section. More figures of the evolution of parts can be seen in Appendix B

The bottom part is the part of the setup where the air bubbles are distributed using an air stone commonly used in aquariums. This air stone distributes the incoming air into loads of smaller bubbles rather than a limited number of larger bubbles and is originally used to diffuse air into a tank and provide oxygen for fish to breathe. They are made of a non-toxic mineral material, are sturdy and durable and have a high dissolved oxygen rate. Air stones come in various shapes and sizes and several have been used for testing this experiment both a MARINA 50 mm spherical air stone and Aqua Nova 25 mm long cylindrical air stone.

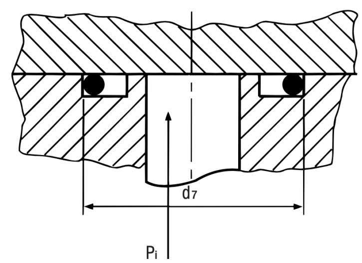

(a) Slice across the setup with the O-ring groove shown on each side. The O-ring is placed towards the outer side of the groove, since the pressure (albeit small) is coming from the water column.

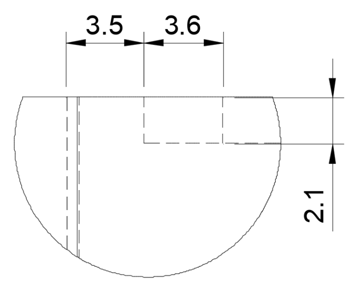

(b) Cross section across a groove with width 3.6 mm and depth of 2.1 mm. This follows the design guides for o-ring grooves. The groove has a distance from the edge to the outer groove diameter of 3.5 mm

(c) Yada yada yada

5.1.1 O-rings

Between each of the connected parts in figure B.1 is an o-ring of size 2.62 mm x 58.42 mm to prevent leaks of the water inside the setup. Various types of o-ring grooves have been considered but for the final setup a standard rectangular cut was used[1]. Besides the o-ring, four threads for a M6x1 bolt is used for tightening the parts together making sure the o-ring prevents leaks. To make sure the o-ring fits as good as possible the final setup uses a round outer shape rather than a square as earlier iteration of models that have been improved upon. This previous shape left too much space in the o-ring groove and caused leaks.

The square for the frozen ice core resembles the size of gas and chemistry pieces ice core cut sections which will be explained more in depth later but this is created one mm larger (35x35 mm) to each side to account for melt as the ice core has to be slid out of the setup after freezing. This size was chosen to be used for a setup that re-

[1] https://www.sealanddesign.com/technical/o-ring-groove-design/

sembles most other measurements of an ice core - a size that the sound recording experiment also accommodates thus making it a useful component in gas or chemistry melt campaigns without further changes. 35x35 mm was also deemed sufficient in creating and measuring enough bubbles since the bubbles can spread out but are not just centered in the middle

5.1.2 *3D printing*

The parts presented previously and throughout the thesis are printed on a PRUSA I3 MK3S 3D printer.

The three parts were meant to be printed as a size that resembles the length of an ice core bag of 55 cm. Due to limits on the printer each part is limited to 21 cm in height and 4 pieces were estimated to be a much more fragile setup. Therefore the final setup consists of the two top pieces each being 21 cm and the bottom part being only for the air stone and other relevant sensors. It is still a very fragile setup as there are many potentials for leaks. The three parts are tightened together, filled with water and placed in the freezer. As the water freezes the air bubbles produced by the air stone should be trapped comparably to that of an actual ice core.

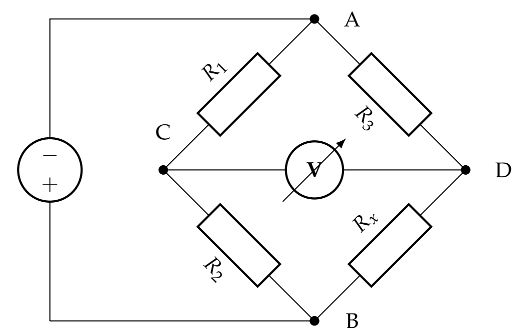

Figure 5.2: Wheatstone Bridges measure tiny variations in voltage since voltage going across R_1 C R_2 is kept constant whereas voltage across R_3 D R_x shows a voltage change when the two are compared.

5.1.3 *Air flow sensor*

The air provided comes from compressed technical dry air supplied in the lab facilities and is regulated with a pressure regulator. Along the flow line from the gas tank to the freezer an air flow sensor is used to observe the air flow over time. This air flow sensor is built using an arduino and a mass airflow sensor.

The analog Honeywell AWM3100 Microbridge mass airflow sensor [2] is used as the sensor and is based on the principles of wheatstone bridges to measure tiny variations in the resistance used for sensing purposes. A wheatstone bridge (see fig 5.2) works by measuring the voltage drop across two voltage dividers from A to B - one going across R_1 C R_2 and one going across R_3 D R_x. Because the resistors R_1 and R_2 are kept constant any changes across R_3 and R_x shows a voltage change. It is this change in voltage from one side to the other that is the principle of the wheatstone bridge. The variations change the voltage between point C and D giving a nonzero value. This means that the bridge is unbalanced. When the voltage on C and D is the same the bridge is balanced. As the resistance changes on R_x it becomes unbalanced and the measurement can be translated from voltage change to temperature, flow or whatever the sensor measures.

[2] Honeywell AWM3100 manual, Honeywell Sensing and control, https://sensing.honeywell.com/honeywell-sensing-airflow-awm3000-series-catalog-pages.pdf, Accessed: 2020-09-08

An arduino is used to convert the analog voltage output from the sensor to standard cubic centimeters per minute (SCCM) a third degree polynomial fit was applied to the conversion output flow vs. interchangeability performance characteristics from the installation instruction at 10 VDC as applied in the setup. This fit can be seen in Figure 5.3. The range of the Honeywell AWM3100 sensor is 0-200 sccm. The performance characteristics can be found in the manual referenced previously. The 10 VDC was controlled using a UA7810 voltage regulator giving a steady supply at 10 VDC.

The arduino circuit is connected to a screen to display the sccm value coming through the sensor. The circuit saves the values of sccm over time with values being measured every second. Other sensors could potentially also be added to the circuit as for example a temperature logger by the air stone but was not installed before it would work.

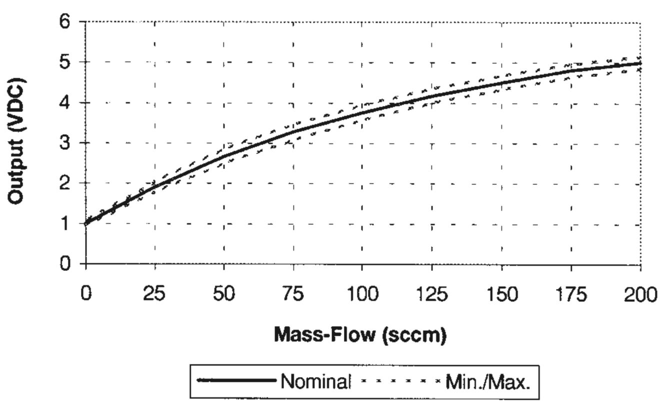

Figure 5.3: Voltage change vs. Flow change in standard cubic centimeters per minute with uncertainties. The change in the voltage across the wheatstone bridge describes the mass-flow.

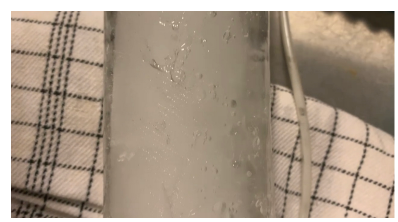

Video 5.1: Video spanning artificial ice core produced. [link]

5.1.4 *Results*

After several tests this method did not seem to work. Some bubbles did form but they were big and only placed in random sections around the ice core. The bubbles were also quite big and did not resemble the bubbles in an ice core even remotely. We also had no success with adjusting neither the size nor the amount of air in artificial ice cores. This was most likely due to bubbles not freezing instantly and thus not freezing in place. Several iterations of the setup and changes of the parts described previously was tried but even improvements in the setup showed none to little improvement in creating ice with small bubbles. If in the future somebody has a way of creating ice that resembles that of an ice core this would be of great value for test ice.

Due to the faulty results this part of the project were stopped and work began on more promising work.

5.2 *Bubble-free ice and bubble transitions*

Since the production of a bubbly ice core was unsuccessful the focus changed to working on a bubble-free ice core. The gas lab had a previous setup that creates 25 cm long samples of ice core, though often with bubbles (R > 2mm) in both top and bottom of the core. With this setup it takes up to 3 days to create a new sample.

5.2.1 *Method*

An overview of the method is provided in this section, but a more thorough and step-by-step guide can be found in Appendix C.

The setup consists of a cylinder held tight by wingnuts and long bolts from the top to bottom. On the lid several valves are present for air evacuation explained in a minute.

The general method applied is to first fill the cylinder with mQ water. It is placed on a magnetic stirrer and both stirrer and heating is turned on. The valve on the lid is connected to a pump through a pressure sensor as well as a water trap placed in nitrogen. The pump is turned on to evacuate the air dissolved in the water. First the lid valve is closed and the pressure is reduced to below 0.1 mbar. The valve is then opened and many bubbles are produced in the water. This is the evacuation process of air dissolved in the water. Let it run for at least 30 min. until only few bubbles are still formed. When the air is evacuated to a satisfying result the cylinder is put in the freezer. In the freezer there is a a heating jacket kept around 4°C which at first covers the whole cylinder. This way the water does not freeze immediately. The heating jacket is connected to a motor which moves it up and down at defined speeds. The heating jacket is slowly moved up the cylinder in around 3 days. This way the water is frozen so slow that the air is pushed up and not trapped in the ice as bubbles. Often some bubbles of R > 2mm are created towards the top of the bubble-free ice cores giving 10-15 cm of completely bubble-free ice.

By varying the evacuation time and the velocity of the heating jacket the amount of bubbles can be varied. Therefore various parameters were changed and experimented with. As will be explained later in this section the transition between when the ice is bubble-free and some bubbles are formed is experimented with to investigate the change of bubble size.

From the previous setup some things have been improved upon to provide more options in changing parameters. One thing is the motor which previously only had one speed setting which was really slow. This meant that it also took 3 days to move the heating jacket

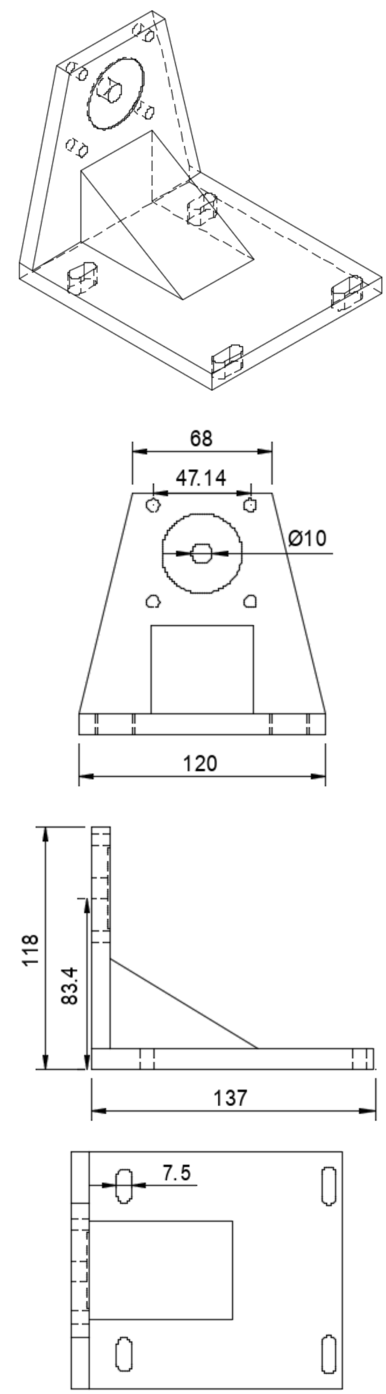

Figure 5.4: The base plate used to keep the motor held tight to the system seen from various angles. The pin on the motor goes through the hole and connects to the gear boxes by couplings.

down again which was unproductive for production of bubble-free ice which several labs are interested in.

5.2.2 *Improvements*

Motor improvements The old motor used for the bubble-free ice setup only had one speed setting. Therefore an IHSS60-36-30-21-38 JMC Closed Loop Integrated Step Motor[3] was added. This needed to be tightened to the base plate and for this a 3D print was designed for the motor to be in the right position according to the gear boxes which lowers the rotations per minute (RPM) by a factor of 1000. The base plate can be seen in figure 5.4. The pin on the stepper motor goes through the whole in the base plate and is then connected to a backlash-free coupling and further on to the rest of the components via a 3D printed knob. These connectors make sure that small off-axis movements are not breaking the setup by dampening the small movements and absorbing the energy. It is this pin on the stepper motor that is doing steps in a rotational movement. Through the other components using gears the movement on each step is reduced to a very slow movement on the coil with the wire moving the heating jacket up and down.

[3] https://www.rocketronics.de/shop/de/IHSS60-36-30-21-38.html

The motor is powered using a power supply and a voltage of 24-50 V and it is operated using an arduino. This arduino setup is copied from Kerrtu Maria Peensoo's[4] setup [Peensoo, 2021].

[4] Contact: kerrtumariapeensoo@gmail.com

By experiment the minimum delay in the motor, which describes the minimal steps per time and thus the movement, was found to be 32767 ms which relates to 30 steps/s with the step size being varied through micro stepping. The motor utilizes micro stepping which is a method for controlling stepper motors typically used to achieve higher resolution or smoother motion at low speeds. It divides each step into a number of sections providing finer resolution. From this we get the minimum velocity of the motor but it also has a maximum velocity although the specific maximum delay is not easily found. Therefore, the need for a fine micro stepping resolution that provides low speeds but also has the option to reset the motor to its previous position fairly fast eg. moving 27 cm in minutes, not days as the previous motor. Below are some calculations for various microstepping settings with minimum velocity calculated.

For 800 steps/rev it makes 0.00125 rev/step since it takes 5000 steps/rev. The pitch (the length moved per revolution) is 0.14 mm/rev.

$$30\frac{steps}{s} \cdot 3600\frac{s}{hr} \cdot 0.14\frac{mm}{rev} \cdot 0.00125\frac{rev}{step} = 18.9mm/hr \tag{5.1}$$

For 40000 steps/rev it makes 0.000025 rev/step:

$$30\frac{steps}{s} \cdot 3600\frac{s}{hr} \cdot 0.14\frac{mm}{rev} \cdot 0.000025\frac{rev}{step} = 0.378mm/hr \tag{5.2}$$

For 5000 steps/rev it makes 0.0002 rev/step:

$$30\frac{steps}{s} \cdot 3600\frac{s}{hr} \cdot 0.14\frac{mm}{rev} \cdot 0.0002\frac{rev}{step} = 3.024mm/hr \tag{5.3}$$

With these velocities the optimal micro stepping was set to 5000 steps/rev since the full bubble-free length could be done in as slow as 3-4 days but still had the flexibility in moving fast with a maximum velocity of around 1 mm/s. 800 steps/rev moved too fast and 40000 steps/rev moved too slow at max speed.

The script provided by Kerrtu Maria Peensoo was also modified slightly for possibilities of making automatic transitions in speed and direction after moving a certain distance. This can be found in Appendix D

5.2.3 Results

Using the method described above and in Appendix C various ice cores are produced with more or less success. The improved setup allows more testing and variations in parameters especially in speed and transitions from one speed to another.

All ice cores produced for bubble-free ice consistently resulted in bubble-free ice though with bubbles forming in the top as previously explained. Examples of these can be seen in figure 5.5.a-c. For ice cores tested with various parameter settings changed they produced bubbles of roughly the same size but in varying patterns and varying places through the process. Some examples for this is figure 5.5.d and 5.5.e.

As can be seen in figure 5.5 each run of bubble-free ice core is very different. Most consistent they would be bubble-free in the lowest part and larger bubbles (radius > 3 mm) in the top third. By varying the amount of time air is evacuated, the speed of the heating jacket and doing transitions various ice cores with different properties have been produced. The most important aspect though was to get some completely bubble-free ice to test the background and noise signal in the freezer as ice is being melted but without bubble signals. This was produced in mass production of bubble-free ice with the improved setup.

(a) (b) (c) (d) (e)

Figure 5.5: Various results from the bubble-free ice setup. a-c) shows regular bubble-free ice produced with bubbles in the top due to water freezing faster than air can diffuse through the water. Some parameters were changed and transitions were produced in d-e)

6 *CFA System and Improvements*

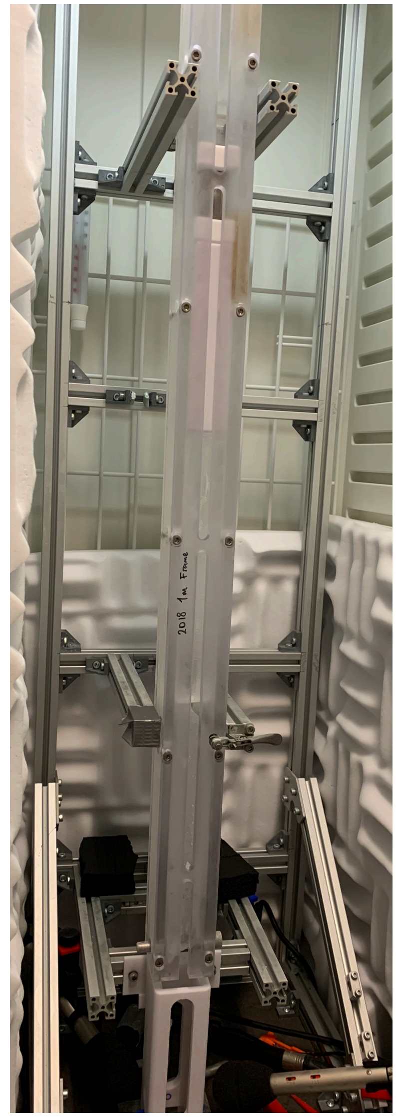

Figure 6.1: The inside of the freezer. The CFA frame holder is shown with the plastic frame put in. Inside the frame some ice and the weights are shown. In the bottom the ice core guide can be seen above the melt head as well as some microphones in the bottom.

This chapter will focus on the freezer setup both the original and optimized setup as well as parameter tuning in a flow rate experiment.

Contents

6.1 *CFA setup*

Continuous flow analysis (CFA) is a method of continuously melting and measuring various isotopes, chemistry and gas measurements instead of the previously used discrete measurements. The CFA setup in Copenhagen follows the standards of CFA labs around the world using the same general setup of melthead, pump and heater based on [Bigler et al., 2011]. The surrounding setup varies from laboratory to laboratory. The CFA setup at PICE (Physics of Ice, Climate and Earth, Niels Bohr Institute, University of Copenhagen) uses a smaller singular freezer, whereas in Bern they use the freezer in which they also store the ice cores but with a glass window to follow the melting. These can make it difficult to make general improvements in the noise spectrum of the rooms as the acoustics are very different and so is the possibility to turn off the freezer for shorter and longer time. In the following section I will go through the CFA setup in Copenhagen and the improvements we have implemented and tested. I will explain whether this could be a general improvement to the CFA system overall or if this method applies only to the freezer setup in Copenhagen. The improvements done had a focus of reducing noise in the freezer but also improves the CFA setup for any measurement.

For this setup we have used the simplest setup of the CFA system with just the melthead, pump and heater.

Thanks to Helle Kjær and Meg Harlan for helping set up the CFA system[1].

[1] Contact info. Helle Kjær: Hellek@nbi.ku.dk and Meg Harlan: Margaret.Harlan@nbi.ku.dk

6.1.1 *Frames and freezer*

The freezer is a Vibocold display freezer with a glass front and temperature regulation of -30°C. The whole CFA system holder is build using aluminum profiles of 25x25 mm groove 5 which aligns and holds the ice core frame in place. The ice core frame is made of plexiglass and has a free space of 39x39 mm inside. The ice core frame is held by two arms in the top with some hooks on the frame and is then aligned and held in place by the middle arms (see figure 6). The bottom arms hold the ice core guide (the white in the bottom) and here the frame does not touch the aluminum profiles. These two points (top and middle) align the ice core frame so it hits perfectly on the melt head for a stable melt. The ice core guide in the bottom aligns it further. The bolts holding the aluminum profiles tight get loose over time - possibly due to freeze-reheat cycles. These were tightened to make sure that the frame was stable.

6.1.2 *Melthead*

The melthead follows that of [Bigler et al., 2011] with ice core cross sections of 34x34mm. The melthead is made in such a way that only the central part (26x26mm) of the ice core is sampled by the central line and the outer is discarded. This is done to minimize contamination from touching the ice and handling and thus the setup also needs an overflow from the central part to the outer. The inner and outer sections are separated by a 2mm triangular ridge. The central section only has a single drain channel maximizing the amount of water collected by carefully controlling the pump settings and setting it a bit lower than the amount of water melted in the

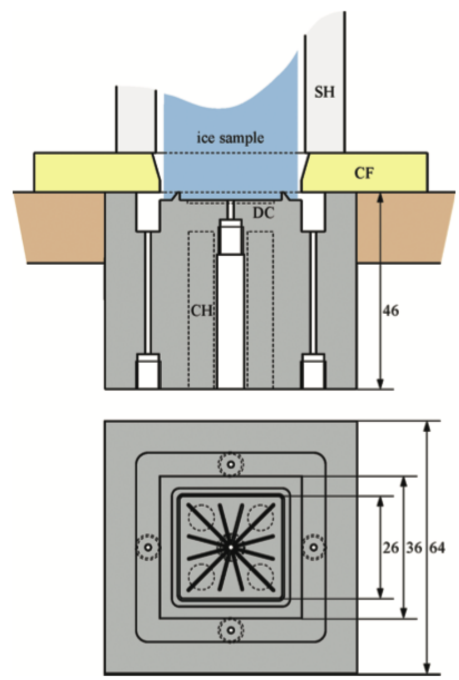

Figure 6.2: CFA Melthead from [Bigler et al., 2011]. The ice core is guided by a sample holder (SH) and a centering frame (CF). The cartridge heaters (CH) melt the ice and is pumped away through the drain channels (DC). Measures are in mm. The top figure shows the setup from the side and the bottom from the top.

central section as to create overflow. On the outer section there are four drain channels to remove the contaminated water. The melthead is cleaned daily after usage using ethanol and cotton swabs.

6.1.3 Pumpsystem

The pumping is done using peristaltic pumps of the type Ismatech IPC with Tygon tubing and the tubing is teflon tubing. The pump settings are easily controlled using the display and buttons. The control of the system has been tested for various settings in section 6.3.

For the audio recordings it is of the utmost importance to control the melt speed and keep it stable. If too much water is pumped away pumping sounds are very prominent will disturb the audio signal making it virtually impossible to resolve the amount of bubbles in a section. Therefore it is advised in order to melt a section of mQ-ice first to adjust the settings. If too little water is pumped away it will overflow from the outer section - so this is a very important feature to constantly be aware of and control. For a normal CFA measurement these sounds do not matter and are typically ignored.

If the freezer is crooked then the melthead is also crooked and the water accumulates differentiated. The freezer was aligned using a big spirit level for the overall freezer alignment and a small one on the melthead to make sure this was level as well.

6.1.4 Melter controls

The melthead is heated using four 125 W heating cartridges with an embedded thermocouple of type J. The temperature is controlled using a temperature regulator (JUMO, dtron 308 plast) with melting temperatures around 20-35°C depending on the melt rate required. Various temperatures have also been tested in section 6.3.

To achieve a stable meting speed a weight is placed on top of the core resulting in a constant downward force on the ice. Usually this is done using a 370 g steel cylinder with plastic endpieces. This is connected to the encoder which pulls down on this cylinder with a force of 1.2 kg. As a supplement, a square plastic container was 3d printed with enough space for an iron bar of 1.5 kg to fit inside in case the encoder could not be used due to changes in the freezer. Besides the added weight on top, the ice core itself further up adds extra weight.

A full frame with ice core is 110 cm (2x55 cm ice cores) and the weight would thus be $0.917 g/cm^3 (3.4cm \cdot 3.4cm \cdot 110cm) = 1166$ g. This is almost a doubling of the weight when the frame is full compared to the last section of ice not melted. If the top weight is heavier this change will not vary as much and it can be argued that this weight should be increased but has not been as this might have changed the melt rate which we wanted to remain stable.

6.2 *Improvements*

6.2.1 *Thermal capacity in freezer*

The freezer temperature has been investigated due to the freezer being shut off during measurements as well as to see the rate of cooling to below freezing and changing from freezing to above freezing. In figure 6.3 the temperature of a freezer in the span of 42 hours can be seen. As the freezer is turned on at room temperature it reaches freezing within an hour but it takes 4.5 hours from room temperature to -28°C. When the freezer is turned off, as it will be during audio recordings, the freezer goes from below -28°C to above freezing in a span of 2 hours and this is without the door being opened and closed every time something happens or a frame has to be changed.

Due to this, more thermal capacity was attempted added to the freezer. This was achieved using freezing elements like the ones used in regular freezers, camping boxes or for shipments. These took upwards of 5 days before they were completely frozen as they were placed in several layers. Besides this, they were also placed on grid shelves which interrupted the encoder cable and movement - yet another reason the 3d printed plastic container with a bar of iron was used as the weight on the ice, just as explained in the previous section.

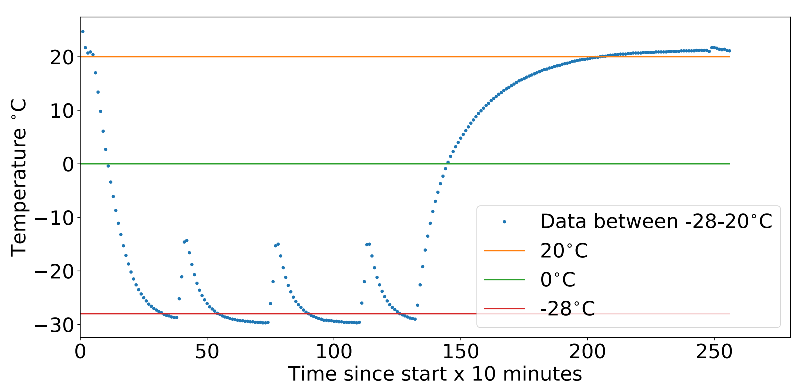

Figure 6.3: The temperature logger data. The freezer defrost every 7 hours causing the temperature rise in periods. at time 0 the freezer is turned on from room temperature and at time step 132 the freezer is turned off to investigate freezing and heating of the freezer.

The effect of the extra thermal capacity was limited. It did stop some air from flowing around but as the door was opened quite often the thermal capacity did not cool the freezer down much between door openings. In the final setup the thermal capacity was removed. The problems with temperature is something that should be looked into for longer melt campaigns. The main problem being the hot air flowing in as the door is opened frequently. This could possibly be solved with a plastic plate covering the opening, such that less air flow in. This is something that is a greater problem with the Copenhagen freezer compared to e.g. Bern due to the size of the freezer.

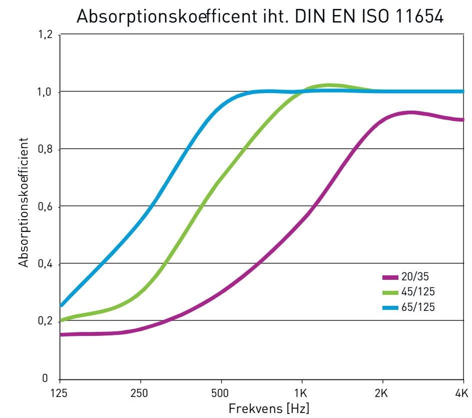

Figure 6.4: The absorption rate vs. the frequencies for the current setup. Figure from IAC acoustics [Link here]

6.2.2 *Sound absorbing materials*

Since the freezer is of limited size there is a high chance of reflection of sound on the walls which could disturb the signals. This is something sound absorbent materials could help prevent by absorbing some of the energy Each frequency reacts differently to various materials but the general rule of thumb is light and porous materials absorb more of the high frequencies (above 1kHz). More sturdy, heavier and compact materials absorb the lower frequencies more effectively. In general the materials decrease in efficiency if they get wet or saturated so this is a point of note to be aware of.

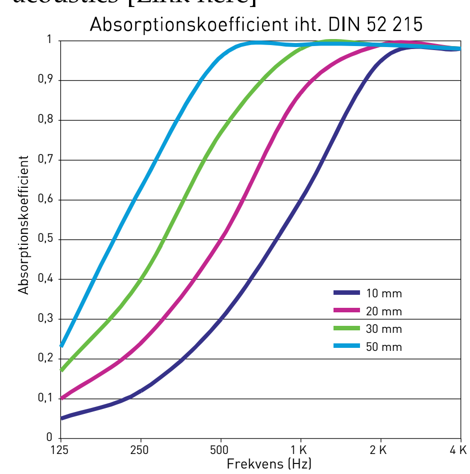

Figure 6.5: The absorption rate vs. the frequencies for the recommended setup with heavier material. Figure from IAC acoustics [Link here]

Currently the Labyrint sound absorbent (DIN EN ISO 11654) from IAC acoustics is used in the freezer. This material is a light, elongated pyramid shaped material ideal for reducing reflection from the walls from the ice popping sounds. The absorption response by frequency can be seen in figure 6.4 in which the low frequencies generated by the noise is still very present and not diminished.

For a future purchase IAC Acoustics recommended, for a setup like this, the IKALON 135 MK (DIN 52 215) made specifically for reduction in mechanic noise resembling that coming from our freezer and surrounding machines. The response can be seen in figure 6.5. It has a quicker increase in absorption of the low frequency noise though it does not absorb all. It should be noted that all IAC acoustics materials have only been analyzed up to 4 kHz which is in the low end of our bubble signature spectrum but it can be expected it follows the response curve shown in figure 6.4 and 6.5 which shows a bit more absorption but generally not much.

This could be of help in many freezers to screen for various noises but should be analyzed specifically for each freezer which frequencies the sound absorption material should target.

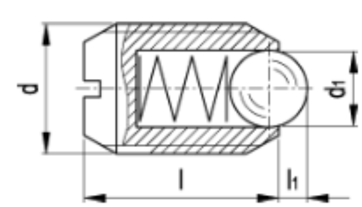

Figure 6.6: Spring plunger length l, width d, ball width d_1 and the ball extension h. As a forcie is applied on the ball the spring is compressed resulting in an opposite force.

6.2.3 *Ice core alignment*

As the ice is placed in a vertically standing frame in the freezer we want to make sure that the ice is aligning with the melthead, and with the center of the ice core hitting the center of the melthead. Usually, this would be done using plastic elements that are held in place between some clamps and with a plastic alignment element on the melthead as the one in figure 6.1. The element on the melthead is not held in place and in practice does not do a very good job of holding the core in place. The top element is not very nicely aligned either but does have various options for longer elements guiding the core for a longer path. Since these are not optimal and we wanted a steady and controlled melt of the ice core these systems were improved.

Now, it is connected to one single ice core guiding system which guides the ice perfectly to the center of the melthead. The inner diameter is 36x36 mm so that it holds the regular 34x34 mm ice core size but also smaller cut variations. To make sure the guide goes towards the centre of the melthead and in order to keep it stable, small legs were extended down into the melthead troughs to make sure it was perfectly aligned with the melthead. In the lowest part of the guide spring plungers have been utilized to keep the ice still and in the center while still being able to handle variations in size. These are presented in figure 6.6. A small ball on the end is connected to a spring on the inside. This configuration guides the ice perfectly to the melthead without creating noise and lets the water get away and into the troughs to get pumped away.

The top element is changed to a more stable element that is now connected to and held tight to the frame behind the core holder. This frame uses 5 mm bolts and is easy to move to the side for a better configuration if the elements do not align. There will be a small gap between the frame and the guiding element. The inner and outer dimensions of the guiding part is the same as the previously used plastic frames which have a bit excess space for variations in width of cut ice cores pieces. In the front there is a slit for a view of the ice core to be able to track it all the way through the system. The older pieces were transparent and this could be as well, but none of the 3D print material we had was see-through. In the bottom there are two holes designed for a pin to hold the ice core, exactly as we have it in the core holders. All edges are rounded for less chance of the ice to get stuck. The prints for the ice core guide can be seen in figure 6.7.

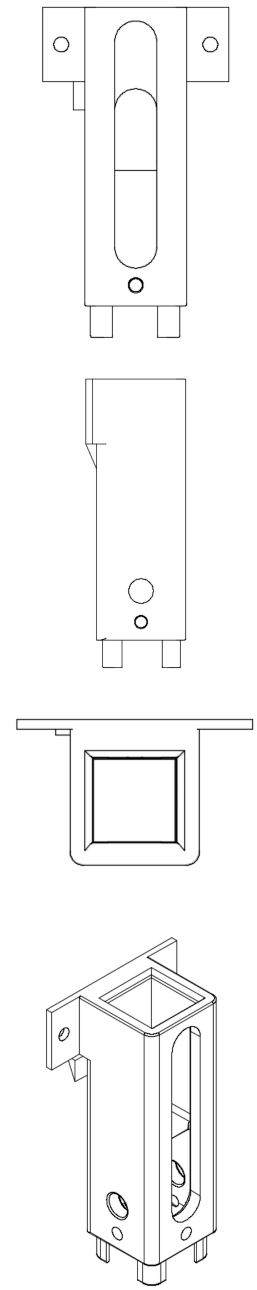

Figure 6.7: The ice core guide at the bottom of the ice core frame. This piece guides the ice core the last way ad centralises it on the melt head. This is done using spring plungers towards the bottom and the legs extending into the melt head troughs. The width is bigger than the ice core to adjust for cutting deviations. The front and back is open to follow the ice and see if it gets stuck.

6.3 Flow rate experiment

The meltrate of the ice core is a significant factor in the amount of air bubbles being released per second. Therefore a good basic knowledge of the flow controls i.e. the melthead temperature and the pump speed is needed. A small experiment was set up to get this required knowledge. The following parameters were tested in this experiment: new vs. old tubes, temperature variations from 15°C to 35°C in increments of 5°C with a pump speed of 10 ml/min, and finally the pump speed was varied from 4 ml/min to 18 ml/min in increments of 2 ml/min with a constant melthead temperature of 25°C. The amount of water being melted in the central area is from the dimensions in [Bigler et al., 2011] with the central line being 26 mm by 26 mm and 5 cm ice core equals 33.8 ml per 5cm sample.

The hypothesis before the experiment was that a high melthead temperature means a higher meltrate of ice. When the central pump line takes away all water collected by ice being melted then the meltrate is going to be higher and the ice is progressively going to melt slower due to less weight being on top of the ice being melted. It is also expected that the meltrate of the ice core is going to be different depending on which type of ice being melted. With this experiment it should be possible to know how much to adjust the various settings. All data can be found in Appendix E.

6.3.1 Method

The regular setup for the CFA system was used. Before putting the ice core in the frame, freezer markings were made at 5 cm separation from 0 to 40 cm. This would give eight meltrates for each ice core in order to obtain an average meltrate with uncertainties. The best measurements were when there was an extra amount of ice to melt both before and after the 40 cm. This would make sure the melt was stable when reaching the point of measuring.

As the point of measurement was reached the time was started and the water collection began. The central line went in a separate container to get a measure of the amount of water overflowing from the central to the outer lines. As the first 5 cm mark is reached the time is noted through a time lap measurement and the containers are changed as well. There was some delay from the 5 cm mark being reached to changing the containers but since this was done in the same rotation and routine each time the uncertainty was systematic and will not be incorporated in the uncertainty analysis since there was also a delay from water being melted and reaching the containers through the pump system.

There was also collected eight volume samples per ice core when the 5 cm marks were reached. The volume samples have a correlation with the meltrate since there is a delay from the marking being reached to that water sample reaching the collection containers. So if the the melt rate changed it has a delayed effect. This also means that the first volume sample will be less than average since the water has not gone through the pump system yet. One exception is if there is extra ice to melt before measuring then this will have filled the pump system prior to recording.

After the ice core is melted the cups are measured on a scale with ±0.001 g precision. The weight of the containers are removed as the results are written into the datasheet.

6.3.2 *Results*

The results are analyzed using python and both the excel datasheet and the python analysis is appended in the separate drive.

The mean and standard deviation are found using numpy nanmean and `nanstd` functions, which gives the mean and one standard deviation values, but disregards NaN values. When same parameters were used for several measurements these were added together using propagation of uncertainties.

Melthead temperature vs. meltrate

Figure 6.8 shows the melthead temperature vs. meltrate. The data tends to show a linear tendency at all datapoints except 30°C. This linear tendency fits the hypothesis that raising the temperature increases the meltrate of the ice core. It does so with an increase of 0.81 ± 0.01 cm/min per 1°C increased.

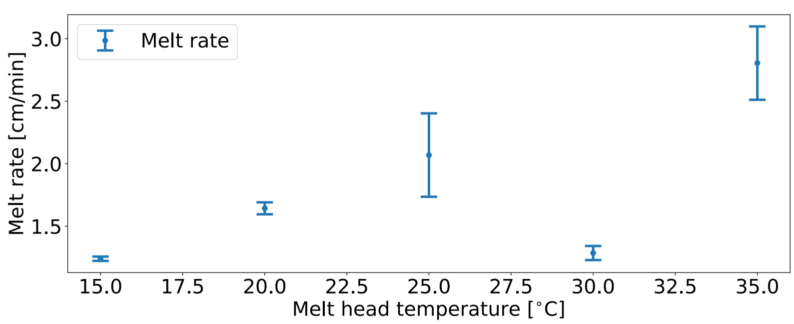

Figure 6.8: The melthead temperature vs. the meltrate of the ice core. The orange fit includes all datapoints from 15°C to 35°C and the green is only using 15°C to 25°C. The value for the 30°C point is measured twice and still looks like an outlier as the rest follows a linear tendency. All measurements are done at a flow rate of 10 ml/min.

The outlier at 30°C does not seems to be an outlier as it is well beyond a standard deviation away from the linear tendency as well as being repeated twice giving the same result. The best explanation is that with the flow rate of 10 ml/min this meltrate is enough for there to be a layer of melted, cold water on the central line that is neither pumped away quickly enough or enough for it to spill over to the outer lines fast enough. This gives a cold layer on top of the melter that decreases the meltrate significantly.

Flow rate vs. meltrate

In figure 6.9 the flow rate vs. meltrate is shown. The variation is high and does not exhibit a clear tendency. Some data points show high uncertainties resulting in an unclear notion on the flow rates influence on the melt rate. There are some variations but concluding a specific relation is problematic. For a future improvement it would be beneficial to do this analysis with various temperatures rather than only 25°C. This could provide greater knowledge on the hypothesis on whether the flow rate in the central line gives rise to an increase in melt rate if the central pump removes all melted water. The top around 12-14 ml/min could suggest that there is an optimized suction for melt rate increase. This decreases greatly when the potential pumping is more than melted water and with a meltrate of 2.1 cm/min this is 33.8 ml/ 2.1 min = 16.1 ml/min. If the flow rate is higher then this could also result in impurities and water outside the central area to get sucked in. If the flow from the central line is too weak there is overflow from the central to the outer lines. This keeps out impurities and is especially important for regular CFA chemistry and gas measurements.

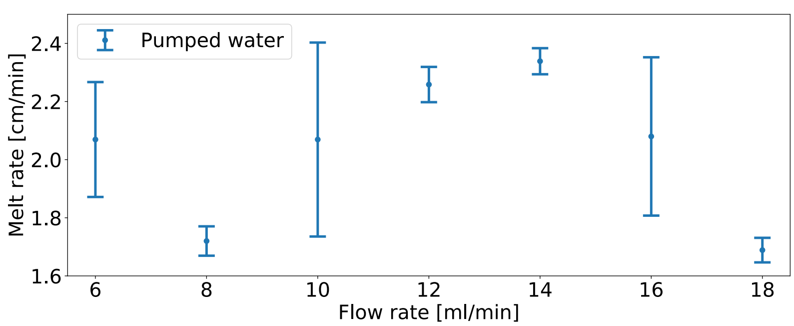

Figure 6.9: The flow rate vs. meltrate of the ice core. The orange fit shows an oscillating fit with optimized parameters. All measurements are done at 25°C.

Melt head temperature vs. pumped water

As previously mentioned the pumped water has a correlation to the meltrate as this determines how fast the core is melted. If it melts fast more water is gonna spill over to the outer lines. In figure 6.10 the melthead temperature vs. pumped water is shown. Once again the 30°C data point is off axis with the rest of the measurements, most likely due to the same effects mentioned previously with a cold water layer on top of the melthead. If the 30°C datapoint is excluded this tends to a linear tendency with a decrease of pumped water of 0.88 ± 0.22 ml/°C. This is not completely linear since below 15°C more water being pumped than being melted. At 15°C the central line pumps all water that is melted resulting in zero spillover to the outer lines. 30°C is beyond the 5 cm volume and must therefore have sucked in water from outside the central area. It could also be due to some of the effects mentioned in the method section. It can only have done this in relation to the low meltrate with low water levels in the central area.

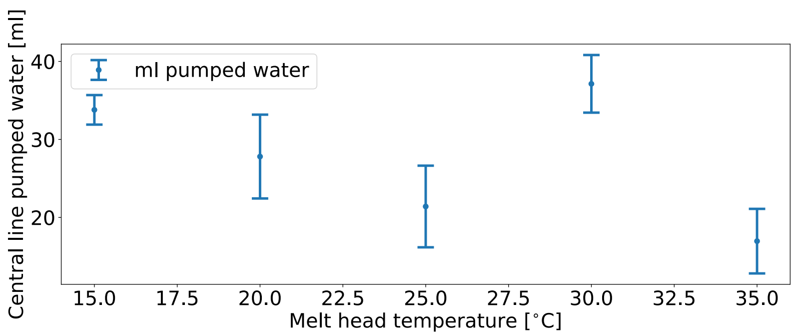

Figure 6.10: The melthead temperature vs. pumped water volume. The orange fit includes all 5 data points and the green fit excludes the 30°C data point. At 33.8 ml the 5 cm volume is noted. All measurements done at a flow rate of 10 ml/min.

Flow rate vs. pumped water

Figure 6.11 shows the flow rate vs. pumped water from central line. If the flow rate increases so does the volume of pumped water. This intuitively makes sense since pumping more water away creates less of a spillover to the outer lines. With a linear relation we see an increase in pumped water of 0.92 ± 0.19 ml per 1 ml/min increase in the pump parameter. The relation seems to be of higher order but without further data points it seems futile to guess at the exact relation. A data point at 4 ml/min was attempted but sucked too little water was sucked in from both the inner and outer lines and created an overflow from the melthead. At 18 ml/min we are way beyond the 5 cm volume suction and it must be pulling in water from the outside area. The relation would be better estimated by doing the same measurements at other temperatures besides 25°C.

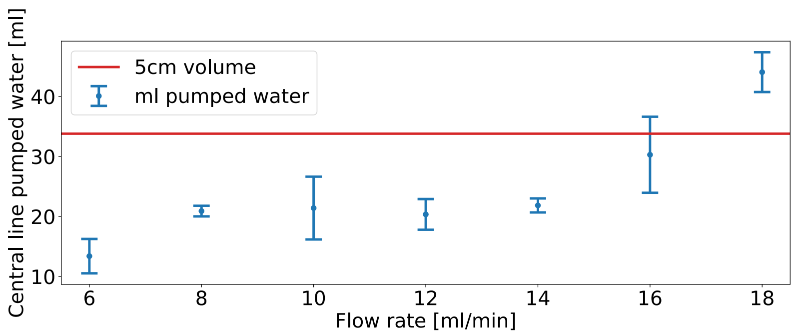

Figure 6.11: The flow rate vs. volume of pumped water. The fit follows a linear tendency with optimized parameters.

Statistical uncertainty of general runs

To get a measure of the general uncertainty, not regarding a change in the parameters, several runs using the same parameters of 25°C and 10 ml/min flow was conducted. These showed a variety of changes in the melt rate resulting in a value of 2.07 ± 0.33 cm/min. This uncertainty should be applicable for all other settings of parameters or at least a general magnitude of the uncertainty.

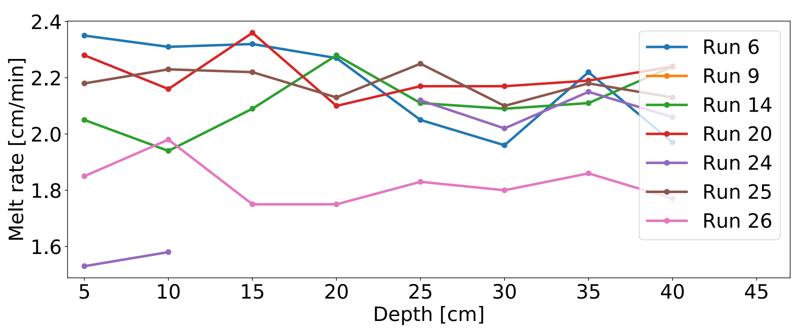

Figure 6.12: Several runs were made using the same parameters of 25°C and 10 ml/min. This gives a statistical uncertainty of 2.069 ± 0.334 cm/min, from which the uncertainty can be projected to all runs.

A problem observed during melting was that if the ice core top was not horizontal then the weight on top would make the ice core tilt and melt at an angle or change the meltrate. If there was a crack along the ice core then the horizontal forces pushing to the sides made the ice core get stuck on the frame. When cracks, even internal cracks, reached the melthead this gave a path for the water on the central part of the melt head to escape which raised the meltrate of the ice core.

From the results of this analysis the parameters are chosen to be 25°C and a flow of 14 ml/min. This gives a bit of overflow from the central line. Every single run is different and should be carefully observed and from the analysis this gives a basis of changing the parameters if something is to change for the setup. One thing to be aware of is to keep water in the outer troughs otherwise the suction from the pump line creates noise which is undesirable for audio recordings.

7 Recording Bubbles

This chapter goes into the main results from melting ice and doing audio recordings based on the work from previous chapters. Two setups have been constructed to examine bubble signatures in water and from ice-bubble, ice-water and water-air transitions as well as audio origins.

Contents

This chapter demonstrates the steps taken towards designing a system that outputs TAC values based on the audio frequencies measured from the bubble signals as explained in Section 3.5.

Company	AKG	AKG	AKG	Shure	Aquarian
Model	C451B[1]	C417PP[2]	C411PP[3]	VP82[4]	H2a-XLR[5]
Type	shotgun	Lavalier	Contact	shotgun	Hydrophone
Cartridge type	Condenser	Condenser	Condenser	Condenser	
Sensitivity	9 mV/Pa	7 mV/Pa	2 mV/Pa	15.8 mV/Pa	1 V/µPa
Freq. Range	20Hz-20kHz	20Hz-20kHz	10Hz-18kHz	90Hz-20kHz	<10Hz->100kHz
Polar pattern	Cardioid	Omnidirectional	Figure eight	Supercardioid	Omnidirectional

[1] AKG C451 Specs: https://www.akg.com/Microphones/Condenser%20Microphones/C451B.html

[2] AKG C417PP Specs: https://www.akg.com/Microphones/Speech%20%2F%20Spoken%20Word%20Microphones/C417PP.html

[3] AKG C411PP Specs: https://www.akg.com/Microphones/Condenser%20Microphones/C411PP.html

[4] Shure VP82 Specs: https://www.shure.com/en-US/products/microphones/vp82

[5] Aquarian H2a-XLR Specs: https://www.aquarianaudio.com/AqAudDocs/H2a_XLR_manual.pdf

Table 7.1: Microphone specifications for the different microphones tested in this project.

7.1 *Method*

The method for sound recording includes many options for tuning using various filters, boosts and cut-offs in processing both in post-processing and in the recording programme (DAW). To get the most homogeneous raw signals from each measurement as little tuning as possible have been used. For future optimization the direct tuning of the signals as they are recorded through the DAW might prove valuable, since optimally it can filter out quite a bit of noise. The method has been kept as simple as possible for easy replication.

Below some of the microphone specifications and the recording flow will be explained. A full setup needs only a few parts and can be made more complex as recordings and setup advance. The setup needs a microphone, the cable, a preamplifier and a laptop with a recording programme.

7.1.1 *Microphone specifications*

In Table 7.1 the most important specifications from the used microphones are set up for comparison. These are also the specifications that would be most useful to focus on in more advanced setups in the future. Especially the frequency range, sensitivity and polar pattern have been main points of focus and they are described thoroughly in Section 3. A higher spec in one category is usually a trade-off with one of the others if the price is still in the same range.

As can be seen in Figure 7.1 the comparison of the three main microphones frequency response to the exact same 10 second signal sample can be seen. Here, it is seen that none of them have the exact

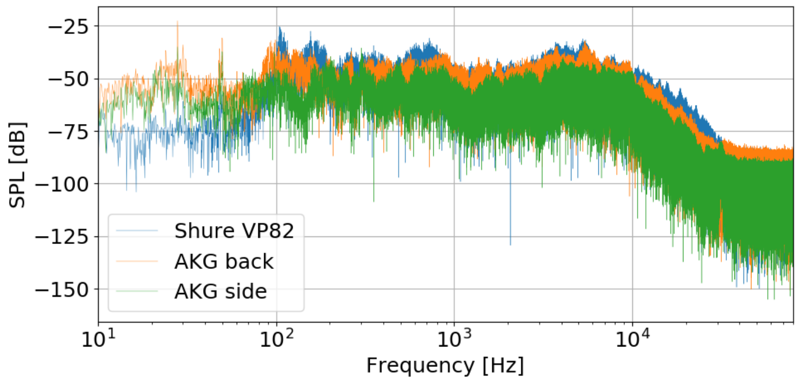

Figure 7.1: SPL vs. frequency of the same 10 sec. signal including bubbles. Blue is Shure VP82, orange is the AKGC451B shot from the back of the freezer and green is the AKG C451B from the side.

same frequency response. The AKG C451B from the side records the weakest throughout the full frequency spectrum followed by the AKG C451B microphone from the back which gets a more powerful signal. In the low frequency spectrum the AKG C451B microphones are more prominent in the signal compared to the Shure VP82. As the frequencies get beyond 100 Hz the signal is strongest in the Shure VP82. Beyond 20000 Hz they all drop out as this is beyond their frequency response. For all measurements in the coming sections the same microphone has been used: The Shure VP82 since it provided the most powerful response and the low frequency response overlaps the background noise frequencies. The two AKG C451B microphones have been matched exactly and should therefore have the same response. This leads to the conclusion that even small variations in the setup and whether the microphones are directed directly towards the ice recordings or have a slight tilt causes a change in the response.

The preamplifier, Steinberg UR816C, was chosen due to its high sampling rate of up to 192 kHz and 32 bit and due to its many inputs of eight microphone inputs. This provides the option to be able to record using multiple microphones simultaneously. It supports phantom powering[1] of 48 V for the microphones and came with the programme Cubase LE AI Elements 11, which was used for measurements. It was connected to a laptop using USB C 3.1 for fast and high quality data transferring.

[1] See section 3.3

It was found through audio analysis that the contact microphones showed a varying background signal as can also be seen in Figure 7.2. It was later found that this signal matched exactly the heating cartridges in the melthead turning on and off to keep the melthead temperature stable. Due to this the contact microphones (AKG C411PP) were omitted from use for now but with further analysis and sig-

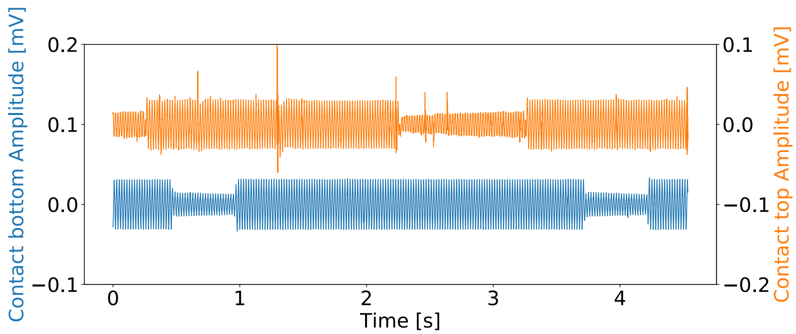

Figure 7.2: Raw signal from the contact microphones. The blue data is from the contact microphone on the bottom of the melt head. The orange is from the top of the melt head.

nal clean-up they might have potentially valuable knowledge since they have no background noise besides material vibrations which might be introduced as bubbles pop. The lavalier microphone was also omitted for now until the setup and recordings are optimized. As mentioned in the previous section, to keep the setup simple and for easy comparison only the signals recorded with the Shure VP82 microphone is presented. For several of the presented measurements data is also available for the AKG microphones.

Audio 7.1: Shure VP82 [link]

Audio 7.2: AKG side [link]

Audio 7.3: AKG Back [link]

7.1.2 *Recording flow*

The microphones were placed in the freezer from different directions. Since this freezer is quite narrow and shotgun microphones are quite long due to their (super)cardioid polar patterns[2] they can be tricky to place. It was managed to place the Shure VP82 and two AKG C451 microphones, the VP82 and one AKG C451 shooting from the back while just the other AKG C451 from the side. The microphones were connected tightly to the frames for stable measurements, although this might introduce some vibrations in the microphones as the holders are not vibration diminishing.

[2] See section 3.3

Using XLR cables the microphones were connected directly into the Steinberg URC816 preamplifier. The preamp is connected to the laptop by USB C. For the recordings the programme Cubase LE AI Elements 11 has been used. Each single audio recording made in the programme was saved separately in a programme subfolder with the file name and recording number e.g. file_name_01.wav. These files are stored for further analysis as explained in the next section.

A more detailed and specified method description can be found in Appendix F.

7.2 Data analysis

Once the signal has been recorded it is analyzed into detail and examined for resemblance to the bubble signals. The raw signal always contains noise even though much of the noise has been removed through the improvements described in Section 6.3.2. More noise can be removed through post-processing signal analysis and the method is described later in this section.

The full algorithm for the data analysis can be found in Appendix G with comments.

7.2.1 The raw signal

The raw signal coming directly from the microphone gives the time domain mV variations in the cartridge. This displays the noise level in between bubble signatures as can be seen in Figure 7.3. A bubble signal shows a sharp increase in pressure and a slower decrease resembling the bubble signals seen in [Lee et al., 2013, Pettit et al., 2015, Al-Masry et al., 2005] and gives the same signature whether it is the bubble release frequency in water or the release of bubble pressure from glacier ice. The bubble signal for this signal can be seen in Figure 7.4 which also displays a short section of the signal in Figure 7.3 as the sound pressure level.

The sound pressure level (SPL) can be found using the sensitivity of the microphone (see Table 7.1) by first taking the root mean square (rms) of the signal.

$$p_{rms} = \sqrt{(\overline{signal^2})}, \tag{7.1}$$

and then dividing by the sensitivity. This gives us the signal SPL in the time domain in Pascal. To find it in dB the 20·log10() is taken of

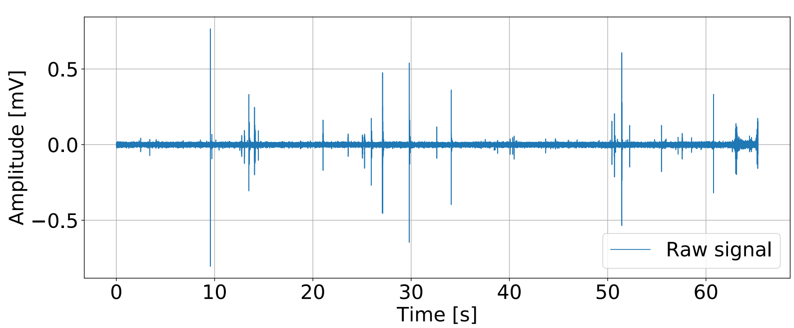

Figure 7.3: The raw audio signal directly from the microphone in pressure on the diaphragm.

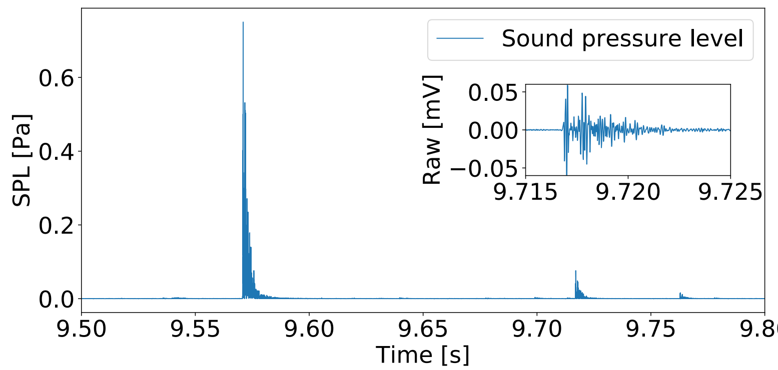

Figure 7.4: The sound pressure level (SPL) in Pa. showing a bubble signal. The inset is the raw signal in Pa. showing the sharp increase and slower decrease in pressure.

this fraction

$$SPL_{Pa} = \frac{p_{rms}}{sensitivity}, \tag{7.2}$$

$$SPL_{dB} = 20 \cdot \log_{10}\left(\frac{p_{rms}}{sensitivity}\right). \tag{7.3}$$

To find the SPL in the frequency domain it is common to use a window such as hamming before doing a discrete fourier transform (DFT) to adjust the feeds to the DFT, making smooth repeating transitions for the furier transform [Ryan, 2019]. The spectrum in the frequency domain of the signal is found and a two-sided, equal negative and positive valued spectrum is obtained. Since the spectrum is equal in both negative and positive values only the positive side is analyzed but the energy in each band is conserved by multiplying by two. This relates to the Nyquist theorem considered in Section 3.2.3. Once again the RMS is found in the frequency spectrum and is converted to dB by the same method that applied to the time domain.

The SPL in the frequency spectrum found by the previous method consists of the total energy of the full signal but for a setup where the bubble signals are only present at certain times and each individual

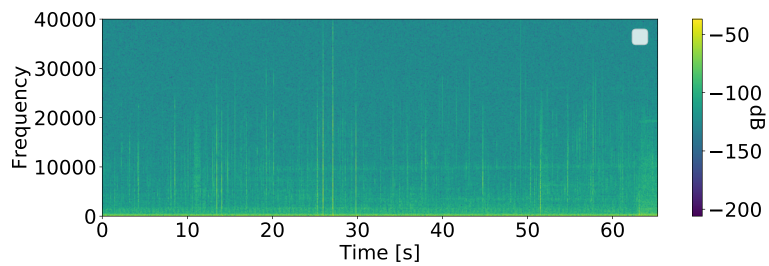

Figure 7.5: A spectrogram displaying the frequency spectrum by time. The colors display the dB pressure on the diaphragm.

bubble signal should be investigated, another method can apply: A spectrogram. The spectrogram analyzes small sections in the frequency spectrum and is able to show variations in the frequency density over time, rather than a DFT of the full signal only showing the average energy in various frequencies over the full measurement. The spectrogram gives an insight into the change of the frequency spectrum with time. The function used is `matplotlib.pyplot.specgram()` which takes in the signal, the sampling frequency, the amount of data points NFFT to perform FFT on and the overlap in amount of datapoints N between consecutive steps. An example can be seen in figure 7.5 with the signal being displayed in dB values.

7.2.2 *Filtering*

Noise has been mentioned previously in this section and the best way to examine a given noise distribution is to measure the background signal. By looking at the background signal in the time domain (Figure 7.3) it is easily seen that there is a significant amount of noise. To get a better view into the specifics of the noise it was analyzed in a spectrogram to see in which frequencies the noise was present. As can be seen in Figure 7.6 most of the noise is in the low frequency range and it stems mostly from lab equipment running in the background or general machine rumbling in the building.

A good way of removing noise is by using a frequency filter on the measured signal and for that there are many choices. By comparing the background signal to the recorded signals it is very clear to see that the background noise is in the low frequency range below 3 kHz and especially below 1 kHz. Whenever there is a bubble signal we see this in the 5-15 kHz range as in Figure 7.5 and therefore we would want to remove the background noise below 3 kHz. Just

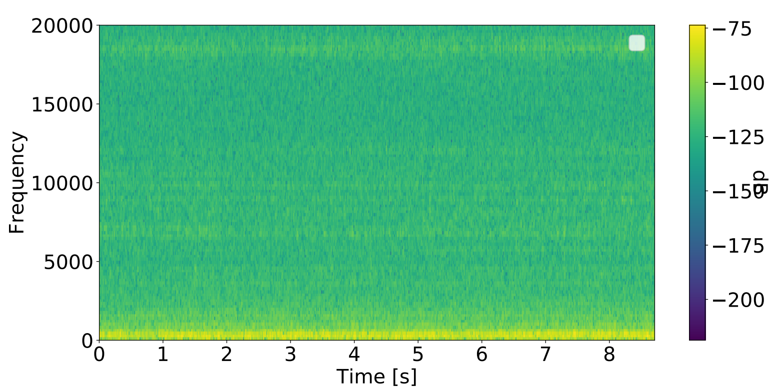

Figure 7.6: A spectrogram of the background signal by frequency over time. Most of the power present is in the low frequency.

subtracting the background signal is not an option as the amplitude of the signal might change from recording to recording. A better way is to deal with the low frequency noise for each run.

It is worth noting that if there are any high frequency events that are not just background noise, eg. a crack happening or ice sliding heavily along the frame in the freezer, these are not filtered out with the current state of the data analysis. These could be removed by identifying specific bubble signatures by fitting a bubble signal to whenever there is a signal but this has not been done.

Difference filter A difference filter takes the difference between data point `k` and `k-1` [Proakis and Manolakis, 2007], defined as

$$y[k] = x[k] - x[k-1], \tag{7.4}$$

where x is the input signal and y the output signal, k is the index.

This is easy to implement numerically and decreases the amplitude significantly of low frequency noise. The difference filter can easily be implemented using the Pandas dataframe package using `pandas.DataFrame.diff()`.

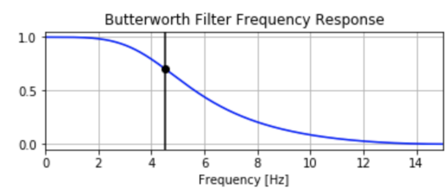

Figure 7.7: The butterworth filter signature

Butterworth high pass filter The butterworth filter can be adjusted to both a low or high-pass filter and is used as a high-pass filter here. The filter follows the frequency response described by

$$H(z) = \frac{1-\alpha}{1-\alpha z^{-1}}, \tag{7.5}$$

with α describing the attenuation. An example can be seen in Figure 7.7.

This version uses `scipy.signal.butter` from the Scipy library. It takes in the order N, the cut-off frequency, the sampling frequency and whether the filter is low-pass or high-pass.

As can be seen in figure 7.8 the two filters are compared to the original signal. The difference filter is more smooth but does not remove a lot of the low frequency noise. The butterworth filter is really efficient at reducing the low frequency noise below the cutoff frequency and let the high frequency energy pass.

7.2.3 *Estimating bubble-size distributions*

As mentioned previously the bubble signals are clearly seen in the 5-15 kHz bands when comparing with the background signal in the spectrograms. Since the background power level is constant those bins in the time domain in the spectrogram that have more power

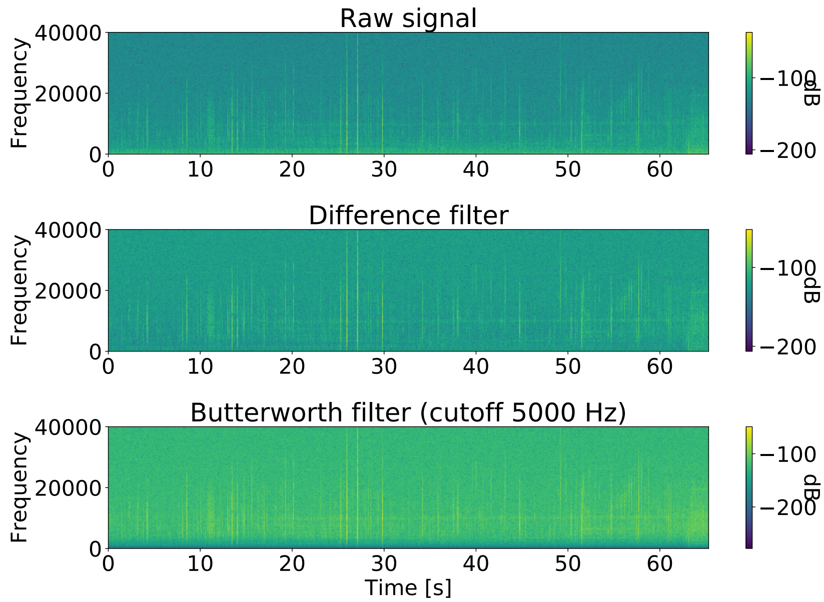

Figure 7.8: The spectrogram of a) the raw signal, b) the difference filter and c) the butterworth filter.

than others must be the ones that have an extra signal eg. bubbles and often in the 5-15 kHz bands. Therefore, the total power of all frequencies for each time bin/column in the spectrogram is found.

Using `scipy.signal.find_peaks()` the bins with most power are found. It takes in the signal, a height criteria and a distance criteria. By defining the height criteria based on a certain percentage of the max power value and a distance criteria as to not find shoulders on peaks they were analyzed and the smaller noise peaks were not used for calculating bubble sizes. This height criteria is based on a fixed value as the code is now. It should be updated so as to find an automated criteria as to get enough signal but as little noise as possible.

If a peak is detected, meaning a lot of power is prominent for this time bin, the frequency spectrum for this time bin is analyzed. The time/bubble spectral density has several prominent peaks as can be seen in Figure 7.11. The most prominent peaks are found and their frequencies are used in a weighted average based on their prominence compared to the most prominent peak. This gives one value describing a weighted average frequency from the prominent peaks. Once the peaks in the frequency spectrum of the time bin has been analyzed this frequency is used as the Minnaert frequency in Equation 3.23 to find the bubble radius. This is then done for each time bin that shows a peak due to power in that bin based on the previously described method. The values used in the Minnaert

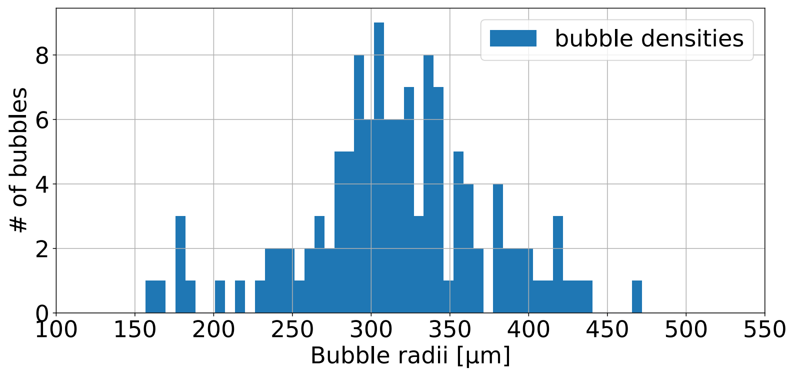

Figure 7.9: A histogram of the bubble-size distribution. The bubble sizes are displayed in μm and distributed over a variety of sizes.

equation are taken from [Lee et al., 2013] which analyzes bubbles emitted from glacier ice in water and are the best values compared to the specifications which resemble our setup.

From the bubble radii a bubble-size distribution can be obtained and the TAC can be calculated using the volume of a sphere $V = \frac{4}{3}\pi r^3$ for each of the found bubble weighted average frequencies.

The variations in the bubble frequencies should be studied further since the bubble radius changes significantly with frequencies of both 5 kHz and 15 kHz. Therefore this is just a first order bubble size distribution estimate since there are still quite a few processes to be optimized.

7.3 *Controlled bubbles experiment*

To check whether the signal recorded is similar to that of a bubble and what the origin of the sound signal is an experiment was set up. This experiment utilizes the same method as [Lee et al., 2013, Pettit et al., 2015].

7.3.1 Capillary

Audio 7.4: Single bubble capillary audio [link]

Using capillaries of size 25 μm, 40 μm and 50 μm bubbles of various sizes were made and with a varying pressure the spatially and temporal variations could be handled to observe individual and multiple bubble signals as they occur in water.

A plastic box of size 34x26x20 cm was filled with pure mQ water to prevent clogging of capillaries and build up of bubbles around impurities. The water was kept at room temperature and to prevent ground vibration interference the tank was placed on a towel. To minimize external noise everything was shut off in the room and

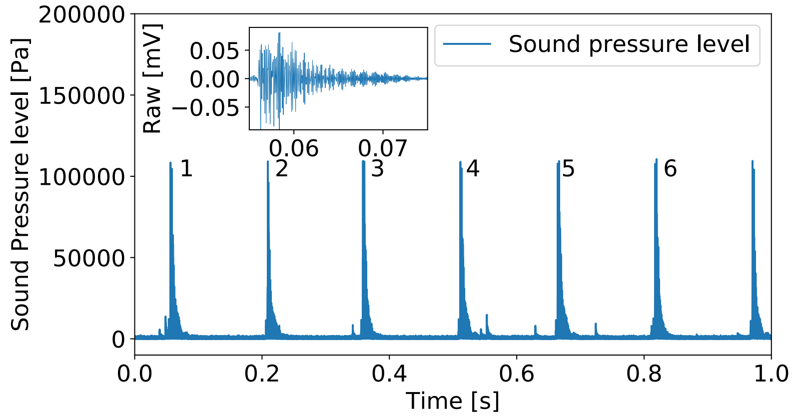

Figure 7.10: Single bubble capillary SPL with inset showing a single bubble signature. Several repeating bubble signals are shown.

recordings were made outside work hours due to doors shutting and cars driving by affecting the signal which can be heard when the signal is set to full gain. Using the Shure VP82 microphone and the Aquarian hydrophone (specs in table 7.1) the signal was investigated both in and out of the water. These are both connected to the Steinberg preamplifier and uses the recording method described previously and in Appendix F.

The capillaries are placed centrally in the water close to the bottom and below the Shure microphone. The hydrophone is placed slightly to the side of the bubble column as to not disturb the bubbles ascending to the top. The recordings were captured at a sampling rate of 192 kHz and a sample resolution of 32 bit to get the highest resolution possible.

Single bubble For a deeper understanding of a bubble signature a discrete single bubble signal was analyzed by turning down the pressure. This signal can be seen in figure 7.10 which also focuses specifically on the bubble signature from a single bubble signal. Here it is clearly seen that the signal has a sharp increase followed by a slower oscillating decrease lasting upwards of 15 ms. The tail of the signal shows some interference most likely due to the reflection of the walls of the container which prolongs the signal even further. From apparent analysis the individual bubble signals look very alike with peaks occurring every 160 ms. It seems that the bubbles grow large and are released 6 times a second. By analyzing the frequency spectrum for individual bubble signals, as can be seen in figure 7.11, it is apparent that they are found to be very similar with the same power spectral density but with minor variations. The second bubble signal shows peaks at the same values, but were more spread out in

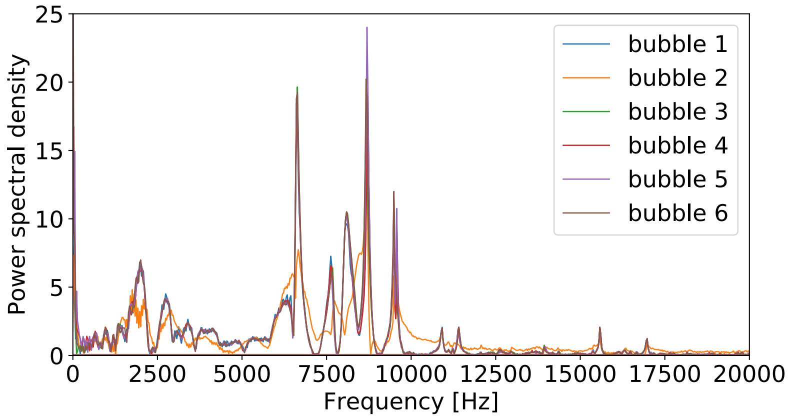

Figure 7.11: Spectral density of several bubble signals shown in Figure 7.10. There are minor variations, but in general fits good. The second bubble signal shows the highest variations but peaks at the sam frequencies.

energy.

The same repeated signal which is seen in Figure 7.11 gives basis for an understanding of the bubble radius estimate variations of bubbles of the same size. This bubble-size distribution can be seen in figure 7.12 and shows a quite wide distribution with $r_{single} = 470$ µm and is wider than expected considering the similarity in the frequency spectrum. This is mostly likely due to using the weighted averages and due to some bubble signals like the second bubble signature deviating more than others from the average. The size estimate of the bubble seems reasonable with capillaries of 25, 40 and 50 µm, but in general bubbles grow larger before releasing.

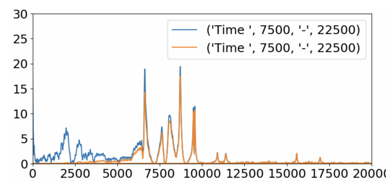

Video 7.1: Video of the frequency spectrum as a running mean is taken of 7000 consecutive datapoints.

Double bubbles By analyzing a double bubble signal it can be investigated whether they can be detected separately in size and whether they can be individually distinguished when they overlap. A segment of the signal in the time domain can be seen in figure 7.13 and dis-

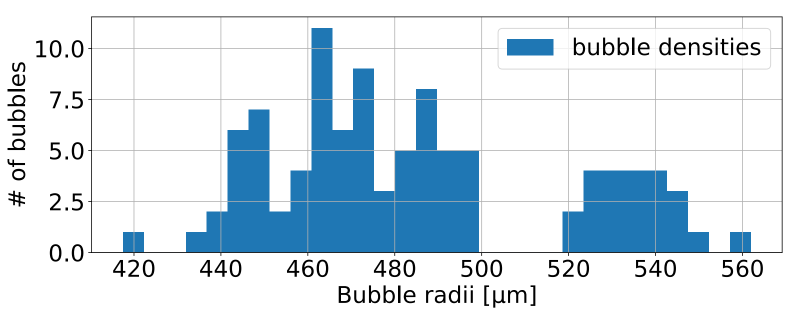

Figure 7.12: Bubble size distribution of single bubble signal. It is spread out between 430 and 550 µm and could be two different distributions around 470 µm and 530 µm, but need more data.

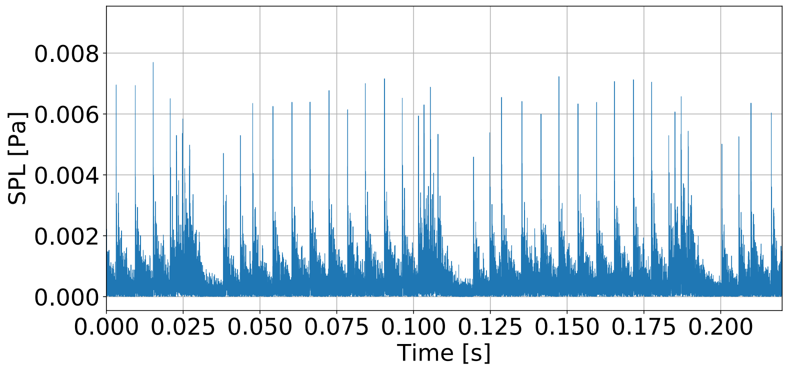

Figure 7.13: The SPL [Pa] for the double bubble signal. Two periods are present in the 0.2 second signal.

play two bubble periods with the first signal period of 6 ms and the second of 90 ms. It is also clear that the signals overlap.

Audio 7.5: double bubble capillary audio [link]

Investigating the bubble-size distribution of the double bubble signal the bubble size is much more defined compared to the single bubble signal with the average bubble size $r_{double} = 210 \pm 11$ µm though they should show two gaussian distributions which seems to be present. It also shows much smaller bubbles released compared to the single bubble distribution, since the period between bubble release is much smaller for the double bubble experiment and these bubbles do not grow as big as with the single signal this also results in smaller bubble radii.

The distribution resembles the signal of two gaussian distributions likely from the rapidly and slower repeating periods of the two bubble signals. The reason the lower distribution around 190 µm is of higher value might be that these bubbles get to form bigger bubbles compared to the quicker release from the rapid release distribution.

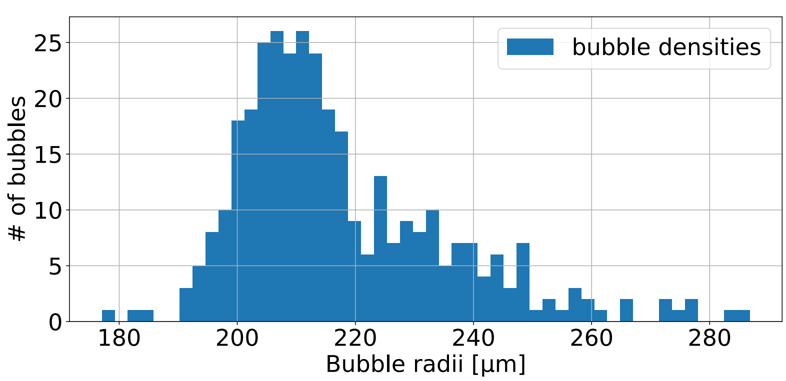

Figure 7.14: Bubble size distribution for the double bubble experiment. The distribution is quite wide spread possibly with two distributions, one around 210 ± 11 µm and one around 232 ± 15 µm.

7.3.2 Iceberg ice cube

Audio 7.6: Iceberg in water audio [link]

After doing measurements of bubble signals in a controlled environment a piece of ice cube originating from an iceberg was melted. These ice cubes are known to have air bubbles that have undergone the same process as the air bubbles in ice cores (at least it says so on the box). From this the estimated bubble-size distributions can be determined to estimate the size of these types of air bubbles. The measurements are done in the same way and with the same setup as the capillary experiments - just now the bubbles are released from the ice cube to the water.

The bubble sizes are more widely spread out from 100 µm to 500 µm which fits fairly well with the results from [Lee et al., 2013] with bubble sizes of 230-500 µm. It is not known where the icebergs came from or how they have been transported through the ice sheet. It is also possible that for ice that is stored for longer periods of time the pressure inside the pores might decrease.

7.3.3 Takeaways from the controlled bubble experiments

From these experiments it can be concluded that bubbles of certain sizes produce repeated signals, with a specific period, that are very similar in the spectral density, but even small changes in the spectral density distribution for a peak can vary the estimated bubble size.

From both the capillary and iceberg experiments it was very clear that most of the signal comes from the bubble breaking free from the ice or the capillary rather than the bubble popping on the water surface. This is observed and [Minnaert, 1933] reaches the same conclusion.

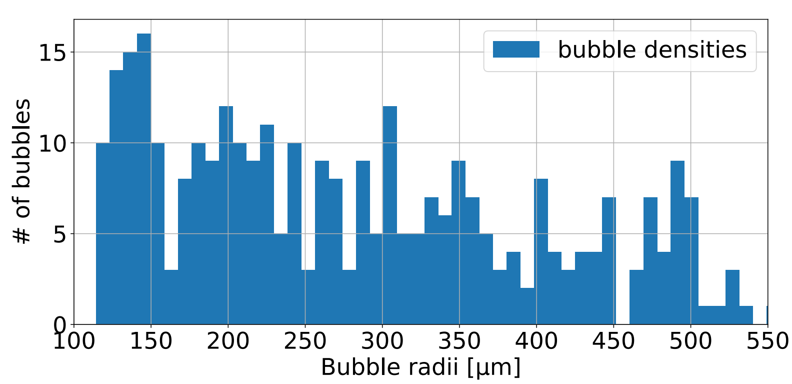

Figure 7.15: Bubble size distribution for iceberg recordings. They are widely spread out between 100 and 550 µm.

7.4 *Melting ice*

The improvements, tests and preliminary recordings has constructed the basis for analysis of melted ice recording. Four different types of ice have been melted and will be presented one by one: frozen mQ ice core, bubble-free ice core, bubbly section of bubble-free ice core and a short section of the DYE-3 ice core. Besides this, the background signal has been analyzed again before melting and all the audio files can be found by pressing the link in the captions of the audio segments in the margins.

Audio 7.7: Background noise with freezer on [link]

Audio 7.8: Background noise with freezer off [link]

Background noise As previously discussed the freezer background signal is most prominent in the low frequency spectrum which can be seen in both Figure 7.16 and 7.17.

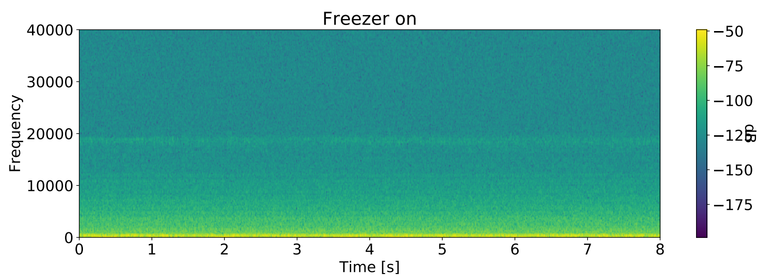

(a) The spectrogram of the background signal with the freezer on

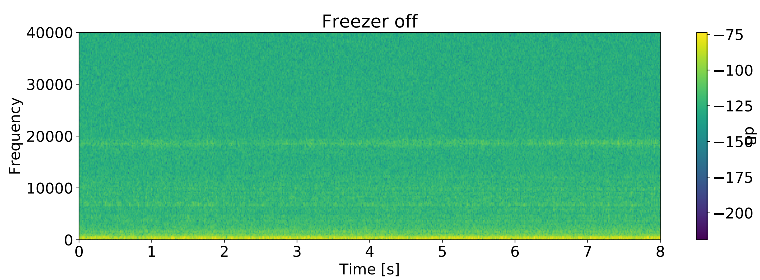

(b) The spectrogram of the background signal with the freezer on

Figure 7.16: The spectrogram of the background signal with the freezer on and off. With the freezer on a lot of power is present in the low frequency spectrum whereas when the freezer is off the power is more equal in frequency bands.

In Figure 7.17 the SPL of the frequency response of 5 second signals can be seen. It is clear to see that there is a significant decrease in the SPL just by turning off the freezer, though this creates problems with the temperature as discussed previously. This is also clearly heard by listening to Audio 7.7 and 7.8. The decrease in the background signal as the frequency increases is similar in both the freezer on and off signals. By recording while the freezer is turned off the only background signal to take into consideration is below 1-2 kHz whereas the strong freezer on signal decreases steadily down to 20 kHz which is well beyond the bubble signals as can also be seen in

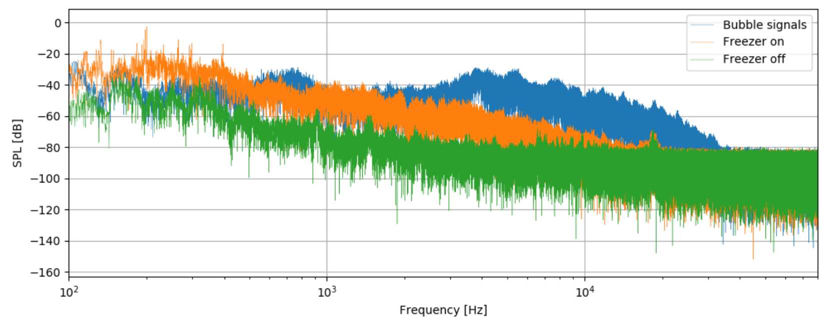

Figure 7.17: SPL of the background signals all of 5 seconds. Blue is a bubble signal, orange is the freezer on background signals and the green signal is the background signal of the freezer off.

Figure 7.17. This green noise level in Figure 7.17 is the level after all the improvements described previously and has to be dealt with in post-processing.

Audio 7.9: mQ ice core melting audio [link]

7.4.1 mQ ice

mQ is a very purified type of water that works well in laboratories as no impurities build up and clog the system. The mQ ice cores are just made by filling an ice core bag and freezing the water, making sure not to fill it completely so there is space for it to expand and reduce cracking along with other features. They are usually filled with small bubbles but these are of course not formed and compressed under the same pressure as an air bubble in an actual ice core.

It works brilliantly as test ice since small bubbles constantly pop but the pressure coming from the signal is much smaller, though the frequency response to these signals are comparative to true bubble signals. The smaller pressure means the signal is not quite as clear as e.g. in the Bern video (Video 4.1). In Figure 7.18 the frequency response over time can be seen. This shows the variation in smaller and bigger signals as one would expect.

mQ ice results in more systematic errors when estimating the

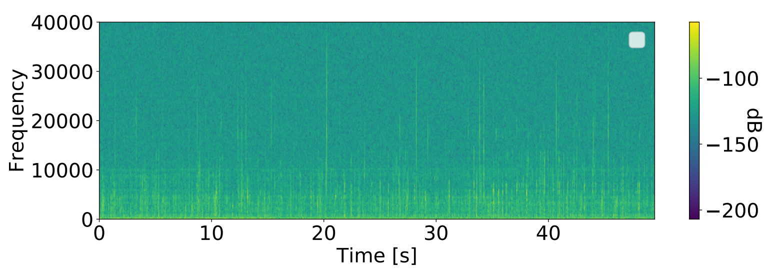

Figure 7.18: SPL of the background signals all of 5 seconds. Blue is a bubble signal, orange is the freezer on background signals and the green signal is the background signal of the freezer off.

TAC as e.g. cracks and micro fractures as well as bubbles that are being formed in an irregular way through the freezing process. By observation the bubbles are also formed in more varying ways and shapes and are also more elongated due to the freezing process than air bubbles in ice cores that are densified as explaind in Section 1.1. Some of these variations can be seen in Appendix H.

7.4.2 *Bubble free*

Audio 7.10: Bubble free ice melting audio [link]

Bubble free ice gives the exact opposite signal of the one wanted and that is why it is one of the best measures of how well all the improvements implemented in the previous chapters work. This has all audio signals, from the freezer, to ice scraping the core guide, cracks, and anything else, besides the bubble signals explored. Listening to Audio 7.10 it can be heard that none or very little audio signal is introduced by ice melting, moving or cracking. This suggests that no other origins of noise have been introduced. Inspecting the spectrogram in Figure 7.19 some small signal is seen but since the signal and most of the frequencies are bright green it means that the signals are not powerful and the signals and the background is very similar. These few signals need to be studied in the further work of this project to examine whether they can be classified and omitted from the final signal should they need to, since these could be cracks or other features present in ice cores as well.

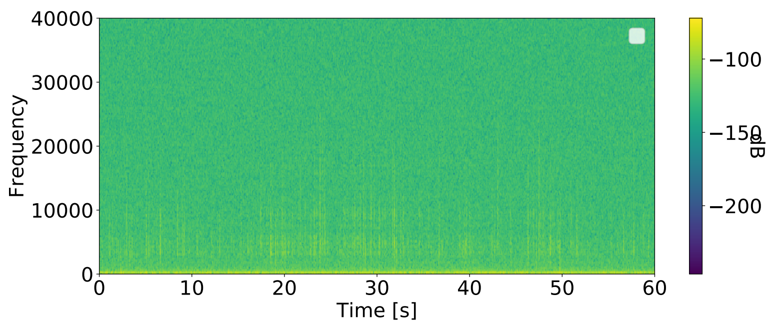

Figure 7.19: Spectrogram of the bubble free ice core signal

Audio 7.11: Bubbles in bubble free ice melting audio [link]

7.4.3 *Bubble free with few bubbles*

As explained in Section 5.2 sometimes bubbles of radius > 2 mm were introduced. These bubbles are quite larger than air bubbles in mQ ice and ice cores and should therefore introduce a different response in the frequency spectrum since they are released under the same circumstances as both mQ and DYE-3. This means the values

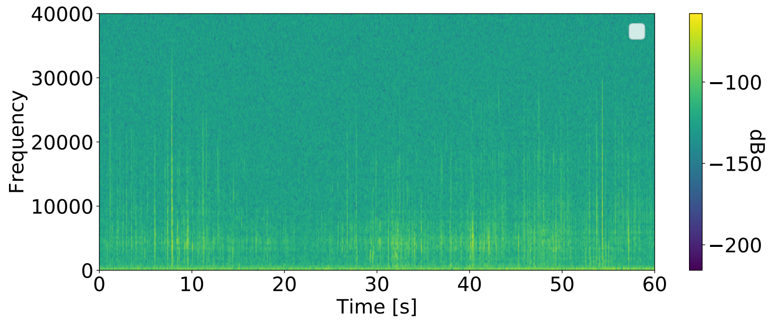

Figure 7.20: Spectrogram of the bubble-free ice with bigger bubbles

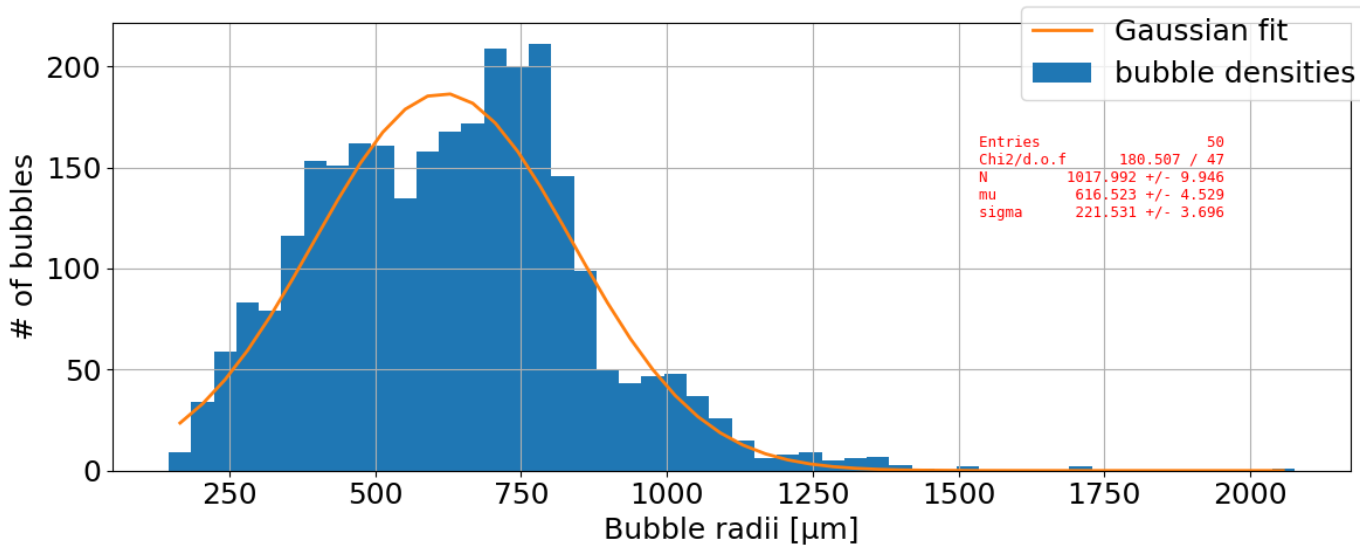

Figure 7.21: Bubble-size distribution of the ice core with big bubbles from the bubble free ice.

in the Minnaert equation (Eq. 3.23) are all the same except the radius. This should introduce a theoretical response that are in a lower frequency band than those of mQ and ice core air bubbles. Therefore this type of ice has also been recorded to test this hypothesis.

The spectrogram in Figure 7.20 shows the frequency as a function of time containing the ice core with few but bigger bubbles. The signal is very prominent around 5 kHz and much weaker in the higher frequencies compared with the true bubbles that are more spread out. The conversion to bubble sizes can be observed in Figure 7.21.

As the bubbles are estimated to be radius > 2mm these are not found using this method. Only few bubbles are estimated to have over 1 mm in radius. This suggests something is wrong in the analysis and in the estimate of the bubble amount and size as there is, by observation, not thousands of bubbles.

7.4.4 DYE-3

Audio 7.12: DYE-3 sample melting audio [link]

All improvements, tests, melting of ice and optimization has led to melting a real ice core with bubbles formed during the densification process explained in Chapter 1.1. It was deemed that the noise level was reduced sufficiently and the test of bubble signals and method both during the controlled experiment and by melting ice was of high quality for a test of principle on a 20 cm sample of real ice core, DYE-3.

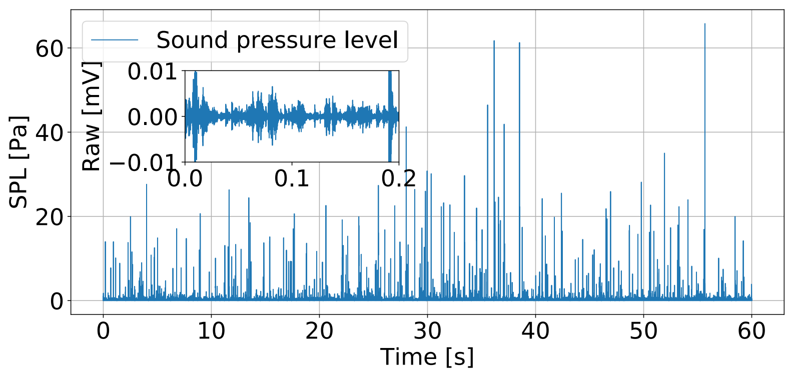

Figure 7.22: Rms signal of the DYE-3 core melted with inset of the raw signal.

The ice melted was not documented in an ice core bag and has not been marked for a specific depth or even a specific core. It is thought to be DYE-3 scraps but it is not certain. Therefore the TAC value can not be compared directly with values from a certain depth of the DYE-3 TAC record but will be compared to the general and average

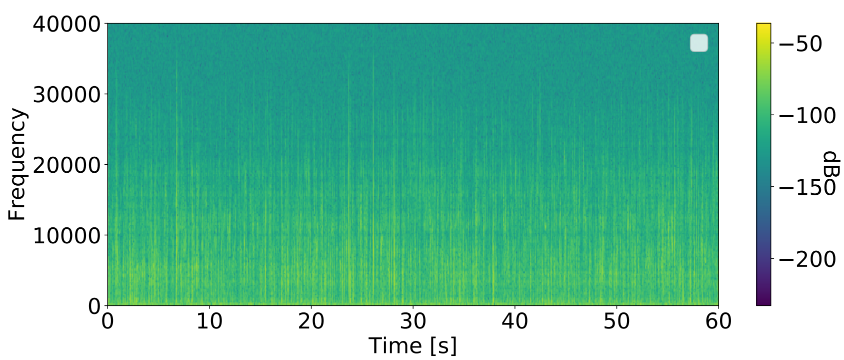

Figure 7.23: Spectrogram of the DYE-3 recording

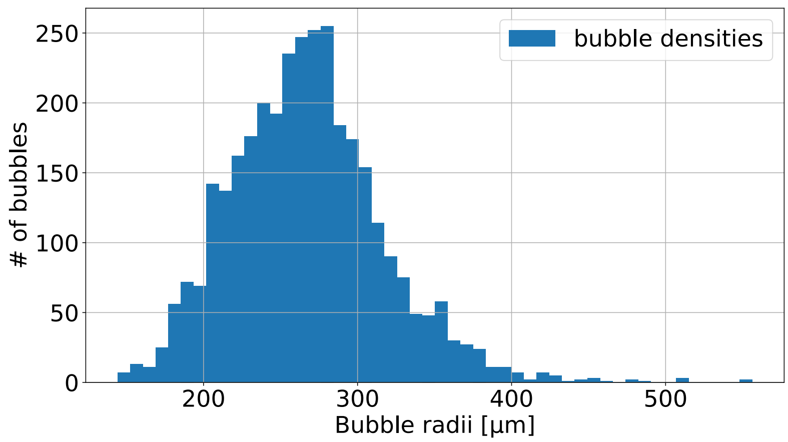

Figure 7.24: Bubble-size distribution of DYE-3 recording.

value of around 10% air content as explained in section 2.1.

In Figure 7.22 the RMS signal is clearly seen with quite a few prominent signals present. When inspecting the raw signals in the inset it is clear that the bubbles are constantly popping and often the bubble signals overlap. The signal show the tendency of a sharp increase in pressure followed by a slower decrease as expected for bubbles.

By investigating the spectrogram in figure 7.23 the SPL is most prominent below 10 kHz but has significant power levels up through 20 and 30 kHz. From this the same analysis as previously used is implemented and the bubble size distribution is found.

This bubble-size distribution can be found in Figure 7.24. Through the analysis described previously 3336 individual signals are investigated and the bubble radii is estimated which gives the bubble-size distribution in Figure 7.24 and the total air content value described in Table 7.2. In Table 7.2 the theoretical value of the TAC is compared to the value obtained from the data analysis. The theoretical value comes from a melt rate of 2 cm/min and a core cross section of 34x34 mm. The experimental value is taken for one minute of recordings.

Theoretical	Experimental
$2.31 \cdot 10^{-6} m^3$	$2.95 \cdot 10^{-7}\ m^3$

Table 7.2: The theoretical value of the TAC is compared to the value obtained from the data analysis. The theoretical value comes from a melt rate of 2 cm/min and a core cross section of 34x34 mm and the average value of 10 % TAC. The experimental value is taken for one minute of recordings.

The data analysis value is a factor of ten lower than that of the theoretical which could be due to a variety of parameters especially in the peak finding part of the data analysis. The current script finds the most prominent peak of the raw signal and finds and includes all peaks that has a power a thousand times weaker than this signal which might be too much or little but at the same time the signal is almost of the right order at 10^{-7}m^3. Therefore this parameter should not be tuned much. The average weighting of the power peaks for each signal might include too much or too little of the peak signal.

The values used in the Minneart equation might not be correct even though, as explained previously, the same values are used in [Lee et al., 2013] with glacier bubbles being released to water. These are estimated to work accordingly to this setup and the air bubbles being released into water, thoug some might be released directly to air which changes some of the parameters.

The bubble-size and bubble-number distributions found in section 1.3 are also far from the values given by the data analysis. The physical bubble size is quite a bit smaller but this is also a different core with new parameters and the depth is unknown for the melted ice. Comparing to [Lee et al., 2013] the bubble sizes are also significantly bigger suggesting that something went wrong, though the bubble sizes vary a lot. These bubble values are also bigger than the average values of Antarcic ice cores presented in Section 1.3. This is also the same for the bubble amounts found by the analysis. Using a value of 400 bubbles cm^{-3} from Section 1.3 and with a meltrate of 2 cm/min there should be upwards of 9200 individual bubbles that are being popped in a 2 cm core section. Though many bubble signals are found it is not quite enough. With over 9000 bubble signal per minute several of these are most likely going to be overlapping and at the data analysis' current state this problem has not been addressed.

Many of the parameters used are initial values of values estimated by observation or from other papers and can definitely be fine tuned for a more automatic system in the future. It should be further investigated in the future work of this research project.

This method does describe a way of estimating TAC values for ice core and is a proof of concept which still has to be fine tuned.

8 Conclusion and further work

Through the tests, optimizations, improvements and system design implemented it has been proved that estimating total air content (TAC) values in ice cores is possible. This is done through audio recordings of ice cores, from which the prominent frequencies can be detected and used to estimate the bubble radius by the Minnaert equation described in Section 3.5. Though it is possible several things both in the setup and the data analysis needs to be improved upon.

This point has been reached by doing preliminary recordings of ice cores being melted during a melting campaign in Bern. From this the proof of concept of detecting single bubble signals in the frequency spectrum was proved.

By learning and improving the current CFA setup in Copenhagen through e.g. a new ice core guide and sound absorption the ice has been possible to melt and origins of noise has been limited. An experiment was conducted to estimate the melt rate parameters as this is an important parameter for knowing the amount of ice melted during a certain period of time. This increased the knowledge significantly of how changing parameters affect the melt rate. The melting rate can be improved upon in the future and made more stable and adjusted automatically through the temperature variation in the melt head.

To test the setup several designs were constructed and tested to get both ice cores with varying amounts of bubbles as well as bubble-free ice. The ice core designed to have varying sizes and amounts of bubbles showed little improvement and was therefore stopped. If artificial ice with varying bubble sizes are to be constructed in the future this could prove valuable for testing. The bubble-free setup which already existed was improved upon with a new stepper motor for more possibilities of changing parameters such as speed and transitions. This proved to create bubble-free ice as well as ice with transitions between bubble-free and bubbly ice, though the bubbles were big (radius > 2 mm).

Ultimately the four types of ice: mQ, bubble-free, bubble-free with bubbles and the ice core DYE-3 was melted and their audio signals were analyzed. This improved the knowledge on sources of noise and was used to estimate TAC values which was compared to the average of 10 % TAC in previous ice cores as described in Section 2.1 and proved to be of the right order. They were also compared to the bubble-sizes and bubble-number distributions described in Section 1.3. Through the current data analysis the bubbles are estimated have fewer but bigger bubbles which most likely stems from the data analysis which needs to be improved upon.

This thesis lays the foundation for further research and implementation into using microphones and audio signals in ice core research in the future. This signal has not been thoroughly investigated previously and does not need more ice to be melted. It could in future melt campaigns be included in the setup after more optimizations.

8.1 Further work

The first step of improvements in this 3 year research project should be to improve the data analysis. The foundation has been established with estimations of steps to be taken but at this moment the cut off values of included peaks are just best guesses. Besides this signals that are not bubble signals need to be identified and discarded as well as overlaying bubble signals that need to be separately analyzed. When Minnaert did his experiments in 1933 the digital and highly advanced microphones used today did not exist. The individual bubble spectral densities are more complex than described in [Minnaert, 1933] and should be handled accordingly. This focus of understanding the individual bubble spectral densities are important for getting the specific frequencies used in the Minnaert equation to get the radius and give a significant source for error. The values used in the Minnaert equation are stolen from [Lee et al., 2013], but should be looked into whether it is the right values. For estimations of TAC a more accurate melt rate needs to be incorporated as this describes the amount of ice melted within a certain time limit and thus how many bubbles should theoretically be released. This can also be improved by using OpenCV for feature tracking and estimating melt rates.

As has been explained during the thesis the effect of microphone placement as well as various microphone specifications can be made further complex and microphones which records above 20 kHz might be of interest to investigate. The data analysis at this point only includes the Shure VP82 microphone but at a further state signals radiating from different sides of the ice core might show various responses in microphones placed in different spots in the freezer and a future data analysis might be able to incorporate several microphone signals in the process.

9 Bibliography

W.A. Al-Masry, E.M. Ali, and Y.M. Aqeel. Determination of bubble characteristics in bubble columns using statistical analysis of acoustic sound measurements. *Chemical Engineering Research and Design*, 83(10):1196–1207, 2005. ISSN 0263-8762. DOI: https://doi.org/10.1205/cherd.05014. URL https://www.sciencedirect.com/science/article/pii/S0263876205728203.

J. M. Barnola, P. Pimienta, D. Raynaud, and Y. S. Korotkevich. Co2-climate relationship as deduced from the vostok ice core: a re-examination based on new measurements and on a re-evaluation of the air dating. *Tellus B: Chemical and Physical Meteorology*, 43(2):83–90, 1991. DOI: 10.3402/tellusb.v43i2.15249. URL https://doi.org/10.3402/tellusb.v43i2.15249.

Verena Bendel, Kai J. Ueltzhöffer, Johannes Freitag, Sepp Kipfstuhl, Werner F. Kuhs, Christoph S. Garbe, and Sérgio H. Faria. High-resolution variations in size, number and arrangement of air bubbles in the epica dml (antarctica) ice core. *Journal of Glaciology*, 59(217):972–980, 2013. DOI: 10.3189/2013JoG12J245.

Matthias Bigler, Anders Svensson, Ernesto Kettner, Paul Vallelonga, Maibritt E. Nielsen, and Jørgen Peder Steffensen. Optimization of high-resolution continuous flow analysis for transient climate signals in ice cores. *Environmental Science & Technology*, 45(10):4483–4489, 2011. DOI: 10.1021/es200118j. URL https://doi.org/10.1021/es200118j. PMID: 21504155.

C. Buizert. *Studies of Firn Air*, pages 361–372. 01 2013. ISBN 978-0-444-53642-6. DOI: 10.1016/B978-0-444-53643-3.00330-7.

K. M. Cuffey and W. S. B. Paterson. *Physics of Glaciers*, pages 11–28, 614–660. 2010. ISBN 978-0-12-369461-4.

O. Eicher, M. Baumgartner, A. Schilt, J. Schmitt, J. Schwander, T. F. Stocker, and H. Fischer. Climatic and insolation control on the high-resolution total air content in the ngrip ice core. *Climate of the Past*, 12(10): 1979–1993, 2016. DOI: 10.5194/cp-12-1979-2016. URL https://cp.copernicus.org/articles/12/1979/2016/.

Jared H. Microphone basics: The beginner's guide stuff you need to know: Ln, May 2021a. URL https://ledgernote.com/columns/studio-recording/microphone-basics/.

Jared H. The types of microphones amp; their uses (when amp; why), May 2021b. URL https://ledgernote.com/columns/studio-recording/types-of-microphones/.

Jared H. Microphone pickup patterns: Understanding amp; using directionality: Ln, Feb 2021c. URL https://ledgernote.com/columns/studio-recording/microphone-pickup-patterns-directionality/.

Michael Herron and Chester Langway. Firn densification: An empirical model. *Journal of Glaciology*, 25: 373–385, 01 1980. DOI: 10.3189/s0022143000015239.

Susan Herron and Chester Langway. Derivation of paleoelevatio ns from total air content of two deep greenland ice cores. *The Physical Basis of Ice Sheet Modelling, Proceedings of the Vancouver Symposium*, 170, 01 1987.

ISO 3744:2010(en). Acoustics — determination of sound power levels and sound energy levels of noise sources using sound pressure — engineering methods for an essentially free field over a reflecting plane. Standard, International Organization for Standardization, Geneva, CH, October 2010.

Finn Jacobsen, Torben Poulsen, Jens Rindel, Anders Gade, and Mogens Ohlrich. *Fundamentals of Acoustics and Noise Control*. 09 2011.

D. Jensen, Mary Albert, Ala Aldahan, Nobuhiko Azuma, David Balslev-Clausen, Michelle Baumgartner, A. Berggren, M. Bigler, T. Binder, T. Blunier, J. Bourgeois, Edward Brook, Susanne Lilja Buchardt, C. Buizert, Emilie Capron, Jérôme Chappellaz, J. Chung, H. Clausen, Ivana Cvijanovic, and Jiancheng Zheng. Eemian interglacial reconstructed from a greenland folded ice core. *Nature*, 493:489–494, 01 2013. DOI: 10.1038/nature11789.

J. Jouzel. A brief history of ice core science over the last 50 yr. *Climate of the Past*, 9(6):2525–2547, November 2013. ISSN 1814-9332. DOI: 10.5194/cp-9-2525-2013. URL `https://cp.copernicus.org/articles/9/2525/2013/`.

Takao Kameda, Masayoshi Nakawo, Shinji Mae, Okitsugu Watanabe, and Renji Naruse. Thinning of the ice sheet estimated from total gas content of ice cores in mizuho plateau, east antarctica. *Annals of Glaciology*, 14:131–135, 1990. DOI: 10.3189/S0260305500008429.

Qingkai Kong, Timmy Siauw, and Alexandre M. Bayen. Chapter 24 - fourier transform. In Qingkai Kong, Timmy Siauw, and Alexandre M. Bayen, editors, *Python Programming and Numerical Methods*, pages 415–443. Academic Press, 2021. ISBN 978-0-12-819549-9. DOI: https://doi.org/10.1016/B978-0-12-819549-9.00034-8. URL `https://www.sciencedirect.com/science/article/pii/B9780128195499000348`.

Benny Lautrup. *Physics of continuous matter. Exotic and everyday phenomena in the macroscopic world. 2nd ed*. 01 2004.

K. Lee, P. Wilson, and E. Pettit. Underwater sound radiated by bubbles released by melting glacier ice. *Journal of the Acoustical Society of America*, 20:070004, 2013.

T.G. Leighton. 3 - the freely-oscillating bubble. In T.G. Leighton, editor, *The Acoustic Bubble*, pages 129–286. Academic Press, 1994. ISBN 978-0-12-441920-9. DOI: https://doi.org/10.1016/B978-0-12-441920-9.50008-0. URL `https://www.sciencedirect.com/science/article/pii/B9780124419209500080`.

V. Lipenkov. How air bubbles form in polar ice. *Earth's Cryosphere*, 22:16–28, 01 2018. DOI: 10.21782/KZ1560-7496-2018-2.

V. Lipenkov and Andrey Salamatin. Steady-state size distribution of air bubbles in polar ice. *Ice and Snow*, 128, 03 2015. DOI: 10.15356/2076-6734-2014-4-20-31.

V. Lipenkov, F. Candaudap, J. Ravoire, E. Dulac, and D. Raynaud. A new device for the measurement of air content in polar ice. *Journal of Glaciology*, 41(138):423–429, 1995. DOI: 10.3189/S0022143000016294.

Vladimir Ya. Lipenkov. Air bubbles and air-hydrate crystals in the vostok ice core. In *Physics of Ice Core Records*, pages 327–358. Hokkaido University Press, 2000. URL http://hdl.handle.net/2115/32474.

Vladimir Ya. Lipenkov, Andrey N. Salamatin, and Paul Duval. Bubbly-ice densification in ice sheets: Ii. applications. *Journal of Glaciology*, 43(145):397–407, 1997. DOI: 10.3189/S0022143000034973.

P. Martinerie, V.Ya. Lipenkov, and D. Raynaud. Correction of air-content measurements in polar ice for the effect of cut bubbles at the surface of the sample. *Journal of Glaciology*, 36(124):299–303, 1990. DOI: 10.3189/002214390793701282.

P. Martinerie, V. Y. Lipenkov, D. Raynaud, J. Chappellaz, N. I. Barkov, and C. Lorius. Air content paleo record in the vostok ice core (antarctica): A mixed record of climatic and glaciological parameters. *Journal of Geophysical Research: Atmospheres*, 99(D5):10565–10576, 1994. DOI: https://doi.org/10.1029/93JD03223. URL https://agupubs.onlinelibrary.wiley.com/doi/abs/10.1029/93JD03223.

Patricia Martinerie, Dominique Raynaud, David M. Etheridge, Jean-Marc Barnola, and Danièle Mazaudier. Physical and climatic parameters which influence the air content in polar ice. *Earth and Planetary Science Letters*, 112(1):1 – 13, 1992. ISSN 0012-821X. DOI: https://doi.org/10.1016/0012-821X(92)90002-D. URL http://www.sciencedirect.com/science/article/pii/0012821X9290002D.

Kyle Mathias. What are bad acoustics?, Oct 2019. URL https://audiouniversityonline.com/studio-acoustics/.

Stanley L. Miller. Clathrate hydrates of air in antarctic ice. *Science*, 165(3892):489–490, 1969. DOI: 10.1126/science.165.3892.489. URL https://science.sciencemag.org/content/165/3892/489.

M. Minnaert. Xvi.on musical air-bubbles and the sounds of running water. *Philosophical Magazine Series 1*, 16: 235–248, 1933.

Kerttu Maria Peensoo. Developing a method for high resolution water isotope measurements in ice cores. Master's thesis, University of Copenhagen, 2021.

Erin Pettit, Kevin Lee, Joel Brann, Jeffrey Nystuen, Preston Wilson, and Shad O'Neel. Unusually loud ambient noise in tidewater glacier fjords: A signal of ice melt. *Geophysical Research Letters*, 42, 03 2015. DOI: 10.1002/2014GL062950.

John G. Proakis and Dimitris G. Manolakis. *Digital Signal Processing - Principles, Algorithms and Applications. 4th ed.* 2007.

D. Raynaud and B. Lebel. Total gas content and surface elevation of polar ice sheets. , 281(5729):289–291, September 1979. DOI: 10.1038/281289a0.

D. Raynaud, J. Chappellaz, J. M. Barnola, Y. S. Korotkevich, and C. Lorius. Climatic and CH4 cycle implications of glacial–interglacial CH4 change in the Vostok ice core. *Nature*, 333(6174):655–657, June 1988. ISSN 1476-4687. DOI: 10.1038/333655a0. URL https://doi.org/10.1038/333655a0.

Dominique Raynaud, Jerôme Chappellaz, Catherine Ritz, and Patricia Martinerie. Air content along the greenland ice core project core: A record of surface climatic parameters and elevation in central greenland. *Journal of Geophysical Research: Oceans*, 102(C12):26607–26613, 1997. DOI: https://doi.org/10.1029/97JC01908. URL https://agupubs.onlinelibrary.wiley.com/doi/abs/10.1029/97JC01908.

Muhammad Ryan. Brief introduction of hamming and hanning function as the preprocessing of discrete fourier..., Sep 2019. URL https://towardsdatascience.com/brief-introduction-of-hamming-and-hanning-function-as-the-preprocessing-of-discrete-fourier-8b87fe538bb

J. Schwander, T. Sowers, J.-M. Barnola, T. Blunier, A. Fuchs, and B. Malaizé. Age scale of the air in the summit ice: Implication for glacial-interglacial temperature change. *Journal of Geophysical Research: Atmospheres*, 102(D16):19483–19493, 1997. DOI: 10.1029/97JD01309. URL https://agupubs.onlinelibrary.wiley.com/doi/abs/10.1029/97JD01309.

M.K. Spencer, R.B. Alley, and J.J. Fitzpatrick. Developing a bubble number-density paleoclimatic indicator for glacier ice. *Journal of Glaciology*, 52(178):358–364, 2006. DOI: 10.3189/172756506781828638.

Kai Ueltzhöffer, Verena Bendel, Johannes Freitag, Sepp Kipfstuhl, Dietmar Wagenbach, Sérgio Faria, and Christoph Garbe. Distribution of air bubbles in the edml and edc (antarctica) ice cores, using a new method of automatic image analysis. *Journal of Glaciology*, 56:339–348, 06 2010. DOI: 10.3189/002214310791968511.

D.S Wilkinson and M.F Ashby. Pressure sintering by power law creep. *Acta Metallurgica*, 23(11):1277 – 1285, 1975. ISSN 0001-6160. DOI: https://doi.org/10.1016/0001-6160(75)90136-4. URL http://www.sciencedirect.com/science/article/pii/0001616075901364.

Part III

APPENDICES

A H-L densification model

Herron-Langway densification model [Herron and Langway, 1980]

The H-L model is a semi-empirical model attempting to predict the depth-density profile using only surface temperature, accumulation rate and initial snow density for a given site without obtaining laboratory measurements. Three stages are parameterized by density with the first from intial snow density to critical density 550 kgm^{-3}, due to rapid densification and snowpacking. A slower stage of densification is the second from the critical density to air close-off density $550 - 820\ \mathrm{kgm}^{-3}$. The final stage of densification is further compaction and compression of air bubbles in the ice from $820 - 917\ \mathrm{kgm}^{-3}$. The last stage is not used in this model as the rapid densification is the investigated area.

The main assumption is that the densification is proportional to the stress of the load of overburden snow.

$$\frac{\mathrm{d}\rho}{\rho_i - \rho} = \mathrm{constant}\rho \mathrm{d}h \tag{A.1}$$

where ρ_i is the density of ice $917\ \mathrm{kgm}^{-3}$. This implies a linear relationsip between $\ln[\rho/\rho_i - \rho]$ and depth.

To solve for the densification rate the accumulation rate and temperature is constant at each site, but with varying dependencies for the different stages.

$$\frac{d\rho}{dt} = A^a K_0(\rho_i - \rho) \qquad \rho < 550\ \mathrm{kgm}^{-3} \tag{A.2}$$

$$\frac{d\rho}{dt} = A^b K_1(\rho_i - \rho) \qquad 550\ \mathrm{kgm}^{-3} < \rho < \rho_i \tag{A.3}$$

Where a and b are values determined by slopes of densification for each stage at equivalent accumulation and temperature rates. These values are often set as 1 and 0.5 respectively derived from graphs of depth vs. $\ln[\rho/\rho_i - \rho]$ at different sites. K_0 and K_1 are determined using Arhenius type equations

$$K_0 = 11\exp\left(-\frac{10160}{RT}\right) \qquad K_1 = 575\exp\left(-\frac{21400}{RT}\right) \tag{A.4}$$

with R = 8.314 $\mathrm{JK}^{-1}\mathrm{mole}^{-1}$.

From this relations of depth-density and depth-age can be found. For the upper stage of the firn.

$$z(\rho) = \frac{1}{\rho_i K_0}\left(\ln\left(\frac{\rho}{\rho_i - \rho}\right) - \ln\left(\frac{\rho_0}{\rho_i - \rho_0}\right)\right) \tag{A.5}$$

$$t(\rho) = \frac{1}{K_0 A}\ln\left(\frac{\rho_i - \rho_0}{\rho_i - \rho}\right) \tag{A.6}$$

and for the second and lower stage of firn the density at depth h and age

$$z(\rho) = \frac{\sqrt{A}}{\rho_i K_1}\left(\ln\left(\frac{\rho}{\rho_i - \rho}\right) - \ln\left(\frac{\rho_c}{\rho_i - \rho_c}\right)\right) + z_c \tag{A.7}$$

$$t(\rho) = \frac{1}{K_1\sqrt{A}}\ln\left(\frac{\rho_i - \rho_c}{\rho_i - \rho}\right) + t_c \tag{A.8}$$

These analysis can be used to predict climatic changes by variation from the model. See rest of [Herron and Langway, 1980]

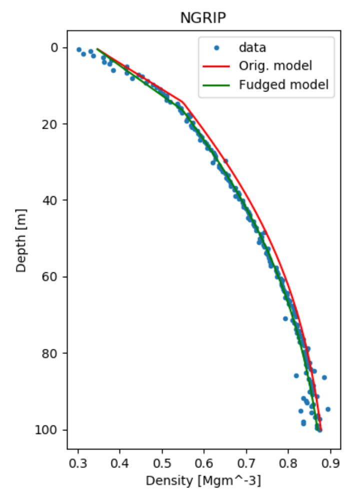

Figure A.1: NGRIP density profile using an H-L model and an H-L model with optimized parameters.

B Bubble creation models

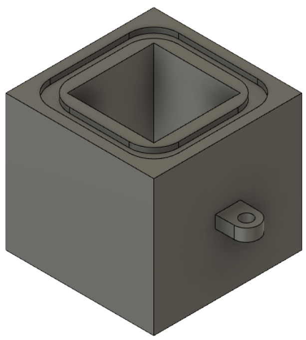

(a) Setup 2.0

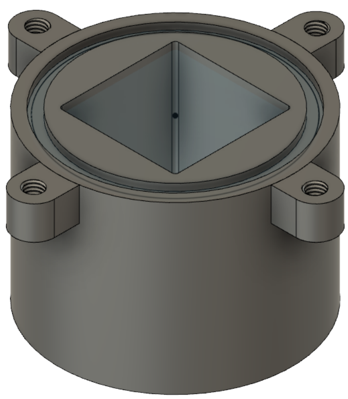

(b) Setup 3.0

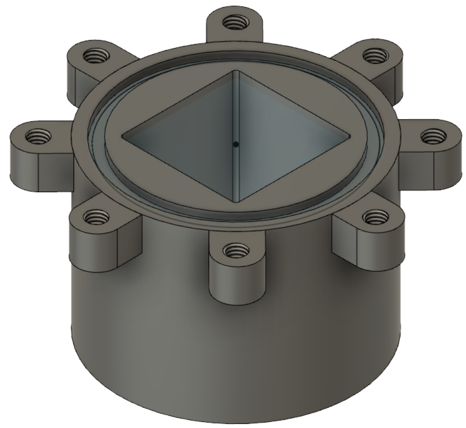

(c) Setup 4.0

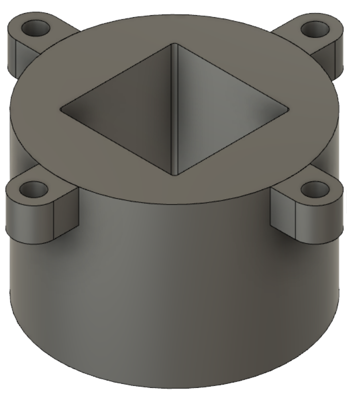

(d) Setup 5.0

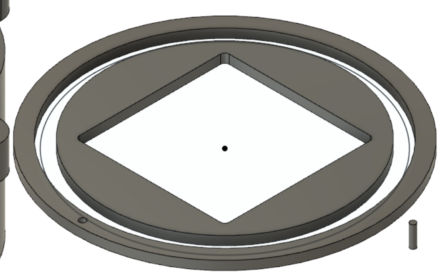

(e) setup 5.0 middle

Figure B.1: Several iterations of the bottom part's evolution from a square piece in a) to a round with more bolts in b) and c). The final setup consisted of separate pieces in between the parts on the next page.

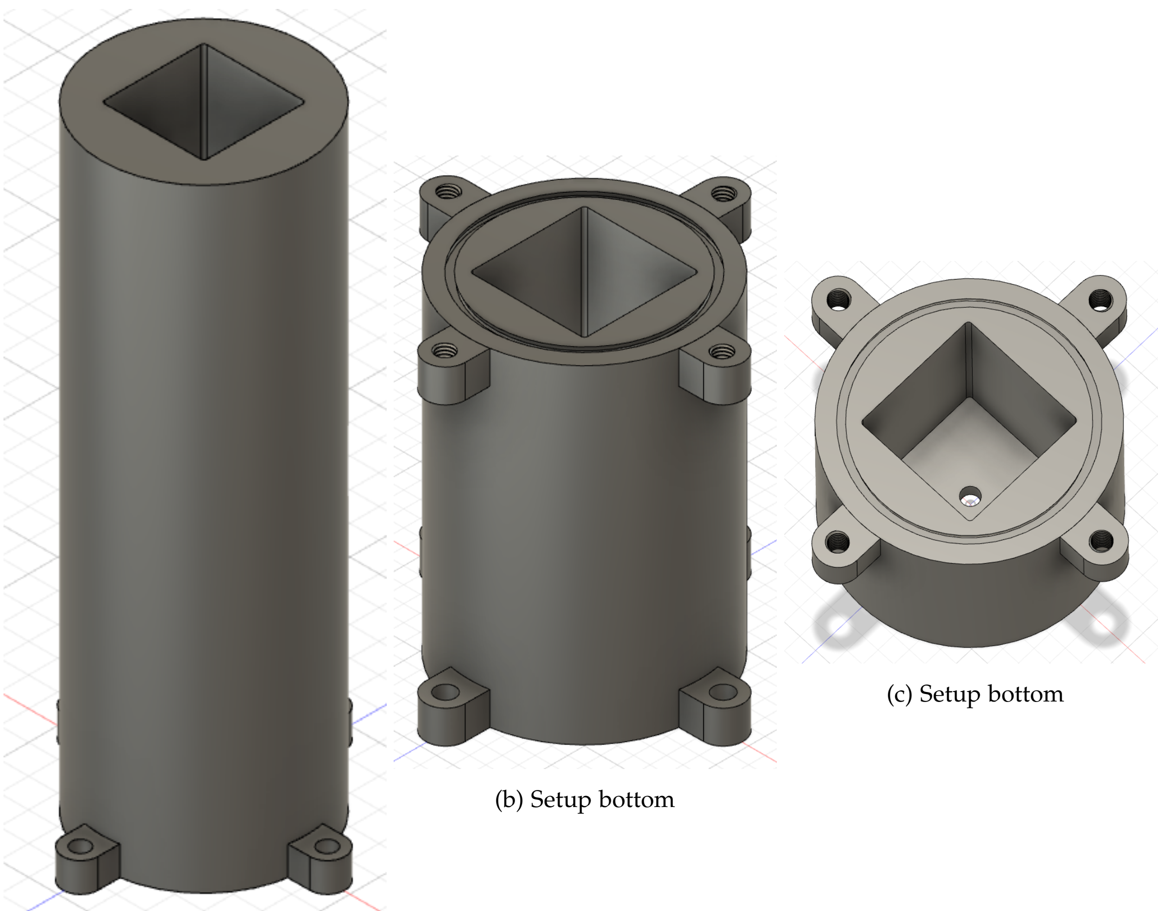

(a) Setup bottom

(b) Setup bottom

(c) Setup bottom

Figure B.2: The three components of the artificial ice core with bubbles experiment. They are set on top of each other and are connected by bolts. An o-ring is in between the parts to prevent leaks.

C Bubble-free method

Most of the bubble-free ice setup procedure follows the one described on the Gaslab wiki.

Description

The bubble-free ice setup produces - as its name implies - bubble-free ice. This ice can be used for a variety of tests e.g. blank tests on various extraction systems. The heating wire is Type RS 379-722, Resistance is 1920 Ohm.

Degassing under vacuum

The cylindrical holder is filled with milliQ water, which can be found in the CFA and Chemistry labs. As a first purification step the water is degassed under vacuum by connecting it to a roughing pump. A liquid nitrogen cooled water trap is inserted in the pump line to prevent water damage to the pump. The setup can be seen in Figure C.1

The steps are:

- Screw off the wing nuts and take the top off. Fill the holder with milliQ water (does not need to be the highest purity). Push the cylinder down to prevent leakage at the bottom.

- Make sure the magnetic stir bar is in and quickly put on the lid and screw in the wing-nuts. As it gets tight it prevents leakage. Make sure to use a polymer stirring rod. The glass ones damage the aluminium of the bottom plate, causing black metal particles in the ice.

- There have been problems with supercooled water in the past (not recently). If this happens, then put a little bit of regular tap water in to give the ice crystals a site to nucleate.

- Make sure to close the swage valve (the one on the lid).

- Place the holder on a magnetic stirrer and turn on both stirring and heater. The heat makes the air easier to remove from the water.
- Make sure there is no water in the water trap, will it with liquid nitrogen and cool down the trap.
- Connect all connections on the pump lines and tighten them.
- Start the pump and keep the swage valve closed.
- Evacuate below 0.1 mBar.
- Keep the pump on and open the swage valve, this should produce plenty of bubbles in the water.
- Leave the water for at least 30 min, preferably more than 60 min. If less than 30 min. bubbles will form throughout the ice.
- Close the swage valve and cap it. Turn off the pump. There is water in the valve and we do not know whether the vacuum holds if it freezes.

  The vacuum on the holder should hold for a few weeks at most.

Slow freezing from bottom up

The purification step described above is insufficient to completely degas the water. In the second phase of the procedure the water is frozen slowly from the bottom up. As long as the dissolved gas can diffuse faster than the ice grows the gas will not be trapped inside the ice crystal. The holder gets covered with the black heating tube. The tube consists of a copper sheet with heating wire wrapped around it. This is covered by 2 cm of insulating material. The tube temperature is controlled by the output voltage of an AC power source. The heating tube is slowly raised by a motor through a gear bow that lowers the RPMs by a factor of 1000, so that the tube is raised slowly and around 10 cm per day.

The steps:

- Place the holder with the degassed water on the floor of the freezer.
- Make sure the heating jacket is all the way down and place the heating jacket over the holder.
- Turn on the heating jacket and the motor power supplies.
- Set the speed parameters on the pc.

  - Log in to guest account on the pc. password is: isolab-x20-1
  - Open the terminal and go to stepper_motor folder by typing `cd documents/stepper_motor/`
  - Run python file LA_GUI_v2.py by typing `python LA_GUI_v2.py` which should open a new window and say "connection is established2 in terminal.
  - Turn on power supply and set voltage between 24-30 V
  - In the GUI/opened window choose your preferred settings (standard is direction 1, speed 0.0011 mm/s and distance 270 mm)
  - Direction: 1 moves the heating tube up, -1 moves it down.
  - Speed: set the speed. Highest around 1mm/s, lowest 0.0009 mm/s.
  - Distance move the tube the set distance in mm.
  - ignore the rest of the parameters.
  - Run it.

  Some numbers and good advice:

- Always check the logbook for the latest numbers and comments on ice growth.
- A voltage of 150 V on the heating tube has given good results. At this voltage the temperature inside the tube stays around 4°C.
- If need be for trouble shooting, try putting a temperature logger on top of the holder during the process.

Getting the ice out

Several days have passed and your bubble-free ice has now been created with more or less success.

- Take out the holder and place it at room temperature. Leave it for a minimum of 20 min. Do not pour water on the holder as this will just cause the ice to crack. Take it easy - get a cup of coffee, and when you come back the ice is ready to be removed from the holder.
- After +20 mins unscrew the wing nuts and let out the pressure by opening one of the connections. Your ice should then slide right out.
- Go fill the holder and prepare a new bubble-free section so that you do not run out.

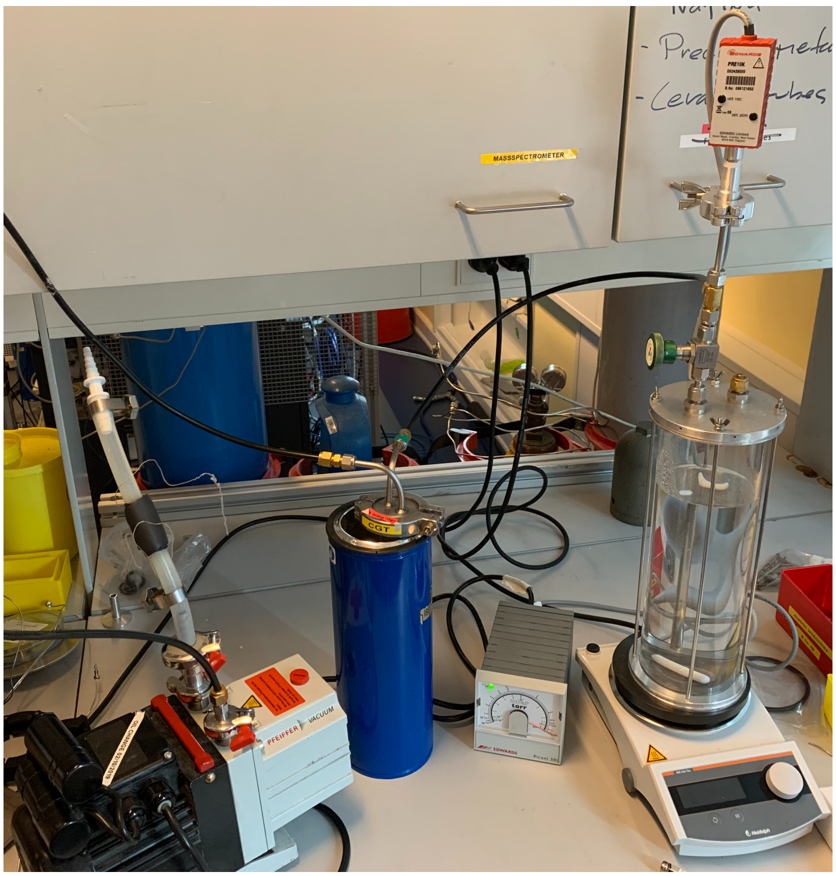

Figure C.1: The bubble-free ice setup. The holder is standing on a magnetic stirrer and heater. It is then connected to a pressure sensor which is further connected to a water trap. The water trap is cooled by liquid nitrogen. From the water trap it is connected further to the roughing pump.

D Bubble-free script improvements

Script improvements The script, both arduino, GUI, JSON and python base were kindly provided by Kerttu Maria Peensoo.

A function was added for manually taking in a list of [Direction, velocity, distance], for us to experiment with transitions in ice. This could be a very slow movement in the first half to ensure no bubbles were formed and then faster movement in the second half to still trap some air bubbles (these can be seen in figure 5.5). It was known from previous creations of bubble free ice that if the freeze was too fast air bubbles would get trapped.

```python
def sequence(self, seq_list):
        """
        Executes a series of moves with a motor taken from a tuple of lists.
        Finishes a full move before moving on to the next command in the tuple.
        Logs data every 2 seconds.

                Parameters:
                        seq_list        : A tuple of lists. Each list is structured as:
                                         [(Direction (1 for up, -1 down), velocity (mm/s), distance (mm))]

                Outputs:
                        log.log         : a log file containing: time since start, direction, spd_us/step, spd_mm/
                             s, dis_steps.
        """
        f = open("./log.log", "w")
        t_init = time.time()
        t_1 = time.time()
        write_delay = 2
        for j in seq_list:
            self.set_dir(int(j[0]))
            self.set_speed(spd = float(j[1]), unit = "mm/s")
            self.move_dis(dis = float(j[2]), unit = "mm")
            while True:
                t_2 = time.time()
                if t_2 - t_1 >= write_delay:
                    t_1 = time.time()
                    self.ping_arduino()
                    data_s = self.serial_read()
                    str_out = "%0.4f\t%i\t%0.4e\t%0.5f\t%0.1f\t%0.1f\n" %(t_1 - t_init, data_s["direction"],
                         data_s["spd_us/step"], data_s["spd_mm/s"], data_s["dis_steps"], data_s["dis_mm"])
                    f.write(str_out)
                    print(str_out)
                    if data_s["dis_steps"]==0:
                        break
                else:
                    continue
        f.close()
        return
```

E Flow rate experiment data

Overview

	Temp	tube	Flowrate	Central/outer			Done
exp 1	25	old	6	outer			x
exp 2	25	old	6	central			x
exp 3	25	old	6	Central + outer			x
exp 4	25	old	10	Central + outer			x
exp 5	25	new	6	Central + outer			x
exp 6	25	new	10	Central + outer			x
exp 7	15	new	10	Central + outer		Excel crashed	x
exp 8	20	new	10	Central + outer		Excel crashed	x
exp 9	25	new	10	Central + outer	Same as exp 6	Excel crashed	x
exp 10	30	new	10	Central + outer			x
exp 11	35	new	10	Central + outer			x
Exp 12	15	new	10	Central + outer	Same as exp 7		x
Exp 13	20	new	10	Central + outer	Same as exp 8		x
Exp 14	25	new	10	Central + outer	Same as exp 6 + 9		x
Exp 15	30	new	10	Central + outer	Same as exp 10		x
Exp 16	35	new	10	Central + outer	Same as exp 11		x
Exp 17	25	new	4	Central + outer		to flow 6	
Exp 18	25	new	6	Central + outer	Same as exp 5		x
Exp 19	25	new	8	Central + outer			x
Exp 20	25	new	10	Central + outer	Same as exp 6 + 9 + 14		x
Exp 21	25	new	12	Central + outer			x
Exp 22	25	new	14	Central + outer			x
Exp 23	25	new	16	Central + outer			x
Exp 24	25	new	18	Central + outer			x
Exp 25	25	new	10	Central + outer			x
Exp 26	25	new	10	Central + outer			x
Exp 27	25	new	10	Central + outer			x
Exp 28	30	new	10	Central + outer			x
Exp 29	25	new	16	Central + outer			x

Run #1

Cup #	Distance [cm]	Time [s]	g/ml	Melt rate [cm/min]	Comment
1	5	174,09	32,56	1,72	
2	10	177,68	35,47	1,69	
3	15	166,08	39,09	1,81	
4	20	161,23	37,24	1,86	
5	25	159,7	41,69	1,88	
6	30	165,45	40,17	1,81	
7	35	258,75	38,955	1,16	average of cup 7 and 8
8	40	273,99	38,955	1,09	
		192,12	38,01	1,62	

Run #2

Cup #	Distance [cm]	Time [s]	ml/5cm	melt rate [cm/min]	Comment
1	5	151,01	13,72	1,99	
2	10	235,48	17,55	1,27	ice stuck on frame
3	15	136,94	11,39	2,19	
4	20	130,84	11,75	2,29	
5	30	271,19	11,73	2,21	10 cm...
6	35	134,48	11,99	2,23	
7	40	135,48	11,97	2,21	
8	45	126,87	17,26	2,36	
		165,28	13,42	2,09	

Run #3

Cup #	Distance [cm]	Time [s]	ml/5cm inner	ml/5cm outer	melt rate [cm/min]	Comment
1	5	167,43	14,72	39,53	1,79	
2	10	156,96	14,32	37,67	1,91	
3	15	164,98	14,94	42,01	1,82	
4	20	156,43	14,54	38,49	1,92	
5	25	147,98	13,19	37,05	2,03	
6	30	144,94	13,02	35,32	2,07	
7	35	144,92	13,12	32,99	2,07	Thinner in this end
8	40	121,56	11,04	30,16	2,47	Thinner in this end
		150,65	13,61	36,65	2,01	

Run #4

Cup #	Distance [cm]	Time [s]	ml/5cm inner	ml/5cm outer	melt rate [cm/min]	Comment
1	5	138,34	17,84	33,56	2,17	
2	10	142,77	19,6	35,3	2,10	
3	15	139,93	19,67	41,25	2,14	
4	20	142,75	19,69	29,98	2,10	
5	25	144,16	19,4	34,15	2,08	
6	30	142,93	19,99	34,83	2,10	
7	35	143,97	20,64	37,13	2,08	
8	40	142,59	19,81	29,75	2,10	
		142,18	19,58	34,49	2,11	

Run #5

Cup #	Distance [cm]	Time [s]	ml/5cm inner	ml/5cm outer	melt rate [cm/min]	Comment
1	5	166,47	11,96	25,28	1,80	
2	10	170,95	16,83	37,11	1,75	
3	15	162,72	15,31	35,46	1,84	
4	20	274,94	20,88	44,56	1,09	Ice stuck
5	25	145,86	13,54	33,00	2,06	Crack across
6	30	151,31	14,58	39,92	1,98	
7	35	146,87	13,88	40,88	2,04	
8	40	130,57	12,92	34,72	2,30	
		168,71	14,98	36,36	1,85	

Run #6

Cup #	Distance [cm]	Time [s]	ml/5cm inner	ml/5cm outer	melt rate [cm/min]	Comment
1	5	127,5	18,04	28,86	2,35	
2	10	130,1	18,57	29,05	2,31	
3	15	129,48	19,17	29,20	2,32	
4	20	132,08	20,00	29,75	2,27	
5	25	146,27	23,64	26,63	2,05	
6	30	153,18	23,93	26,29	1,96	
7	35	135,38	20,67	26,39	2,22	
8	40	152,56	24,09	27,35	1,97	
		138,31	21,01	27,94	2,18	

Run #7

Cup #	Distance [cm]	Time [s]	ml/5cm inner	ml/5cm outer	melt rate [cm/min]	Comment
1	5		32,8	19,84	#DIVISION/0!	
2	10		31,965	20,665	#DIVISION/0!	
3	15		31,965	20,665	#DIVISION/0!	Average of cup 2 and 3
4	20		33,54	22,4	#DIVISION/0!	
5	25		33,18	21,1	#DIVISION/0!	
6	30		36,24	20,75	#DIVISION/0!	
7	35		31,01	17,46	#DIVISION/0!	
8	40		33,84	18,99	#DIVISION/0!	
		0	33,06	20,23	#DIVISION/0!	

Run #8

Cup #	Distance [cm]	Time [s]	ml/5cm inner	ml/5cm outer	melt rate [cm/min]	Comment
1	5		29,62	15,35	#DIVISION/0!	
2	10		34,35	9,88	#DIVISION/0!	
3	15		33,9	9,2	#DIVISION/0!	
4	20		41,17	14,85	#DIVISION/0!	
5	25		33,16	13,06	#DIVISION/0!	
6	30		39,16	15,86	#DIVISION/0!	
7	35		43,08	14,86	#DIVISION/0!	
8	40		36,41	11,45	#DIVISION/0!	
		0	36,35	13,06	#DIVISION/0!	

Run #9

Cup #	Distance [cm]	Time [s]	ml/5cm inner	ml/5cm outer	melt rate [cm/min]	Comment
1	5		21,65	21,34	#DIVISION/0!	
2	10		27,08	22,47	#DIVISION/0!	
3	15		26,94	22,62	#DIVISION/0!	
4	20		27,98	21,83	#DIVISION/0!	
5	25		26,69	20,5	#DIVISION/0!	
6	30		23,01	21,76	#DIVISION/0!	
7	35		23,61	24,93	#DIVISION/0!	
8	40		25,34	26,39	#DIVISION/0!	
		0	25,28	22,73	#DIVISION/0!	

Run #10

Cup #	Distance [cm]	Time [s]	ml/5cm inner	ml/5cm outer	melt rate [cm/min]	Comment
1	5	247,8	40,05	14,8	1,21	
2	10	238,61	38,64	14,6	1,26	
3	15	233,54	38,75	15,03	1,28	
4	20	225,92	34,98	15,47	1,33	
5	25	214,25	34,4	12,03	1,40	
6	30	230,36	37,31	18,05	1,30	
7	35	228,62	37,08	17,8	1,31	
8	40	231,95			1,29	Forgot to remove
		231,38	32,65	13,47	1,29	

Run #11

Cup #	Distance [cm]	Time [s]	ml/5cm inner	ml/5cm outer	melt rate [cm/min]	Comment
1	5	94,6	14,74	28,04	3,17	
2	10	107,36	16,37	32,7	2,79	
3	15	109,06	17,06	34,52	2,75	
4	20	85,08	13,84	30,53	3,53	
5	25	112,7	17,66	36,29	2,66	
6	30	107,2	17,63	35,73	2,80	
7	35	102,54	16,52	33,93	2,93	
8	40	97,54	15,81	32,31	3,08	
		102,01	16,20	33,01	2,96	

Run #12

Cup #	Distance [cm]	Time [s]	ml/5cm inner	ml/5cm outer	melt rate [cm/min]	Comment
1	5	243,14	33,42	16,58	1,23	
2	10	236,79	32,45	19,3	1,27	
3	15	239,02	32,39	20,81	1,26	
4	20	239,76	33,18	20,6	1,25	
5	25	244,11	33,18	20,6	1,23	Average of cup 4+5
6	30	245,96	33,23	18,97	1,22	
7	35	241,33	33,82	18,19	1,24	
8	40	246,09	38,66	17,83	1,22	
		242,02	33,79	19,11	1,23	

Run #13

Cup #	Distance [cm]	Time [s]	ml/5cm inner	ml/5cm outer	melt rate [cm/min]	Comment
1	5	174,43	22,9	20,9	1,72	
2	10	185,15	26,49	26,66	1,62	
3	15	181,66	25,8	24,76	1,65	
4	20	192,28	27,21	26,1	1,56	
5	25	288,12	40,6	25,6	1,04	Ice stuck
6	30	337,48	25,57	12,53	0,89	Crack along stick
7	35	181,94	26,06	25,14	1,65	
8	40	180,58	39,69	41,18	1,66	Forgot to remove
		215,20	29,29	25,35	1,47	

Run #14

Cup #	Distance [cm]	Time [s]	ml/5cm inner	ml/5cm outer	melt rate [cm/min]	Comment
1	5	146,32	21,29	30,08	2,05	
2	10	154,26	22,41	32,33	1,94	
3	15	143,73	20,77	30,82	2,09	
4	20	131,48	18,63	29,08	2,28	
5	25	142,16	19,65	30,63	2,11	
6	30	143,61	20,05	31,69	2,09	
7	35	142,13	19,22	31,15	2,11	
8	40	134,15	18,5	31,83	2,24	
		142,23	20,06	30,95	2,11	

Run #15

Cup #	Distance [cm]	Time [s]	ml/5cm inner	ml/5cm outer	melt rate [cm/min]	Comment
1	5	228,89	36,35	12,24	1,31	
2	10	234,79	36,63	13,59	1,28	
3	15	238,94	37,57	13,69	1,26	
4	20	239,31	38,28	13,93	1,25	
5	25	240,88	41,81	15,61	1,25	
6	30	240,88	37,68	14,65	1,25	
7	35	230,99	37,5	14,33	1,30	
8	40	232,59	29,66	11,52	1,29	
		235,90	36,93	13,69	1,27	

Run #16

Cup #	Distance [cm]	Time [s]	ml/5cm inner	ml/5cm outer	melt rate [cm/min]	Comment
1	5	130,52	15,99	22,62	2,30	
2	10	134,35	19,81	31,49	2,23	
3	15	122,76	18,33	29,02	2,44	
4	20	123,21	18,54	31,69	2,43	
5	25	128,03	19,24	30,34	2,34	
6	30	131,07	19,64	31,69	2,29	
7	35	134,73	20,21	30,7	2,23	
8	40					Only 7 5cm pieces
		129,23	18,82	29,65	2,32	

Run #17

Cup #	Distance [cm]	Time [s]	ml/5cm inner	ml/5cm outer	melt rate [cm/min]	Comment
1	5				#DIVISION/0!	
2	10				#DIVISION/0!	
3	15				#DIVISION/0!	
4	20				#DIVISION/0!	
5	25				#DIVISION/0!	
6	30				#DIVISION/0!	
7	35				#DIVISION/0!	
8	40				#DIVISION/0!	
		0	0	0	#DIVISION/0!	

Run #18

Cup #	Distance [cm]	Time [s]	ml/5cm inner	ml/5cm outer	melt rate [cm/min]	Comment
1	5	145,99	9,04	27,56	2,05	average 1 and 2
2	10	145,99	12,63	38,32	2,05	
3	15	141,94	12,76	39,75	2,11	
4	20	134,96	12,1	37,1	2,22	
5	25	138,91	12,6	39,36	2,16	
6	30	133,58	12,08	38,72	2,25	
7	35	135,5	11,19	36,27	2,21	
8	40	129,24	11,96	25,87	2,32	
		138,26	11,79	35,36	2,17	

Run #19

Cup #	Distance [cm]	Time [s]	ml/5cm inner	ml/5cm outer	melt rate [cm/min]	Comment
1	5	182,32	22,54	23,33	1,65	
2	10	180,96	21,77	30,28	1,66	
3	15	169,09	20,16	25	1,77	
4	20	169,81	20,1	28,53	1,77	
5	25	169,82	20,16	27,25	1,77	
6	30	172,39	20,3		1,74	Droppped glass 6 outer
7	35	172,6	20,52	27,98	1,74	
8	40	180,86	21,67	29,1	1,66	
		174,73	20,90	27,35	1,71	

Run #20

Cup #	Distance [cm]	Time [s]	ml/5cm inner	ml/5cm outer	melt rate [cm/min]	Comment
1	5	131,53	17,74	29,21	2,28	
2	10	138,83	19,28	32,66	2,16	
3	15	126,97	18,19	30,13	2,36	
4	20	142,92	19,88	30,94	2,10	
5	25	138,08	19,74	28,31	2,17	
6	30	138,56	20,24	24,92	2,17	
7	35	136,77	20,04	22,47	2,19	
8	40	133,71	19,52	22,24	2,24	
		135,92	19,32	27,61	2,20	

Run #21

Cup #	Distance [cm]	Time [s]	ml/5cm inner	ml/5cm outer	melt rate [cm/min]	Comment
1	5	130,15	22,02	46,57	2,31	
2	10	130,15	14,31	19,92	2,31	
3	15	135,53	20,32	28,98	2,21	
4	20	210,39	23,77	25,75	1,43	ice stuck
5	25	257,65	19,81	26,02	1,16	Crack through ice
6	30	137,97	21,08	30,63	2,17	
7	35	134,93	21,05	28,08	2,22	
8	40	128,62	20,43	26,25	2,33	
		158,17	20,34	29,02	2,01	

Run #22

Cup #	Distance [cm]	Time [s]	ml/5cm inner	ml/5cm outer	melt rate [cm/min]	Comment
1	5	113,61	19,73	16,11	2,64	plastic in the way
2	10	124,27	21,23	26,73	2,41	
3	15	125,95	21,32	28,13	2,38	
4	20	132,11	22,05	29,36	2,27	
5	25	129,66	22,16	28,97	2,31	
6	30	127,62	22,025	26,67	2,35	Average of 6 and 7
7	35	127,62	22,025	26,67	2,35	
8	40	130,46	24,21	20,55	2,30	
		126,41	21,84	25,39	2,37	

Run #23

Cup #	Distance [cm]	Time [s]	ml/5cm inner	ml/5cm outer	melt rate [cm/min]	Comment
1	5	192,7	33,165	19,135	1,56	Ice stuck due to crack
2	10	139,81	33,165	19,135	2,15	Crack along
3	15	137,69	26,42	23,7	2,18	
4	20	137,52	28,43	29,22	2,18	
5	25	140,62	29,46	23,05	2,13	
6	30	153,2	32,4	20,04	1,96	
7	35	189,55	43,46	8,19	1,58	
8	40	197,27	44,4	6,73	1,52	
		161,04	33,86	18,65	1,90	

Run #24

Cup #	Distance [cm]	Time [s]	ml/5cm inner	ml/5cm outer	melt rate [cm/min]	Comment
1	5	170,9	38,83	11,7	1,76	
2	10	185,01	43,84	9,16	1,62	
3	15	171,93	38,45	10,01	1,74	
4	20	177,19	45,51	5,65	1,69	
5	25	175,98	44,87	3,21	1,70	
6	30	178,22	46,32	7,34	1,68	
7	35	180,19	47,17	4,53	1,66	
8	40	180,95	47,46	5,24	1,66	
		177,54	44,05	7,10	1,69	

Run #25

Cup #	Distance [cm]	Time [s]	ml/5cm inner	ml/5cm outer	melt rate [cm/min]	Comment
1	5	196,62	29,97	19,25	1,53	
2	10	189,62	29,17	22,32	1,58	
3	15	284,75	27,97	27,1	1,05	Ice stuck due to crack
4	20	276,72	23,31	24,38	1,08	ice stuck
5	25	141,59	19,18	29,02	2,12	
6	30	148,74	20,72	32,12	2,02	
7	35	139,49	19,95	29,47	2,15	
8	40	145,93	20,53	30,17	2,06	
		190,43	23,85	26,72	1,69	

Run #26

Cup #	Distance [cm]	Time [s]	ml/5cm inner	ml/5cm outer	melt rate [cm/min]	Comment
1	5	137,52	19,48	33,49	2,18	
2	10	134,26	18,98	31,08	2,23	
3	15	135,02	19	31,25	2,22	
4	20	140,79	19,87	32,57	2,13	
5	25	133,46	19,47	32,02	2,25	
6	30	142,68	20,59	34,24	2,10	
7	35	137,85	19,59	31,26	2,18	
8	40	140,84	20,06	31,91	2,13	
		137,80	19,63	32,22	2,17	

Run #27

Cup #	Distance [cm]	Time [s]	ml/5cm inner	ml/5cm outer	melt rate [cm/min]	Comment
1	5	162,05	24,03	29,18	1,85	
2	10	151,55	14,25	25,73	1,98	
3	15	171,33	13,58	26,95	1,75	
4	20	171,13	13,48	30,45	1,75	
5	25	164,16	13,65	26,18	1,83	
6	30	166,56	14,27	27,13	1,80	
7	35	160,94	13,94	26,23	1,86	
8	40	169,23	26,81	27,84	1,77	
		164,61	16,75	27,46	1,82	

Run #28

Cup #	Distance [cm]	Time [s]	ml/5cm inner	ml/5cm outer	melt rate [cm/min]	Comment
1	5	114,91	17,87	28,48	2,61	Crack across
2	10	100,25	24,25	26,94	2,99	
3	15	90,94	13,58	30,28	3,30	
4	20	97,8	13,47	31,54	3,07	
5	25	94,56	13,65	30,63	3,17	
6	30	96,95	14,27	32,71	3,09	
7	35	94,6	13,94	29,89	3,17	
8	40	96,37	26,81	56,59	3,11	Forgot to remove cups
		98,29	17,23	33,38	3,06	

Run #29

Cup #	Distance [cm]	Time [s]	ml/5cm inner	ml/5cm outer	melt rate [cm/min]	Comment
1	5	134,4	24,98	26,6	2,23	
2	10	129,95	24,78	23,97	2,31	Crack across - fine flow
3	15	140,54	27,94	22,64	2,13	
4	20	133,91	26,29	23,46	2,24	
5	25	138,87	27,53	23,25	2,16	
6	30	138,21	27,73	21,59	2,17	
7	35	136,87	27,39	20,91	2,19	
8	40	137,05	27,07	32,67	2,19	
		136,22	26,71	24,38	2,20	

F Melting method

In this method description the setup in the freezer and the recordings of the melting will be explained.

Setup in the freezer

Much of the setup in the freezer is explained in Section 6.3.2. The microphones have to be placed around the melt head. There is not very much space so they have to be placed the best way they can. For this freezer three microphones were placed around the melt head.

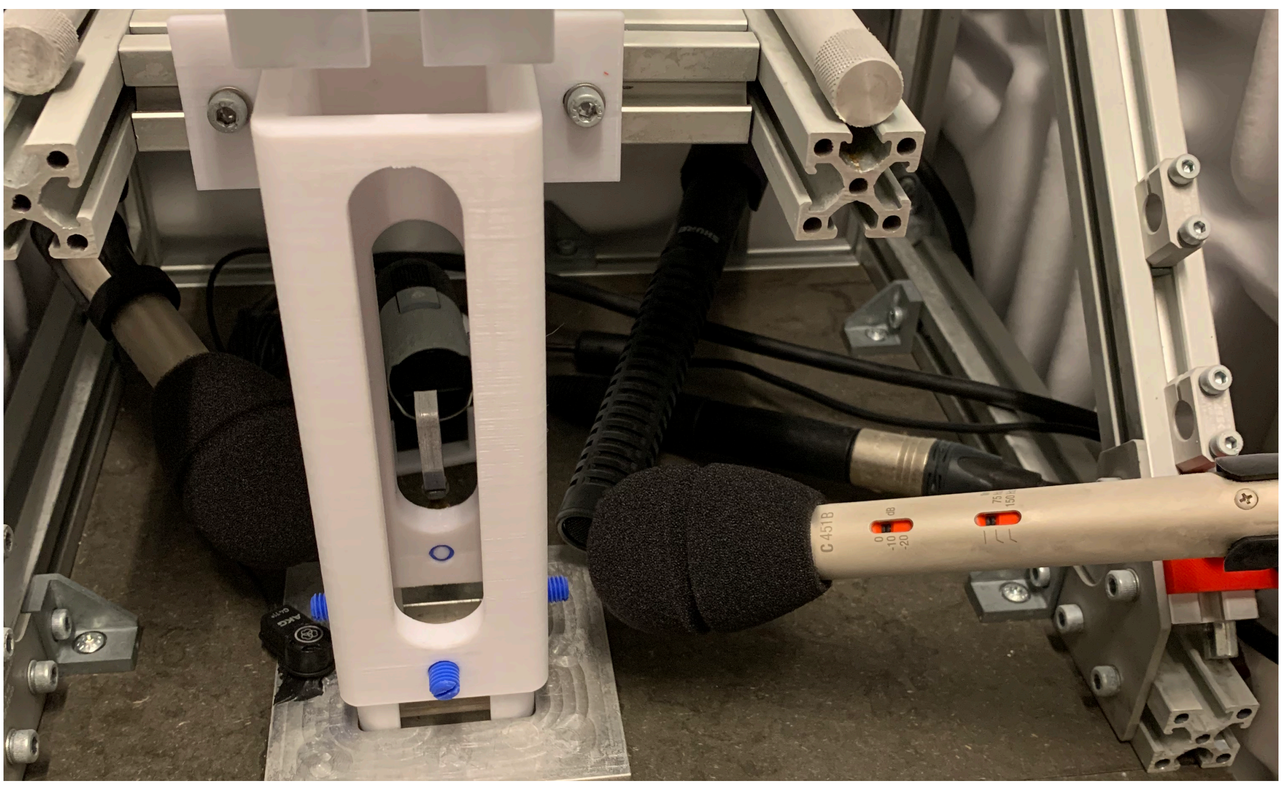

Figure F.1: The microphones are set up with the Shure and one of the AKG microphones from the back and one AKG from the side.

The melting and recording method

The step-by-step method is explained here:

- **Set up and prepare freezer**
- The freezer is cold and the melt head and extraction lines are frozen. Therefore at least an hour before melting turn on the know on the side of the freezer. This is a heater wrapped around the extraction lines and makes sure they are unfrozen and lets the water flow. If this is too slow then use a hairdryer to warm up the extraction lines.
- Turn on the melt head heater and the pump line extractor.
- Once the melt head is heated up spray some mQ water in the troughs on the melt head and turn on the pump extractor to make sure the water is flowing.
- Connect the XLR cables to the microphones in the freezer in the one end and in the preamp in the other.
- Turn on the preamp and make sure to turn on the phantom power to the microphones. Turn up the gain to a satisfying point. This might have to be adjusted just before melting and recording.

- **Set up Cubase**
- Connect the preamp to the computer and open Cubase LE/AI Elements.
- Choose Steinberg UR816C as the audio connection and open an empty project.
- Add each of the microphones by pressing + at a) in Figure F.2 and choosing the inputs that the microphones are at in the preamp.

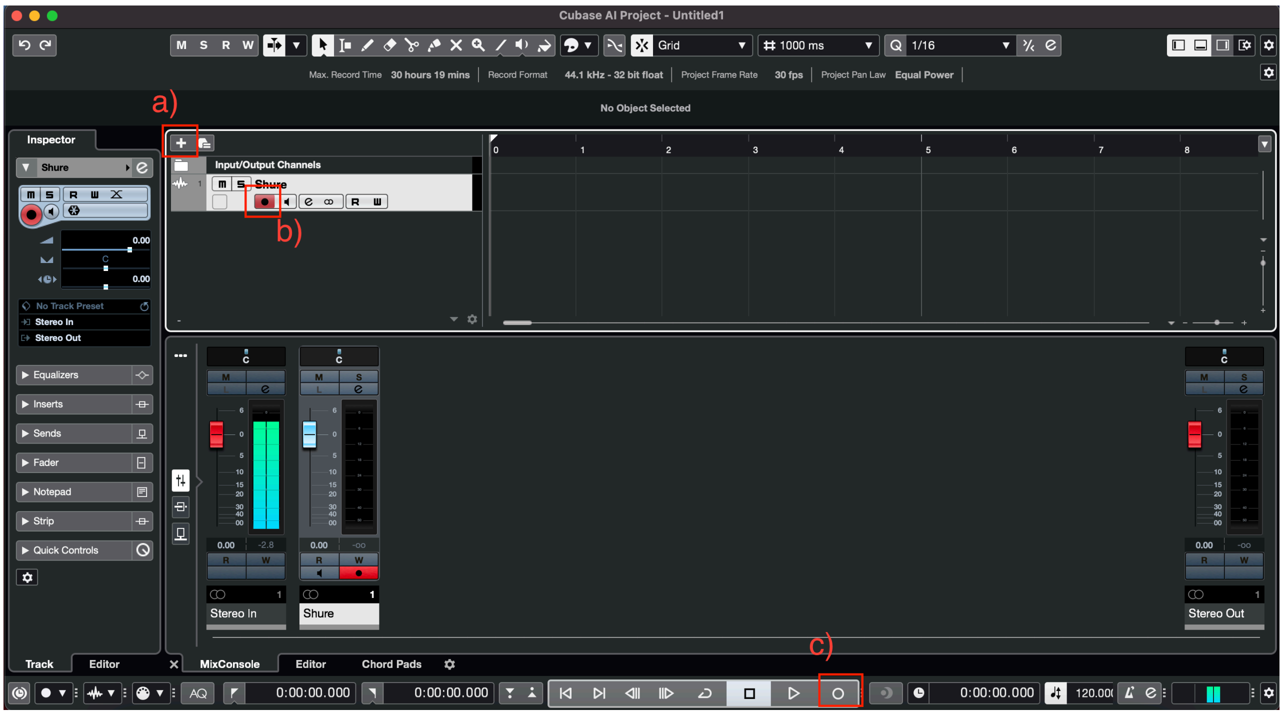

Figure F.2: The Cubase programme interface. This is where the audio recordings are recorded.

- Before recording make sure to "arm" the microphone, making sure it records, by pressing the dot at b) in Figure F.2 and making sure it is red.
- Cubase is now set up and ready to record.

- **Prepare ice for recording**
- Take a piece of ice cut with cross-section of 34 mm x 34 mm and put in the frame. Put pin in the bottom and weight as well as encoder on top.
- Place frame in the freezer.
- Turn off the freezer to reduce noise.
- Change gain on preamp to reduce noise, but still high input.

- **Melting and recording**
- Start the pump extractor at around 6-8 ml/min.
- Start the recording in Cubase by pressing the dot at c) in Figure F.2.
- Remove the pin and start the melting of the ice
- Listen as ice is being melted if something goes wrong.
- Make sure the troughs around the melthead has water in them to reduce noise created by the extraction system.

- **After melting and recording**
- The audio files recorded in Cubase is saved as single files in an audio folder in the Cubase folder system.
- These files can then be analyzed separately as done by the script in Section G.

G Recording ice data analysis script

Code overview

In this script an acoustic signal with background noise is cleaned using high/low pass filter, looking at the frequency spectrum and using a difference function.

Procedure

Step-by-step guide on how the data cleaning is done.

Step-by-step

- Load data using: `from scipy.io.wavfile import read`. Gives sampling frequency and data.
- Convert to pandas datafile `df = pd.DataFrame(data=data_VP82, index=None, columns=['VP82'])` and add columns using: `df['hydro'] = data_hydro.tolist()`
- Filter using a high-pass filter [Butterworth Highpass filter] https://medium.com/analytics-vidhya/how-to-filter-noise-with-a-low-pass-filter-python-885223e5e9b7 . This removes all low frequency noise as we can see all bubble signals are in higher frequency.

```
def butter_lowpass_filter(data, cutoff, fs, order):
    normal_cutoff = cutoff / nyq
    # Get the filter coefficients
    b, a = butter(order, normal_cutoff, btype='high', analog=False)
    y = filtfilt(b, a, data)
    return y
```

- Make a spectrogram using [specgram] https://matplotlib.org/stable/api/_as_gen/matplotlib.pyplot.specgram.html of the butterworth filter: `Pxx, freqs, bins, im = ax.specgram(df['butter_filt'],Fs=samplingFrequency, NFFT=256, noverlap=128`.
- Sum values in all rows of every column: `w = Pxx.sum(axis=0)`

Find peaks https://docs.scipy.org/doc/scipy/reference/generated/scipy.signal.find_peaks.html above some value

- If peak along time axis then analyze the frequency spectrum and find the most prominent peaks using `scipy.signal.find_peaks`
- Calculate frequency value based on weighted average of the most prominent peaks.
- Calculate the bubble/signal radius from the Minnaert equation.
- The volume of a sphere is calculated from the radius and the values for all peaks are summed up.

—

Author: Mikkel Rasmus Schmidt (Niels Bohr Institute)
Date: 04-06-2021 (latest update)

```
from __future__ import division
import numpy as np
import matplotlib.pyplot as plt
import matplotlib as mpl

from scipy.io.wavfile import read
from scipy.io.wavfile import write
from scipy import signal
from scipy import stats
from scipy.signal import butter,filtfilt
import IPython.display as ipd
import pandas as pd
import sys

from iminuit import Minuit                             # The actual fitting tool, better than scipy's
from probfit import BinnedLH, Chi2Regression, Extended # Helper tool for fitting

# Set plotting parameters:
mpl.rcParams['font.size'] = 18      # Set the general plotting font size
%matplotlib widget

# Load raw data and the sampling frequency from the .wav file.
samplingFrequency, data = read("../../../sound_data/21_06_01/21_06_01_Shure_14.wav")

# Filter requirements.
fs = samplingFrequency # sample rate, Hz
cutoff = 1000      # desired cutoff frequency of the filter, Hz ,      slightly higher than actual 1.2 Hz
nyq = 0.5 * fs  # Nyquist Frequency
order = 2       # sin wave can be approx represented as quadratic

# Define lowpass butter filter
def butter_lowpass_filter(data, cutoff, fs, order):
    normal_cutoff = cutoff / nyq
    # Get the filter coefficients
    b, a = butter(order, normal_cutoff, btype='high', analog=False)
    y = filtfilt(b, a, data)
    return y

# Write as audio file and play the audio file using iPython.display
write('ipd_audio/bubble_free_1.wav', samplingFrequency, data)
ipd.Audio('ipd_audio/bubble_free_1.wav')

# Organize data strings in Pandas Dataframe and apply difference and butterworth filters.
df = pd.DataFrame(data[0:192000*60])
df.columns =['signal']
df['diff'] = df['signal'].diff()
df['butter_filt'] = butter_lowpass_filter(df['signal'], cutoff, fs, order)
x = np.linspace(0, len(df['signal'])/samplingFrequency, len(df['signal']))

# Plot the spectrogram. As it is plotted the value matrix, frequencies and center of time bins comes as output.
fig, ax = plt.subplots( figsize=(14,4))
Pxx, freqs, bins, im = ax.specgram(df['signal'],Fs=samplingFrequency, NFFT=256*4, noverlap=128*4, cmap='viridis',
     scale='dB')
fig.colorbar(im, ax=ax)
ax.set_ylim(0,40000)
ax.set_xlabel('Time [s]')
ax.set_ylabel('Frequency')
```

```
ax.legend(loc='best')
fig.tight_layout()
fig.savefig('Figures/spectrogram.png')

# Calculate the total power in each column (the time axis). Find the columns with the most energy and define peaks
    .
Pxx_sum = Pxx_butter.sum(axis=0)
peaks, properties = signal.find_peaks(Pxx_sum, height=np.max(Pxx_sum)*0.0001, distance=1)

# For each peak found along the time axis --> analyze the frequency spectrum and find the most prominent peaks and
      do weighted average.
maxx = []
for i in range(len(peaks)):
    peakss, _  = signal.find_peaks(Pxx_butter[:,peaks[i]], height=(np.max(Pxx_butter[:,peaks[i]])*0.01), distance
         =5)
    freqss = freqs[peakss]
    freq = []
    for j in range(len(freqss)):
        weight = np.abs(Pxx_butter[:,peaks[i]][peakss][j])/np.sum(np.abs(Pxx_butter[:,peaks[i]][peakss][:]))
        freq.append(freqss[j]*weight)
    maxx.append(np.sum(freq))
maxx = np.array(maxx)

# Define the constants for the Minnaert equation calculations
gam = 1.4
rho = 998
p_0 = 101000

# Find the radius that fits with the weighted average frequency value. Calculate the volume of the sphere and the
     Total Air Content
a = (1/(2*3.14*maxx[maxx!=0]))*np.sqrt((3*gam*p_0)/rho)
a_vol = (4/3)*np.pi*a**3
TAC = sum(a_vol)
print(TAC)

##############################################################
#Calculate signal strength for full signal in both dB and Pa.
##############################################################

sensitivity = 9e-3
N = len(df['signal'])

# Calculate the level from time domain signal
rms_time = np.sqrt(df['butter_filt']**2)
db_time = 20 * np.log10(rms_time / sensitivity)

# Apply window to the signal
win = np.hamming(N)
signall = df['butter_filt'] * win

# Get the spectrum and shift it so that DC is in the middle
spectrum = np.fft.fftshift( np.fft.fft(signall) )
freq = np.fft.fftshift( np.fft.fftfreq(N, 1 / fs) )

# Take only the positive frequencies
spectrum = spectrum[N//2:]
freq = freq[N//2:]

# Since we just removed the energy in negative frequencies, account for that
spectrum *= 2
# If there is even number of samples, do not normalize the Nyquist bin
```

```
if N % 2 == 0:
    spectrum[-1] /= 2

# Scale the magnitude of FFT by window energy
spectrum_mag = np.abs(spectrum) / np.sum(win)

# To obtain RMS values, divide by sqrt(2)
spectrum_rms = spectrum_mag / np.sqrt(2)
# Do not scale the DC component
spectrum_rms[0] *= np.sqrt(2) / 2

# Convert to decibel scale
spectrum_db = 20 * np.log10(spectrum_rms / sensitivity)
spectrum_pa = spectrum_rms / sensitivity

# Compare the outputs
print("Difference in levels: {} dB".format(db_time.mean() - spectrum_db.max()))
```

H Pictures of melted ice

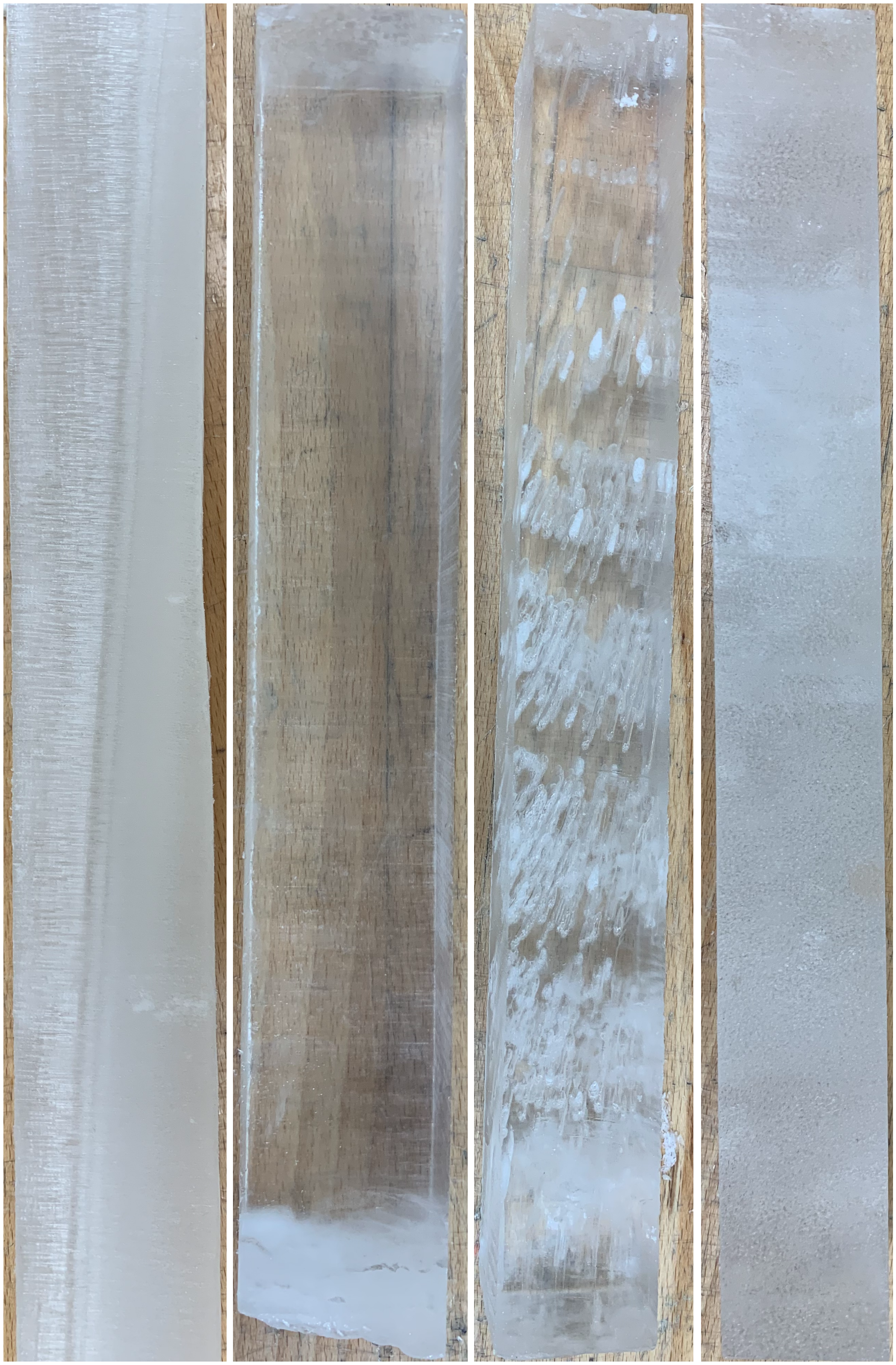

Figure H.1: The four melted types of ice. From left: mQ, bubble-free, bubble-free with bubbles and DYE-3. As can be seen they have a lot of differences.

List of Figures

List of Tables

List of Audio